Doctoral theses at NTNU, 2022:208

Linn Danielsen Evjemo

Additive manufacturing of thin-walled structures by robot manipulator

An experimental approach focusing on arc welding

Doctoral thesis

NTNU
Norwegian University of Science and Technology
Thesis for the Degree of
Philosophiae Doctor
Faculty of Information Technology and Electrical Engineering
Department of Engineering Cybernetics

NTNU
Norwegian University of
Science and Technology

Linn Danielsen Evjemo

Additive manufacturing of thin-walled structures by robot manipulator

An experimental approach focusing on arc welding

Thesis for the Degree of Philosophiae Doctor

Trondheim, June 2022

Norwegian University of Science and Technology
Faculty of Information Technology and Electrical Engineering
Department of Engineering Cybernetics

NTNU
Norwegian University of
Science and Technology

NTNU
Norwegian University of Science and Technology

Thesis for the Degree of Philosophiae Doctor

Faculty of Information Technology and Electrical Engineering
Department of Engineering Cybernetics

ISBN 978-82-326-6853-3 (printed ver.)
ISBN 978-82-326-6624-9 (electronic ver.)
ISSN 1503-8181 (printed ver.)
ISSN 2703-8084 (online ver.)

Doctoral theses at NTNU, 2022:208

Printed by NTNU Grafisk senter

Summary

Additive manufacturing (AM) has, over recent decades, become a quickly evolving and ever more present part of production and manufacturing. It has gone from being a simple prototyping method to building more complex prototypes more quickly and more accurately, and even for manufacturing smaller end products, which is financially advantageous for products in small quantities. Most off-the-shelf AM methods are, however, limited by both the geometry and the size of builds, as they mostly require the component to be built layer-by-layer within a chamber. Robotised AM is on its way to help solve these challenges, making AM technology more useful and available for industry in the future.

This thesis presents contributions in robotised additive manufacturing, focusing on manufacturing metal structures using methods that deviate from the most common methods for AM. The papers present proof-of-concept results of non–layer-wise material deposition as a step towards expanding the range of geometries possible in AM. From there, different challenges related to the construction of thin-walled metal structures using wire-arc additive manufacturing (WAAM) are examined. A set-based control method is examined as a possible solution for enabling non-vertical material deposition in WAAM, and, lastly, more complex structures with overhangs are built by depositing material orthogonally onto surfaces already built.

The accompanying text presents the motivation behind this research, and an introduction to the set-based control method used in some of the experiments. The principles behind the focus on WAAM technology is explained by introducing the main arc welding methods, and examining which method is most easily combined with robotic deposition of material. An overview of the most common methods for AM is also given, in order to fully understand why non-vertical material deposition is a topic worth researching.

Contents

List of figures

ABBREVIATIONS

AM Additive Manufacturing

BJT Binder Jetting

CAD Computer Aided Design

CMT Cold Metal Transfer

CNC Computer Numerical Control

DED Direct Energy Deposition

DLF Direct Light Fabrication

DMD Direct Metal Deposition

DMLS Direct Metal Laser Sintering

DOF Degrees of Freedom

EBM Electron Beam Melting

FDM Fused Deposition Modelling

GMAW Gas Metal Arc Welding

GTAW Gas Tungsten Arc Welding

HAZ Heat Affected Xone

LBMD Laser-Based Metal Deposition

LENS Laser Engineered Net Shaping

LS Laser Sintering

MAG Metal Active Gas

MEX Material Extrusion

MIG Metal Intert Gas

MJT Material Jetting

PAW Plasma Arc Welding

PBF Powder Bed Fusion

RP Rapid Prototyping

RPD Rapid Plasma Deposition

SL Stereo Lithography

SLS Selective Laser Sintering

TAG Tungsten Active Gas

TIG Tungsten Intert Gas

VP Vat Photo-Polymerisation

WAAM Wire-Arc Additive Manufacturing

Chapter 1

Preface

This thesis is submitted in partial fulfilment of the requirements for the degree of Philosophiae Doctor (PhD) at the Norwegian University of Science and Technology (NTNU).

I have done this work at the Department of Engineering Cybernetics (ITK) under the supervision of Professor Jan Tommy Gravdahl. My co-supervisors have been Dr. Signe Moe at SINTEF Digital/Sopra Steria, Dr. Ragnhild Aune at SINTEF Industry, and Dr. Vegard Brøtan at SINTEF Manufacturing AS.

The PhD project was funded by the Research Council of Norway, and undertaken in the SFI Manufacturing cross-disciplinary centre for research-based innovation for competitive, high-value manufacturing in Norway[1] under contract number 237900. SFI Manufacturing has three main focus areas: Multi-material products and processes, robust and flexible automation, and innovative and sustainable organisations. While this project has mainly concerned the Robust and Flexible Automation research area, it has on many occasions touched also upon the area of Multi-Material Products and Processes.

During my PhD studies, I had the pleasure of being co-supervisor to the master students Nora Garcia Leiva, Jørgen Jackwitz, Ingrid Fjordheim Onstein, and Helene Boge.

[1] http://www.sfimanufacturing.no/

1.1 Acknowledgements

More than four years of PhD studies is a long time. Even longer when you throw in a global pandemic with national lockdown and months of mandatory work-from-home into the mix. When you are stowed away in a cramped home office for weeks and months at a time, you get a deeper appreciation for all the people who are there to support you.

First and foremost, I am so very grateful for my main supervisor Prof. Tommy Gravdahl. Your ability to motivate and see the break in the clouds whenever things came to a standstill has been so invaluable to me. When my PhD education started out rough, you got me back in by challenging me just enough to distract me, while staying very understanding and patient at the same time. Thank you for our many discussions related to the research, and for all the conversations dedicated to everything else. I consider myself very lucky to have been given the opportunity to work with you, and for having had you as my supervisor.

Thank you to my supervisor Dr. Ragnhild Aune at SINTEF Industry and my co-supervisor Dr. Vegard Brøtan at SINTEF Manufacturing for valuable feedback and pointers on a field which was very new to me, and for feedback on this thesis. And thank you to my co-supervisor Dr. Signe Moe at Sopra Steria/SINTEF Digital for guidance, discussions and feedback, and for good times at the lab.

I would like to thank Morten Høgseth Danielsen at SINTEF Industry, who genially welcomed me into the welding lab. Your goodwill, high spirits and enthusiasm made the lab work a highlight throughout my PhD studies. I truly appreciate that you never grew impatient with my questions. I would also like to thank Dr. Geir Langelandsvik at SINTEF Industry for our collaboration on the WAAM experiments, and for your contributions related to material analyses.

Thank you to my dear office mate Dr. Kristbjörg Edda Jónsdóttír, who made these years so enjoyable. Thanks for all the interesting, engaging, and loud conversations that were rarely even remotely connected to our fields of study. And thank you for all the encouragement you gave me in the final part of my writing. I am really happy that we will continue to work together, even if we are no longer office-mates.

To all my new colleagues at SINTEF Ocean: thank you for making me feel so welcome from day one, and for the encouragement and support while I finished this thesis. Thank you to Dr. Eleni Kelasidi for valuable input in the final stages of the work on my thesis, and to all of you at Brattøra for

your patience, your understanding, and for backing me all the way. It made every challenge so much easier.

Thank you to my friends in Trondheim (and everywhere else). I am so very lucky to know you, and for having you all in my life. Thank you for your patience and encouraging words while listening to all of my worries and moments of panic throughout these years. A special thanks to the friends at Samfundet, for making me feel seen and appreciated when the impostor syndrome threatened to overwhelm me. And thanks for all the late nights that often became early mornings: *Én gang desker, alltid desker.*

Lastly, I would like to thank my family for all their love and support. To my mother for her endless encouragement and for always having more faith in my abilities than I tend to have myself. To my father, for being an inspiration that I am sorry that I never got time to truly appreciate. To dadda, for being the never-changing safe haven in my life. To my brothers for always seeing me, challenging me, and for treating me as a peer long before my age justified it. And to my brother who was there to see me start my PhD, but not here to see me finish it: I miss you.

1.2 Contributions

The doctoral thesis aiming to address the research questions presented in chapter 4 includes contributions in:

(A) L. D . Evjemo, S. Moe, J. T. Gravdahl, O. Roulet-Dubonnet, L. T. Gellein, V. Brøtan. Additive manufacturing by robot manipulator: An overview of the state-of-the-art and proof-of-concept results. In *22nd IEEE International Conference on Emerging Technologies and Factory Automation (ETFA)*, pages 1–8. IEEE, 2017,

(B) L. D. Evjemo, G. Langelandsvik, and J. T. Gravdahl. Wire-arc additive manufacturing by robot manipulator: Towards creating complex geometries. In *5^{th} IFAC Conference on Intelligent Control and Automation Sciences (ICONS)/IFAC-PapersOnLine*, 52(11): 103–109, 2019,

(C) L. D. Evjemo, S. Moe, and J. T. Gravdahl. Robotised wire-arc additive manufacturing using set-based control: Experimental results. In *21^{st} IFAC World Congress/IFAC-PapersOnLine*, 53(2): 10044–10051, 2020,

(D) L. D. Evjemo, G. Langelandsvik, S. Moe, M. H. Danielsen, and J. T. Gravdahl. Wire-arc additive manufacturing of structures with overhang: Experimental results depositing material onto fixed substrate. *CIRP Journal of Manufacturing Science and Technology*, 38, 186-203 (2022).

These papers follow each other chronologically in methodology and conceptual advancement, as the research progressed from literature reviews and proof-of-concept experiments to welding technology and robotised WAAM.

Paper A presents the state of the art of large-scale AM as of March 2017, looking into some of the projects that had come furthest in utilising AM technology on large structures such as buildings or sculptures. After outlining the the necessary algorithms and components for an AM system that combines robotics with non–layer-wise material deposition, a proof-of-concept experiment using a UR5 robot is performed to demonstrate non–layer-wise material deposition by extrusion by robot.

Paper B presents the transition to building metal structures using CMT welding equipment and a IRB2400/10 robot from ABB Robotics. The focus of the paper is the feasibility of large-scale AM of metallic materials by arc welding. A series of robotic arc-welding experiments is presented and

discussed. These experiments helped map some of the challenges that needed to be addressed in subsequent work.

In paper C, a method for set-based control for WAAM was tested on a cylindrical structure with non–layer-wise material deposition. The set-based control method used to control the robot manipulator allows for some freedom in tool orientation so that the material is not always deposited strictly vertically. Evaluating how non-vertical deposition impacted upon the structure helped map how feasible this solution would be when manufacturing more complex structures.

In paper D, structures with overhangs are constructed using two different approaches: both vertical and non-vertical material deposition. Material tests on two of the structures are presented, examining the porosity and hardness. Tests were done on material in parts of the structure with a prominent overhang, and compared to a part of the structure with little or no overhang. Tests were also performed on a structure with intersections. The final vase and bowl structures presented in this paper show that large overhangs can be constructed using robotised WAAM to perform non-vertical material deposition of material onto a fixed surface.

Other results during the doctoral studies not published as part of this thesis are:

- I. F. Onstein, L. D. Evjemo and J. T. Gravdahl. Additive Manufacturing Path Generation for Robot Manipulators Based on CAD Models. IFAC-PapersOnLine, 53(2): 10037—10043 [1]
- L. D. Evjemo, T. Gjerstad, E. I. Grøtli, and G. Sziebig. Trends in smart manufacturing: Role of humans and industrial robots in smart factories. *Current Robotics Reports*. 1(2), 35—41, 2020 [2].

Chapter 2

An introduction to additive Manufacturing

The term additive manufacturing (AM) is an umbrella term that covers a variety of methods for joining materials together in order to build three-dimensional structures. Techniques include 3D-printing, powder-bed fusion (PBF), direct energy deposition (DED) and binder jetting (BJT), and also find extensive application in rapid prototyping (RP) and free-form fabrication. [3]. The term 'rapid prototyping' refers to creating three-dimensional models of products for testing and prototyping, and was an early use of the technology [4]. Mass production of parts in any industry is, in general, cheaper than producing single, custom-made components. However, AM technology is gradually making custom made parts more affordable. Commercial desktop 3D printers have already been welcomed into the world of prototyping for small businesses and start-ups. As AM technology evolves and becomes more advanced, its availability increases, and the technologies are now used to also manufacture smaller end- products. This is why the term 'AM' has gradually taken over from 'RP' [5, p. 2], although in everyday speech and popular technology, the term '3D-printing' is most commonly used.

The work presented in this thesis examines how the combination of robotics and AM can benefit industry by solving challenges and limitations that limit many of the commercially available AM methods. The main focus is on wire-arc additive manufacturing (WAAM), a welding-based method for additive manufacturing in metals. As this thesis is quite cross-disciplinary, some basic principles will be presented that may be familiar to some readers and new to others: An overview of the most commonly used AM methods

will also be presented in order to understand why robotised AM can increase the flexibility of the design and build, and how this, in turn, can help solve some of the limitations and challenges that other AM methods face today. A brief introduction to welding technology in general, and to the arc welding methods that are of particular interest when considering welding-based AM, will also be given.

2.1 Common methods for AM

The work presented in this thesis focuses on the benefits of depositing material using a robot manipulator with up to 6 DOFs, focusing on WAAM and robotised welding. This method's differences from many of the most common AM technologies are best understood through an overview of the existing and dominant technologies, and what their limitations are.

Powder-bed fusion (PBF)

PBF describes a group of layer-based AM methods that build structures from the bottom layer up. This category includes various methods such as selective laser sintering (SLS) and electron beam melting (EBM) [5]. PBF was one of the earliest AM processes, suitable for metals and polymers, and SLS was the first PBF process to be commercialised [5, p. 125]. All PBF processes that use lasers to perform the fusing of powder particles are known collectively as laser sintering (LS) machines [5, p. 125]. For each layer, which is typically 0.1 mm thick or thinner, an energy source sinters together the powdered material in patterns that match slices of the full 3D structure. Next, a new layer of powdered material is spread out, as shown in Fig. 2.1, and the process is repeated.

When the build is complete, the solid product is enclosed in a powder bed [7]. Because the material is sintered together layer by layer, the bottom-up building process is strictly vertical. However, overhangs can still be constructed because the component is fully submerged in excess powdered material, and each top layer is, at any time, fully supported by this powder bed. When the powdered material is subjected to the energy beam, it melts together in all directions, not only vertically. This makes it possible to construct overhangs and hollow chambers. Even if this AM method is flexible in which geometries can be built, it is still very limited when it comes to size and build time: the size is generally limited to within 2 m^3 due

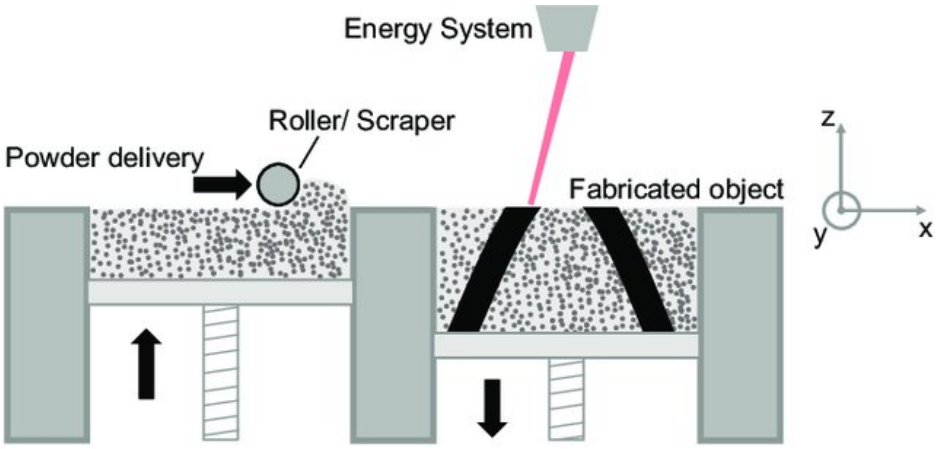

Figure 2.1: **Powder-bed fusion:** This illustration of PBF shows how material from a container to the left is gradually delivered to the container on the right. There, an energy source fuses the material together in a 2D pattern, creating a new layer of the fabricated object. The container holding the fabricated material is gradually lowered, while the container with the building material is gradually elevated. Overhangs are possible because the material at the top is always fully supported by excess powder below. Image from[6], Creative Commons CC BY-NC 4.0.

to the size of the printer and the prolonged build time due to the thin layers, which typically lays down only a few millimetres of depth per hour [8].

Direct energy deposition (DED)

DED methods use an energy source to heat up the material upon deposition, and include WAAM. DED and PDF are, together, the most used methods for constructing metal components. A wide range of more specialised AM methods fall under DED, such as laser-engineered net shaping (LENS), direct light fabrication (DLF), direct metal deposition (DMD), and laser-based metal deposition (LBMD). DED methods are based on welding, and use an energy beam such as an electrical arc or a laser beam to melt solid material as it is being deposited [5, pp. 285–287]. DED is traditionally layer-based, building structures from the bottom-up, and is used almost solely for metals. As shown in Fig. 2.2, powdered material can be fed, for example, through a nozzle along a defined path, and immediately melted using a laser beam. The material deposition rate and build time depend very much on the spe-

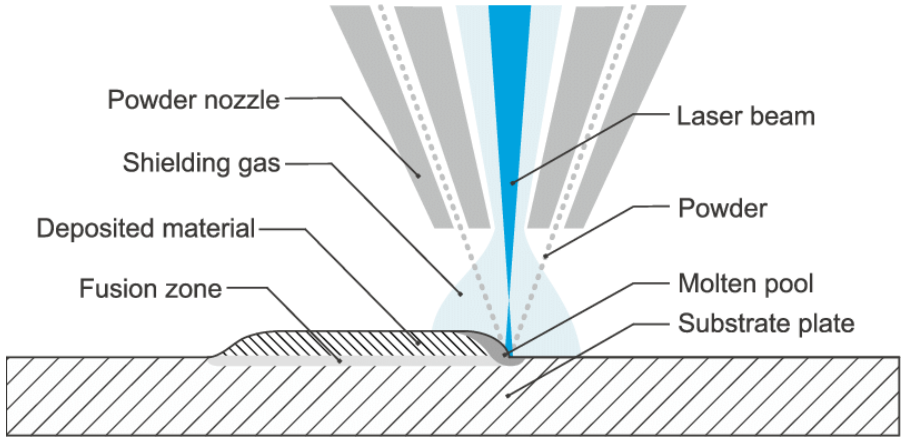

Figure 2.2: **Direct energy deposition:** In this illustration of powder-based DED, powdered metal is deposited and melted together with the substrate using a laser beam. The process is performed vertically, and layer by layer. Image from [9], Creative Commons CC BY-NC-ND 3.0.

cific method, but, like extrusion extrusion-based methods, DED can build much more quickly than PBF because deposition is not confined to very thin layers.

Binder jetting (BJT)

BJT methods are similar to PBF in the sense that both methods entail depositing powder, layer by layer, from the bottom up. The method was developed at MIT in the 1990s, and was the first method to be called *3D printing* [5, pp. 237–239]. Instead of melting the material together in 2D patterns that cumulatively constitute the 3D structure, BJT methods involve depositing a *binder* onto a layer of powdered material, the layer typically being less than 0.1 mm thick. A majority of the materials used for AM using BJT are starch-based, plus a water-based binder which reacts with the powder. The deposited binder droplets make up part of the material in the final structure, though most of the building material is the material from the powder bed. Because the binder reacts with the powder in all directions, AM using BJT also the construction of overhangs, holes etc, but the finished component is commonly less than 1 m^3 due to the limitations of the chamber size and the long building time involved in working with a large number of very to the thin layers.

Material jetting (MJT)

Material jetting (MJT) extrudes material from a printer head, and covers many different kinds of AM technology. To enable the jetting of material, solid material is heated enough to melt, and then cools upon depositing, adhering to previously deposited material [5, pp.203-204]. Finding the right temperature, nozzle diameter, extrusion rate, layer thickness and nozzle speed are the main optimisation challenges at the user end; they're all driven from below by the material's fluidity and freezing rate. The first demonstrations came about in the 1980s, and the first commercially available MJT printer was released in the mid 1990s [5, pp. 203–204]. MJT technology continued to develop to present date. The method can now be used for a variety of materials including various polymers, ceramics and metals, though, in industry, MJT is mostly used for polymers [5, p. 205]. MJT is typically used to build components less than 0.5 m^3 large, and layer-by-layer from the bottom up.

Material extrusion

Material extrusion (MEX) is the most commercially available AM method. Material is fed through a nozzle onto a surface where it adheres to the building surface or the previous layer. Most commonly, material is heated up to a fluid phase before deposition, forced through the nozzle under pressure, and solidifies as it cools down to room temperature. It is also possible to solidify the material chemically, for example by drying a wet material, or by agent-activated curing of an initially liquid material [5, pp. 171–173]. Material is deposited in layers from the bottom- up, accumulating into a final three-dimensional product. Fused deposition modelling (FDM) is a form of MEX, and one of the more commonly known and most available forms of AM. It uses a bottom-up, layer-by-layer approach, melting and extruding a plastic filament through a nozzle that moves along a preassigned path close to the building surface within each layer on the x-y plane. When a layer is completed, the nozzle moves up in the z-direction, to deposit the next layer [4].

Vat polymerisation (VP)

Vat polymerisation (VP) processes, or vat *photo*-polymerisation processes, use electromagnetic waves, mostly in the ultraviolet range, to change the state of materials through radiation. Visible light, gamma rays, x-rays or

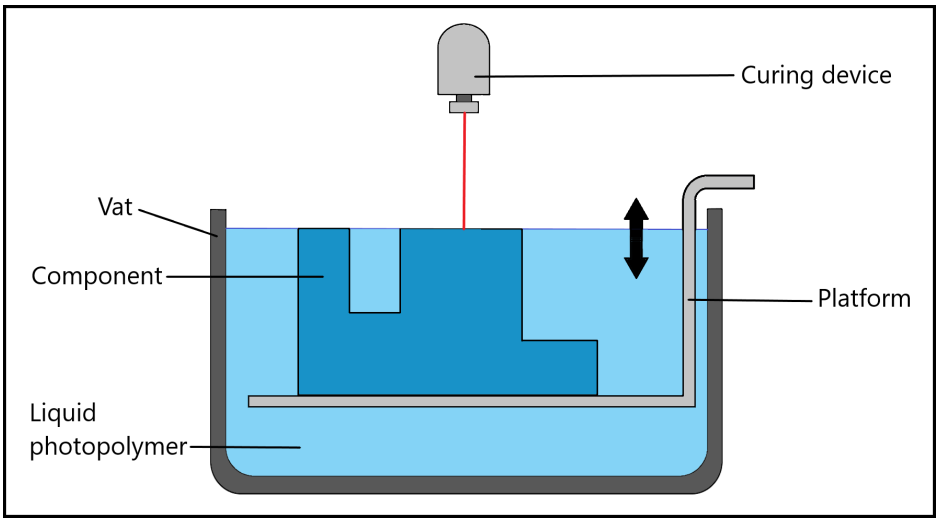

Figure 2.3: **Vat polymerisation:** This illustration of a VP process shows how a vat filled with a liquid photo-polymer, and a component being constructed on a platform moving vertically. The liquid surface is selectively cured, for example by UV light or a laser, and adheres to the rest of the component below. The platform is then lowered to submerge the component just below the liquid surface, and another layer can be constructed in the surface film. Adapted from [10].

electron beams may also be used. Most processes use liquid polymers that become solid when exposed to the right kind of radiation, and are hence called photo-polymers [5, pp. 77–78]. These materials were developed in the 1960s, and mostly used for painting and coating. The first approach towards creating three dimensional parts was done in the 1980s by Charles Hull, and this was the beginning of stereo-lithography (SL).

The method is layer-based. The upper-most part of a vat (tank) filled with liquid photo-polymers are exposed to radiation, shown in Fig. 2.3. The hardened part of the component is then lowered into the liquid, and a new layer is exposed to the radiation. The submerged part of the component and the surrounding liquid provide enough support that small overhangs, of approximately 1–2 mm per layer, can be constructed without needing additional support structures, despite the build being performed strictly vertically from the bottom up [11].

Why the need for robotised AM?

What many of the AM method described in this section have in common, is that they require a strict top-down or bottom-up building approach, where material is deposited or hardened vertically, one layer at a time. Some of the methods allows for the construction of overhangs, but these methods are limited by a slow building process and the size of the build chamber: VP, MJT, BJT and PBF all take place inside a container that must be larger than the structure being built. The deposited layers are also very thin, which allows for a great deal of detail, but makes the deposition rate very low. Building a larger structure is very time-consuming, even if the size of the structure is not limited by the in-box building method. In addition, as the build chamber must be filled with material, whether in liquid or powder form, a lot of excess material is involved. Much of this excess material can be re-used when considering machines that receive heavy use, e.g. producing a large number of small orders, but this can be a big sunk cost in machines used only occasionally.

For methods that can deposit material more quickly, such as MEX and DED, additional support structures must be added if the build involves any overhangs, as material cannot be deposited into thin air [11]. These support structures must later be removed. Some geometries might not be possible to construct at all, depending on the building material and dimensions. Therefore, AM technology would greatly benefit from non-vertical deposition of swiftly curing material.

Consider Fig. 2.4: When material is deposited vertically, but the layers do not overlap completely, the contact surface is reduced, which weakens the link between the layers. This was also the result of the preliminary experiments using viscous glue presented in paper A: a larger contact surface gave a more stable structure [12]. If the overhang shown in Fig. 2.4 were even steeper, the layers might not overlap at all, making it impossible for the layers to stick together when depositing material vertically. However, if the material is deposited at an angle, as shown to the right in Fig. 2.4, the contact surface is increased relative to the vertical deposition of the same overhanging wall. This can enable the construction of overhangs even when using AM methods that such as MEX or DED.

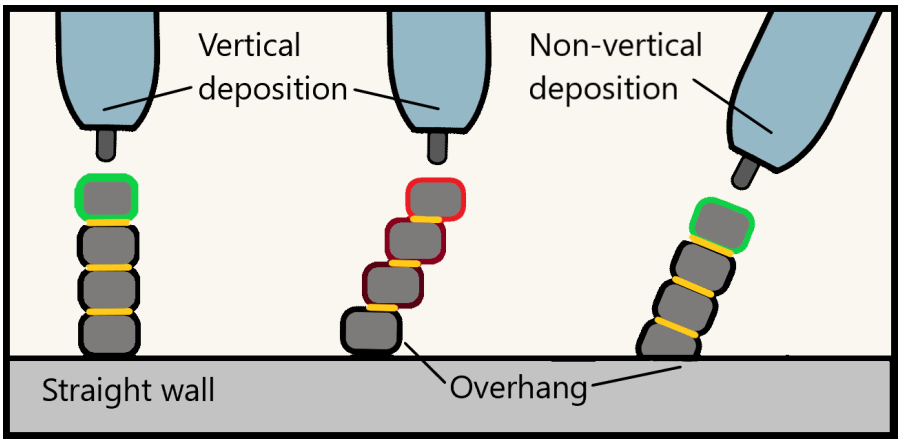

Figure 2.4: **Non-vertical deposition:** In this simplified illustration, it is possible to see how the contact surface between one layer and the next changes with the angle of the wall being built. and the angle of the welding gun. By angling the tool to follow the tilt of the wall, the contact surface is increased, which can enable the newest welding bead to adhere better to the underlying surface.

2.2 Additional benefits of using a 6-DOF robot

Combining material extrusion with a robot manipulator can be beneficial in several ways. Most of the AM methods presented in section 2.1 have hard limitations on the size of the structure that can be built: all in-box building methods require the AM machine to be larger than the component that is being constructed, as the component is built inside a chamber or a basin. Any limitation on the size of the AM machine restricts the dimensions of any component that can be built. “Large” AM-machines are still limited to a volume of a few cubic meters.

One solution to this challenge is to use an industrial robot arm for material deposition. Many industrial, 6-DOF robot manipulators have a reach of 2 meters or more, which in itself creates a total workspace larger than the build chamber of most AM machines. An example is the workspace of the ABB IRB2400/10 robot used in the welding experiments in this thesis, described in Fig. 2.5. Mounting the industrial robot manipulator on a rail or gantry system can increase the workspace almost indefinitely. As long as the material deposition rate is high enough to manufacture components within a reasonable time-frame, such mobility enables the manufacturing of larger

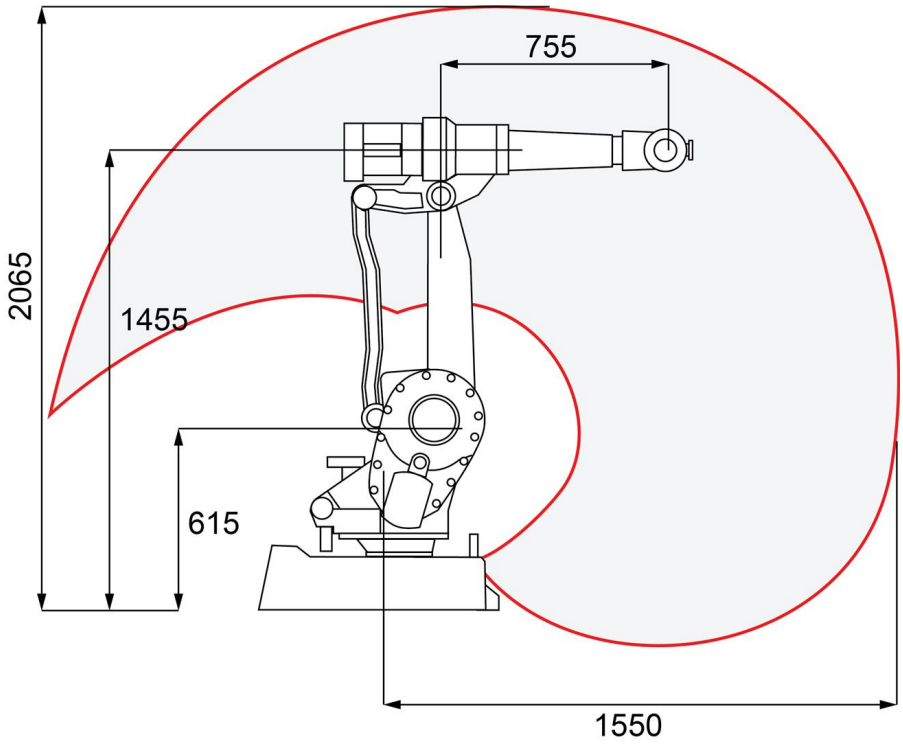

Figure 2.5: **IRB 2400/10:** This 6-DOF robot has a much larger workspace than many traditional AM machines, and can reach points within the workspace with an arbitrary orientation of the end effector. Dimensions are given in mm. Image: www.Abb.com [13]

components. What defines a reasonable time-frame depends on the component that is being used, and on what alternative manufacturing methods are available, just as with other AM methods where the manufacturing time can range from under an hour up to several days.

A larger workspace is only one of the reasons why AM by robot shows promise. Robotised, non-vertical material deposition also broadens the spectrum of what kinds of structures can be manufactured. Compared to, for example, machining, AM has very few limitations when it comes to the geometries of the component. However, most AM methods require the structure to be built layer-by-layer, based on a digital 3D-model which is sliced into thin layers for deposition one at a time [14]. The material is deposited directly and vertically, either top-down or bottom-up, and the process is often time

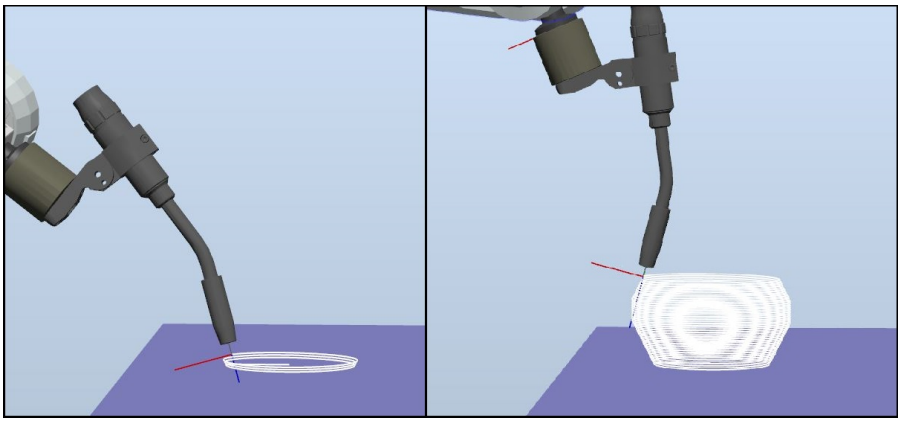

Figure 2.6: **Non-vertical deposition:** Equipment attached to a 6-DOF robot manipulator to deposit material can achieve non-vertical material deposition. This can help build overhangs without needing additional support structures. Simulations were done using the Robot Studio software from ABB.

consuming as very little material is added to the process in each thin layer.

A building method with strictly vertical material deposition is generally unable to build structures with overhangs, so-called 'unsupported geometries' [14], without adding support structures. Unsupported geometries can, in themselves, be quite simple, such as a hollow ball or an arch, and may seem much easier to construct than many other complex geometries that modern AM machines are able to manufacture. For methods such as PBF and VP, smaller overhangs are possible to construct because the component is fully submerged in excess material during the build process, and the fusing or polymerisation can happen horizontally as well as vertically. For extrusion-based AM methods, on the other hand, and other methods which offer benefits such as a higher material deposition rate and less need for excess building material, this is not the case.

While material is deposited directly above the previous layer, any kind of significant overhang requires additional support structures so that the new material can have something to adhere to. This can be understood by studying Fig. 2.4, which shows how the contact surface between layers decreases at steeper angles. Material cannot be deposited onto thin air, so additional support structures are needed for prominent overhangs. Building support structures adds time to the overall building process. In addition,

these support structures must often be removed in post-processing to leave behind the desired shape, which again requires more time and resources. Even if the structure does not, for some reason, require that the support structures be removed, they still represent extra costs in terms of materials and construction time.

If material could instead be deposited in a non-vertical direction, this would greatly expand the range of geometries and structures that can be built. Even though successive layers may not be directly one above the other, it can still be possible for them to adhere to each other when deposited as shown in Fig. 2.6. An industrial 6 DOF robot manipulator can reach a given point in its workspace with an arbitrary orientation of the end effector. If the material extruded through that end effector cures quickly enough to withstand the stresses due to its own weight before reaching a solid state, it will be possible to deposit material non-vertically, as the contact surface is increased as shown in Fig. 2.4. This will not only make it possible to more easily construct geometries with overhangs, but can also remove the need for a strictly horizontal layering approach.

For the preliminary experiments presented in this thesis, tests were done building a small cylindrical cup structure using set-based control and a 6-DOF UR-5 robot arm depicted in Fig. 2.7. This test showed that it was possible to build a structure using a viscous material that was deposited in a non–layer-wise manner: the material was deposited by spiralling the extrusion head upwards along a helix, which sets the method apart from traditional AM. Further details on this experiment can be found in paper A [12]. This is the only build in this thesis that was not done using metals and welding technology, and is an area that needs to be explored further.

2.3 AM using metals and WAAM

This thesis focuses mostly on AM in metals, as this is an important area for industry and manufacturing, as will be further discussed in chapter 4. PBF and powder-based DED are the most-used traditional AM methods for creating metal structures. A great variety of metals can be used to build structures using PBF methods, the most common being stainless steel and tool steels, titanium alloys, nickel alloys, and aluminium alloys, though it is possible to use just about any metal that can be welded [5, pp. 128-130]. These traditional methods are, however, limited to producing smaller components because they are generally so time-consuming. The layers of

Figure 2.7: **Non-layer-wise deposition:** A viscous glue was used in this non–layer-wise build. This preliminary experiment is the only test from this thesis done using material extrusion rather than WAAM, and a 6-DOF UR5 robot from Universal Robots.

deposited materials are thin and, while this allows for a great amount of detail, the deposition rate is relatively low [5, pp. 301–303]. As an example, SLS or DED methods can deposit steel at a rate of 0.1 kg to 1 kg per hour. In comparison, WAAM in the same material can have a deposition rate of 5 kg to 6 kg per hour [15, 16].

Some of the advantages of using WAAM are listed by Williams et al. [17]:

- Low-cost process, cheap robots,
- High deposition rate; can deposit material quickly
- No size limitations, if robot is placed on a track
- Reduces waste of material

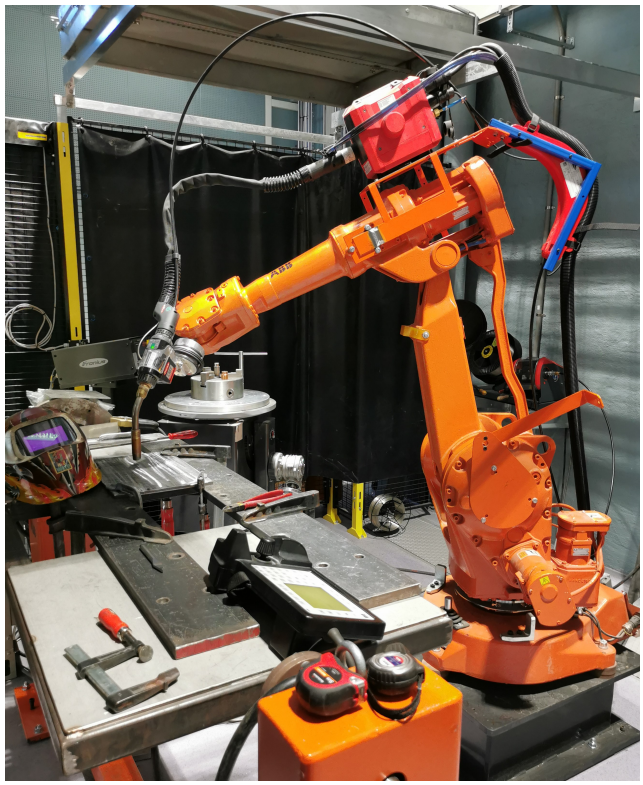

Figure 2.8: **Wire-arc additive manufacturing:** Most of the lab work presented in this thesis was done using this robot cell with a IRB 2400/10 6-DOF robot manipulator from ABB, and Fronius CMT welding equipment.

Most common AM methods are limited to producing small objects because of the enclosed building environment, i.e. the printing chamber of the AM machine. While the machine has to be larger than the component it produces, the benefits of enlarging the machine diminish at a certain point. And, of course, as long as the deposition rate is low, constructing large components will take too long to be practicable.

As explained in section 2.1, the term DED covers a range of AM methods that use an energy beam to melt material as it is being deposited. The arc in a wire–arc welding process can work as such an energy source, motivating the extensive work that has gone into the method known as WAAM. WAAM has grown rapidly in popularity and gained much interest in the industrial manufacturing sector due to its ability to produce large metal

components with a high deposition rate. WAAM can be traced back to the 1920s, when an electric arc was used as the heat source to construct metal decorative ornaments by layered material deposition [18, 19]. The technology has developed gradually from there, and has seen an additional spike in the development over the last decades, which follows the general trend in the use of AM technologies.

WAAM is not restricted by low deposition rates, nor by the size of a printing chamber: combining wire–arc welding equipment with an industrial robot manipulator gives the robot cell a large workspace compared to traditional AM methods. If the robot manipulator is mobile, for example by being installed on a rail or a gantry system, the workspace can be increased even further. The deposition rate is very high compared to PBF or powder-based DED. And, very importantly, the equipment is relatively cheap when considered in a manufacturing setting, and can often be used in other parts of production as well. Both an industrial robot manipulator and welding equipment already exist in many factories, and can often be used for other purposes than WAAM, or can be re-sold if necessary. There are three main types of arc welding, which will be further described in section 3.2: GMAW, GTAW and PAW [18]. The method most commonly used in WAAM, and used in the work presented in this thesis, is GMAW, often referred to only as MIG welding.

In general, building components using WAAM can be more material-efficient, less time-consuming, and environmentally friendlier based on the saving of materials and energy compared to other manufacturing methods. Though all welding faces challenges in its material properties, it has been shown that WAAM samples can have lower porosity, finer micro-structures and higher strength compared to casting when conditioned using post-weld heat treatment [16, 20].

Chapter 3

Arc welding technology

Welding is the joining of two or more parts together by applying heat or pressure. This technology has been utilised in different forms for as long as we have made use of metals such as bronze, iron or gold, and has grown more advanced over time [21]. The technology has evolved especially over the last two centuries, through the significant development and refinement of welding methods following the Industrial Revolution. As of today, over 75 different welding methods, with different advantages and drawbacks, have emerged to meet a growing need for precise and diverse methods for joining metals[22, pp. 3–6]. The common denominator is that all these methods produce a metallic bond between separate pieces of material by exposing them to heat or pressure. The more heat is added, the less need there is for pressure.

3.1 Basic principles for arc welding

This thesis focuses mainly on *arc welding*, which uses heat input from an electric arc to weld metals together. A welding arc is an electric discharge between two electrodes, with a current being conducted through a shielding gas from the electrode to the work-piece. The arc forms initially through dielectric breakdown of the shielding gas, as the electric field between the electrodes pulls the shielding gas atoms apart. This produces ions and free electrons that, accelerated by the electric field, collide with other gas molecules, ionising them to maintain conductive plasma channel – the arc – through the shielding gas.

For traditional welding where separate pieces of metal are joined together, the metal constituting the parts to be joined is called the base metal,

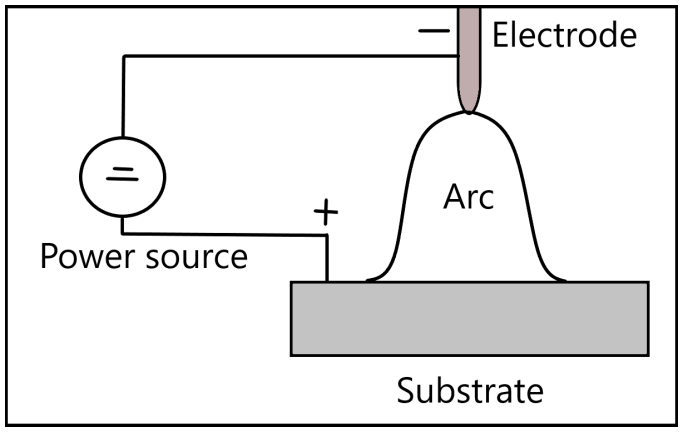

Figure 3.1: **Welding arc:** In this sketch, the consumable electrode is depicted as positive and the substrate is negative, but it can just as well be other way around. Adapted from [24, p. 2.7]

or the substrate. The material added between them during the welding process, such as a welding wire, is called the filler material. The heat input is determined by the amount of electric energy released in the discharge between the electrodes. The heat input controls how much of the substrate and the filler metal melt, and the amount of heat accumulated [23, pp. 6-8]. In arc welding, the heat input is large enough that no extra pressure is required for the metals to bond together. Fig. 3.1 shows the arc between a consumable electrode, i.e. the filler material, and the substrate, which works as the second electrode.

The heated area where base material has melted and can be welded together with the filler metal is called the molten weld pool or molten weld metal, as shown in Fig. 3.4 and Fig. 3.5. The size of this area depends on the heat input, and keeping the size and depth of the weld pool stable is important for determining the outcome of the welding process. A shielding gas protects the electrode, the electrical arc and the weld pool from chemical interaction with the surrounding air. Such gases can be active or inert: an active gas will react with the material in the weld pool and thereby be an active part of the chemical process, while an inert gas will not [23, p. 4-5]. The shielding gas, whether inert or active, must be heated enough to be ionised, in order that it be able to carry the current between the electrodes via its charged particles; different gases require different temperatures for ionisation. This, in turn, impacts upon the heat input to the weld pool.

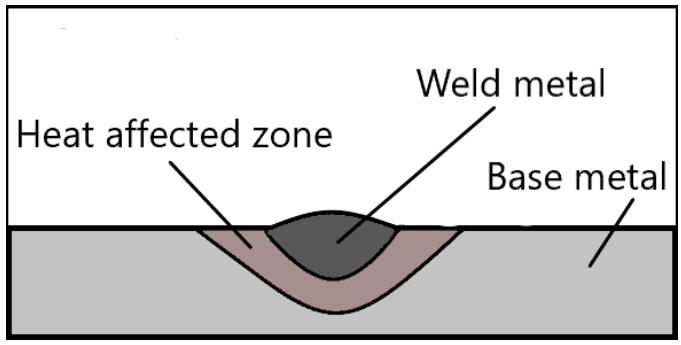

Figure 3.2: **Heat-affected zone:** A cross-section of a welding bead on a substrate. The fully melted metal is called the weld metal and is a combination of melted base metal and filler metal. The heat-affected zone (HAZ) is the area surrounding the welding metal which has not melted, but is still structurally affected by the heat input.

In Fig. 3.2 the cross section of a welding bead on a substrate is shown. The weld metal is the material that has been melted; this will usually be a combination of base material and filler material. The heat-affected zone (HAZ) is material surrounding the weld metal which is affected by the heat, but has not reached the melting point.

Operating variables in arc welding

Several variables control different aspects of the arc welding process. The way these parameters impact upon the welding arc has much to say for the result. The most important parameter are the voltage and current in the welding process, how these are controlled, and how they relate to each other.

The diameter of the weld pool is determined by the current that is added to create the electric charge between the electrodes, as a higher supply current will give a higher heat input at the electrode [22, p. 16]. The welding current is typically somewhere between 100 A and 1000 A [24, p. 2.7]. The voltage is naturally linked to the added current, but not in the classical sense where $U = R \cdot I$, because the welding arc does not work as a Ohmic resistance [24, p. 2.7]. The voltage mainly impacts upon the arc length: the higher the voltage, the higher the arc length, and vice versa.

The wire feed rate also impacts upon the welding process, especially when the wire also functions as a consumable electrode (see section 3.2). As

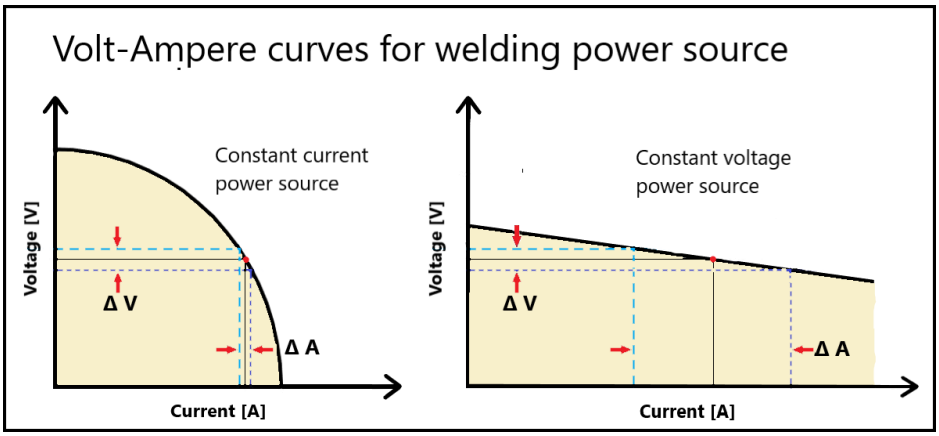

Figure 3.3: **Volt–ampere characteristic curves:** A constant-current supply, with its non-linear volt- ampere curve, can stabilise the current even when the voltage varies somewhat from the target operating point. For a constant- voltage power source, the volt- ampere curve is linear. Depending on the slope of the curve, even a small variation in the voltage can give a significant change in the current. Adapted from [25]

shown in Fig. 3.1, the welding arc stretches between the two electrodes. If the uppermost electrode, i.e. the welding wire, is moved closer to the base material due to an increase in the wire feed rate, the welding arc will shorten. This will, in turn, lower the arc voltage.

How the current, voltage and wire feed are controlled greatly impacts upon the welding process, and different welding approaches can benefit from different control methods. The power sources are generally divided into *constant-voltage* and *constant-current* power sources. As explained, the current, voltage and arc length all impact upon each other. It is therefore possible to choose your main control parameter depending on what type of control is desired for executing the welding procedure.

For example, in manual arc welding, it is not possible to have full control of the arc length: the distance between the end of the welding gun and the surface to be welded will vary throughout the process because a human welder will have some deviations in her movements. When the arc length varies, so will the arc voltage, as these are so closely connected. However, with modern voltage-sensing tecnhiques, it is possible for the power source to adjust the supply voltage to keep the current close to constant, thereby controlling the heat input at the electrode [26]. For these systems, supply voltage

and current are connected in a way so that each current setting results in its own volt–ampere characteristic curve, like those shown in Fig. 3.3: For a constant- current power source, this characteristic is non-linear, as shown to the left. This means that a large change in the voltage will not necessarily lead to a large change in the current, so the welding is kept stable.

On the other hand, automated and robotised welding procedures that are very precisely controlled generally benefit from using a constant-voltage power source. As the arc length does not vary in an unpredictable or sudden way due to close control of both the tool position and the wire feed rate, the system can stabilise the arc based on a constant voltage instead. For a constant-voltage power source, the Volt–Ampere characteristic is linear, as shown to the right in Fig. 3.3. Depending on the slope of the curve, even a small change in voltage can result in a large change in the current [26]. In robotised welding procedures where the surface to be welded and the welding gun are held a fixed distance apart, the voltage is usually kept stable throughout a welding process. Deviations in this distance caused by e.g. an uneven surface can impact upon both the voltage and the current [22, p. 16].

The shielding gas has two main functions: to protect the process from interaction with the surrounding air, and to increase the process's stability, reliability, and quality [23, pp. 49-50]. Inert shielding gases include the helium (He), argon (Ar) and carbon dioxide (CO_2), with helium being particularly costly, and carbon dioxide being cheap but at the practical cost of more spatter. Among the active shielding gases, hydrogen (H_2) is sometimes used for welding austenitic stainless steels, and oxygen (O_2) and nitrogen (N_2) for stabilising the arc [23, p. 19].

3.2 Types of arc welding

Over time, arc welding has become the most important group of welding methods, owing to their wide use in industry [24]. The various kinds of arc welding differ in their characteristics, and hence in their fields of application. The following outline of the most common methods will help us to understand why some kinds of arc welding are more suitable for robotised welding, the focus of this thesis.

Gas tungsten-arc welding

Gas tungsten arc welding (GTAW) uses tungsten or tungsten-alloy electrode separate from the deposited material. This electrode is non-consumable, as tungsten in pure form has a melting point over 3400°C. GTAW welding is also known as *tungsten inert gas* (TIG) welding, mostly using inert shielding gases such as argon and helium. Tungsten *active* gas welding (TAG) also exists, but is not commonly used, and will not be described further in this thesis.

In TIG welding, the electric discharge that comprises the welding arc occurs between the non-consumable electrode and the base metal or welding surface. The added current is usually in the range 20 A to 800 A with regular GTAW equipment [24, p. 3.2]. The arc extends from a tungsten (wolfram) electrode protruding from the mouth of the welding gun, as shown in Fig. 3.4. Shielding gas flows out through the nozzle, enveloping the tungsten electrode. The filler material is added separately, like when using a soldering iron, and angled at the front of the electrode relative to where the welding gun is headed [24, pp. 3.1—3.3]. GTAW welding can be used to weld almost all kinds of metal materials, and the deposition rate for GTAW is typically 1 kg to 2 kg of material per hour.

Plasma arc welding

Plasma arc welding (PAW) also involves a non-consumable electrode and separate feed of filler wire, similarly to GTAW. The mouth of the welding gun is made narrower than in GTAW by adding a nozzle, which concentrates the plasma jet and its power [24, pp. 3.4-3.5]. This leads to an increased heat input when using PAW compared to GTAW, and the deposition rate is typically 2 kg to 4 kg of material per hour [18]. In order to better protect the powerful arc, an extra layer of shielding gas—called plasma gas—is added via an extra mouth piece outside the nozzle that separates the shielding gas and the additional plasma gas, even though these two gases are often the same. One of the drawbacks with PAW is that the equipment is generally very expensive compared to other types of arc welding equipment [26]. The nozzle providing the additional layer of shielding gas also adds bulk to the tip of the welding gun, limiting access to small spaces.

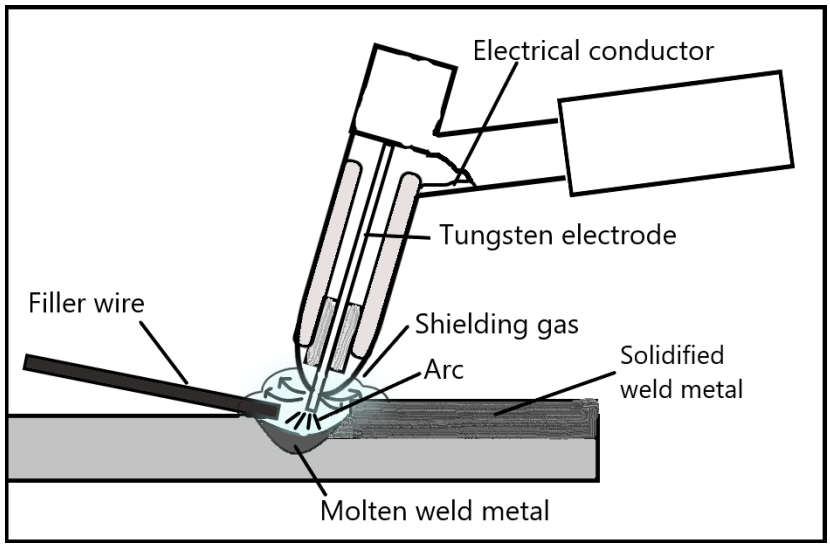

Figure 3.4: **GTAW:** Gas tungsten arc welding, often called TIG- welding from the term 'tungsten inert gas welding'. This process has a non-consumable electrode and a separate filler wire. Adapted from [24, p. 3.1].

Gas metal arc welding

Unlike GTAW and PAW, *gas metal arc welding* (GMAW) has a consumable electrode. The welding wire serves as both filler wire and electrode, as illustrated in Fig. 3.1. The arc burns from the welding thread itself, which is fed continuously through the nozzle of the welding gun, as shown in Fig. 3.5. The shielding gas, electrode and current conductor are all led down through to the nozzle, and, just as for GTAW, the shielding gas covers the electrode. As there are fewer elements involved than in GTAW or PAW, GMAW is often favoured for fully automated welding or WAAM. As the electrode and the consumable filler material are one and the same, there are fewer components to consider when, for example, programming the path for a robot, and less chance of collisions. This makes sense when comparing Fig. 3.4 and Fig.3.5: the latter involves no additional parts to consider when planning the robot's path.

For robotised and fully automated GMAW processes, it is most common to use a constant-voltage power source, as explained in section 3.1. The voltage is typically kept in the range of 20 V to 40 V [22, p. 16]. The average deposition rate is 3 kg to 4 kg of material per hour, depending on the heat

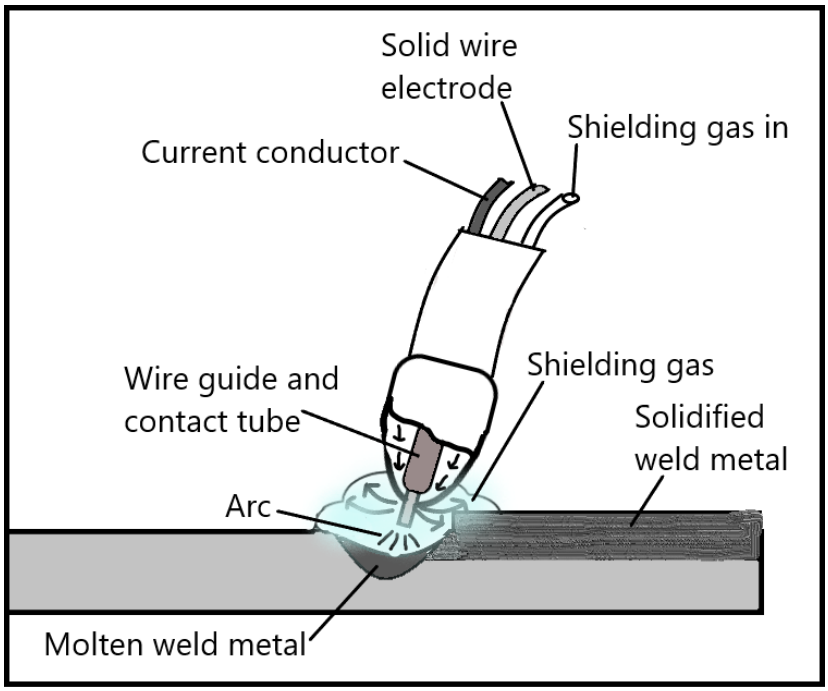

Figure 3.5: **GMAW:** A consumable electrode serves also as the filler wire. Adapted from [24, p.3.6]

input and filler wire material [18]. The method is often referred to as *metal inert gas* (MIG) or *metal active gas* (MAG) welding, depending on whether the shielding gas is inert (e.g. argon or helium) or active (e.g. oxygen or carbon dioxide), i.e. whether it reacts with the molten material.[23, p. 3]. The work presented in this thesis focuses mainly on MIG welding.

There are a few main parameters that affect a MAG/MIG welding process, listed in [23, pp. 19–24]:

- Wire diameter: A thicker wire can carry a higher current, but might also cause feeding problems due to the filler melting into the wire guide and nozzle. This is especially challenging when working with a filler material with a relatively low melting point, such as aluminium.
- Voltage and wire feed rate: Will impact upon both the length of the welding arc and the width of the welding bead.
- Welding speed: How quickly the welding gun and the surface to be

welded move relative to each other. In general, a higher welding speed gives a narrower welding bead, as material is spread out over a greater length, given a constant material deposition rate.

- Inductance or dynamic properties: The inductance of the power source affects the welding properties. This is typically managed by digital control circuits, and will not be addressed further in this thesis.
- Wire stick-out, or electrode extension : How far the consumable electrode sticks out from the nozzle of the welding gun. If this distance is too short, there is a greater chance of the filler metal melting into the wire guide or the nozzle. If the stick-out is too far, stubbing can occur, i.e. longer periods of short-circuiting caused by the welding wire touching the welding surface.
- Choice of shielding gas and gas flow rate: Different welding gases and gas mixtures affect both temperature and other welding arc properties.
- Torch and joint position: The orientation of the nozzle relative to the base metal or welding surface will affect the shape of the welding arc, which, in turn, impacts upon material deposition and arc stability.
- Pulsed wire feed: Affects the deposition rate for CMT welding.

When welding with a consumable electrode, the arc can be classified by how the filler material is transported to the weld pool. For this thesis, it is most important to understand the two most basic transport methods: *short arc welding* and *spray welding*.

Spray arc welding is used only for processes with a relatively high current, normally above 200 A to 250 A. A current this high produces a magnetic field that helps to release a spray of melted material from the electrode surface and directs the droplets down into the welding pool [23, pp. 13–14], as shown to the left in Fig. 3.6. This process avoids short-circuiting, making the welding arc stable and spatter-free, which are highly valued properties for any welding process. If the filler wire is very thin, it is possible to perform spray arc welding at a slightly lower current than 200 A, as the smaller droplets will require less magnetic force to travel the gap between electrodes through the welding arc.

Short arc welding, also referred to as *short-circuiting* arc welding or *dip transfer*, is the most common method when using lower currents. When the current is low, magnetic forces do not push droplets of melted material down into the welding pool, but rather pushes upwards in the welding arc. This

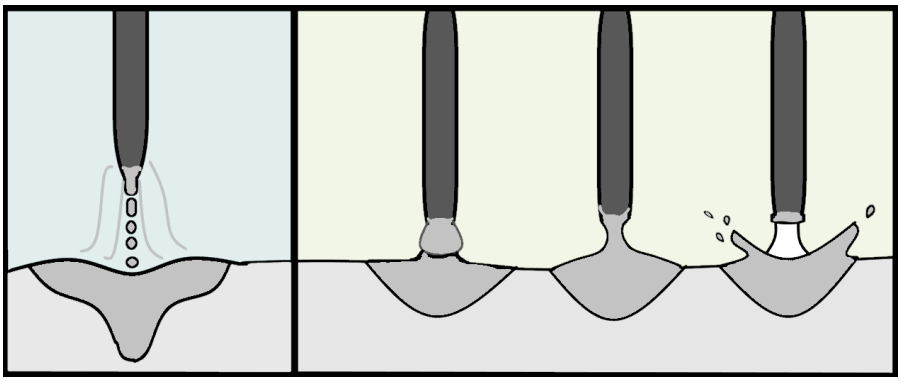

Figure 3.6: **Transfer of filler material:** There are two main arc classifications when using a consumable electrode. Spray arc welding is shown to the left, and the steps of short (-circuiting) arc welding are shown to the right. Adapted from [23, p. 11].

means that the droplet of melted material will not be released immediately, but instead grows in size, which can destabilise the process by affecting the welding arc [23, p. 11]. To prevent the droplet from growing too large, the distance between the consumable electrode and the base or welding surface, i.e. the length of the welding arc, is kept so short that the droplet briefly dips into the welding pool, creating a short circuit. When this happens, surface tension pulls the droplet from the filler wire to the melting bath, and the end of the droplet is eventually pinched off by the magnetic forces at the electrode end. The filler material is hence transferred by direct contact, in contrast to the free droplets used in spray arc welding [23, pp. 11–12]. The steps of short arc welding are shown to the right in Fig. 3.6. If the short-circuit current is too high, the magnetic pinching of the droplet can be affected, causing weld spatter.

In addition to spray arc and short arc transfer, there is *globular* arc welding, which lies somewhere in-between the two. For this method, a larger droplet of molten filler material, i.e. wider than the filler wire, gathers at the end of the feed wire. This droplet is heavy enough for gravity to play a significant role, it is transferred into the weld pool through a combination of gravitation, drag and electromagnetic forces [27]. As the droplet is greatly affected by its weight, this transfer method is generally used only for welding on strictly flat surfaces [26]. Because the molten filler droplet is so large, irregular, and does not necessarily 'fall' straight into the middle of

the welding pool, there is often spattering, though the material deposition rate can be higher than for the other two methods.

Pulsed MAG/MIG

Pulsed MAG/MIG welding can be considered as a fourth transfer mode, or as a modified kind of spray arc welding which uses pulsations in the current. This requires a power source specifically designed to allow for pulsed current control [26, 28]. Spray arc welding gives a more stable arc than short-arc welding, and is generally used with a current range of around 200 A to 250 A [23, p. 13]. Pulsed MAG/MIG uses pulses between 30 Hz to 300 Hz to control the molten filler droplets. The current pulses encourage the formation of small droplets at the end of the welding wire, which move through the arc onto the surface to be welded. This enables greater control over the spray arc welding at lower currents. Pulsed MAG/MIG welding is mainly used for welding stainless steel and aluminium, but can also be used for other materials. Spray welding is both stable and spatter-free compared to short arc welding [23, p. 14, p. 37].

Cold metal transfer

Cold metal transfer (CMT) is a type of short arc MAG/MIG welding invented by the company Fronius [29]. CMT is very stable and spatter-free, even though short arc welding is generally less stable than spray arc welding. This is because of the modified control method: while pulsed MAG/MIG uses a control system to oscillate the current, CMT uses a mechanical oscillation of the filler wire itself. The rate and direction of the wire feed are controlled so that the welding wire oscillates in and out of the welding gun, i.e. towards and away from the surface to be welded [30]. The short circuiting that occurs when the droplet of molten filler material touches the welding surface is detected by process control in the welding equipment, and the filler wire is then immediately retracted. The droplet is thus released, and a gap opened, stopping the short circuiting. This oscillation of the welding wire achieves a more stable short arc welding [31]. The heat input is in the low range of GMAW welding techniques. Consequently, the deposition rate is also slightly lower, about 2 kg to 3 kg of material per hour [18].

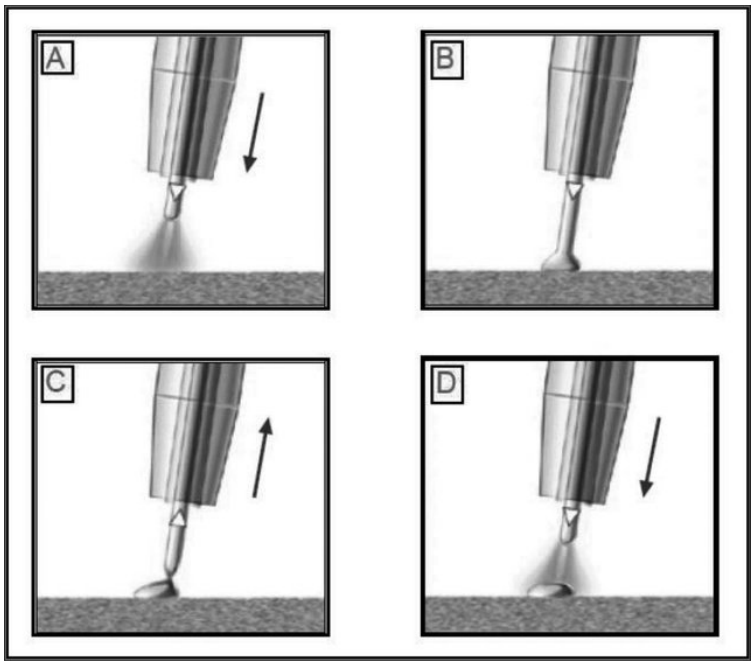

Figure 3.7: **Cold metal transfer:** By oscillating the wire feed, CMT welding achieves a more stable form of short arc welding. When the welding wire is moved close to the surface to be welded, a short circuit occurs. The wire is then retracted, leaving behind a droplet of melted material. Image from[32]/www.Fronius.com, Creative Commons CC BY 4.0.

Chapter 4

Motivation and literature review

The 1980s were the early start for additive manufacturing. Over the decades since then, there has been a boost in the development and use of AM technology. The first commercial systems were available in the 1990s, and were originally based on polymers etc., as the technology was initially focused on prototyping [14]. AM has developed alongside other technologies such as 3D graphics and computer-aided design (CAD), and has numerous benefits when it comes to small series production of three-dimensional parts. The ability for building affordable, small-scale 3D models or prototypes created many new possibilities for developers. The technology has later transitioned from being used solely for prototyping to also producing smaller end products. Gibson et al. (2021) present some of the financial benefits of using AM technology in prototyping and short-run production of components [5, p. 652]:

- If prototypes and end products can be produced in near-net–shape without the need for moulds etc., material consumption could be reduced compared to for example CNC or casting. This will, in turn, lead to lower start-up costs for new and old businesses alike.
- Building structures using AM makes it easier to build them as a whole instead of in pieces that must later be assembled into the composite end product. This can reduce the need for extra equipment or manpower to perform such tasks, and hence the associated financial benefits.
- Having the opportunity to produce components in small runs can re-

lieve businesses of the costs related to the need to store surplus parts, and also avoid the sunk costs of material and time in producing more parts than are presently needed.

An extensive presentation of the most common forms of AM was presented in chapter 2, and researching and writing an early version of section 2.1 was the starting point for the research presented in this thesis. The work on this thesis began at the end of 2016, and as this is a field that is rapidly evolving, much has happened over these last five and half years. The main objective of the thesis is to investigate how robotised AM can be used to extend the areas in which AM could be useful. This include manufacturing structures outside of a restrictive building chamber, and the potential to deposit material non-vertically to construct overhangs without the need for support structures. To fulfil this objective, the following research questions have been identified:

RQ1: *How can a 6 DOF robot manipulator be combined with material deposition to perform AM in order to diverge from many of the standard methods of AM and thus avoid being restricted by a building chamber?*

RQ2: *Can a proof-of-concept build by robot be performed using a building method that is not strictly based on stacking 2D layers of material?*

RQ3: *Is it possible to build thin-walled metal structures in one continuous process using WAAM, thereby avoiding additional issues related to flame-initiation and flame-out?*

RQ4: *When the structure requires intersections within a layer, can an alternative approach using opposing corners to avoid intersections within layers be used on a build with continuous material deposition over several layers?*

RQ5: *Can the suggested framework for set-based control be suited to build a thin-walled, symmetrical structure using WAAM?*

RQ6: *Does freedom in the orientation of the tool significantly affect the build?*

RQ7: *Can an overhang be constructed by depositing material continuously while letting the orientation of the tool follow the tilt of the overhang?*

This chapter will summarise the starting point for the research, the literature that the work presented in each paper is based on, and how the status quo of the AM technologies and research evolved in parallel with this project.

4.1 Robotised AM – proof-of-concept

Based on researching the most common methods for AM, presented in section 2.1, two main challenges was identified: 'In-box' building methods require the AM machine to be larger than the component that is being constructed, which limits the size of the final component, as increasing the size of the AM machine can only be beneficial up to a point. In addition, most methods for AM build up structures strictly layer-by-layer using vertical material deposition, i.e. adding 2D layers onto each other either top-down or bottom-up. This introduces the need for support structures if the build involves overhangs, as material cannot be deposited vertically onto nothing. If material could be deposited at an angle, the contact surface between layer could be increased, allowing to consecutive layers to adhere to each other even at an angle. For a more thorough explanation, see Fig. 2.4 and sections 2.1 and 2.2. The starting point for the work was to perform robotised AM, and to utilise the benefits of this approach, especially considering building large structures.

Paper A [12] includes a literature review conducted at that time investigating the several forms in which other projects were working on realising large-scale or robotised AM. This literature review investigated both projects that built larger structures piece by piece by splitting the final product into smaller parts, such as the 3D Elephant Petition [33], Total Kustom's concrete castle [34], and to some extent the Dragon Bench from Joris Laarman Lab [35].

The 3D Elephant Petition 3D printed a life-sized elephant sculpture over the course of two weeks by combining several 3D printers with an add-on that allowed the printers to move vertically, introducing an additional degree of freedom (DOF) [36]. This use of traditional 3D printers to produce larger structures led to evaluating if a 3D printer head could be used to extrude material while connected to a robot manipulator for some proof-of-concept experiments performed and presented in paper A [12] and section 5.1. The fact that this build also took two full weeks highlights how the high reso-

lution of many off-the-shelf 3D printers also means that they are slow, and that larger builds would take a very long time, and that high resolution or accuracy in many cases must be weighed against efficiency.

The project Total Kustom worked on AM on a much larger scale, using their own apparatus for extruding cement in order to build small houses and other living quarters [34, 37]. As opposed to the high resolution of the structures built in the 3D Elephant project, Total Kustom used a very low resolution material extrusion to deposit large amounts of cement. Another project called Apis Cor had a similar approach: Using their own system for extruding cement, they could build a 38m^2 circular house in approx. 24 hours of machine printing time [38, 39]. In later years, several other companies have followed suit and started their own research into 3D printing of houses, such as the American company ICON who printed a set of 37m^2 homes for the homeless in 2020 [40], the Belgic Kamp C KIEM project which produced their first house in 2020 [41], or the German company Peri who opened their first 3D printed home in 2021 [42].

The work performed by Joris Laarman Lab was especially within the focus area of this research, as they combined robotics with the extrusion of material: Both a fast-curing polymer [43] and metal by laser welding in order to build structures using non-layer-wise material deposition [44]. Their work in metals was focused both on spot welding welding, for example shown in the construction of the dragon bench [35], and continuous arc welding when building the butterfly screen: a 2×3 meter large double curved bronze structure built as a whole [45]. However, as this work is carried out by a commercial actor, their research methods have not been published, and a detailed description of their work is not available. From the time the literature review in paper A was performed, their work has continued developing. A 3D printed metal bridge that were in the planning stages at the end of 2016 has now been built, and more work has been done using CMT and WAAM, culminating in a fully integrated print-on-demand system [46].

Based on the the status of alternative forms of AM investigated, paper A aimed to address **RQ1** and **RQ2** [12].

4.2 Continuous material deposition using WAAM

While mass production of parts and products can bring the cost of manufacturing down, custom-made parts or products are generally costly in comparison. For start-ups and developers, AM is often affordable compared to

other methods for manufacturing custom parts or prototypes. Metal AM is, in general, an interesting field for industry, as metal parts can be costly and time-consuming to manufacture in small quantities. AM can for example be cost-efficient because it saves time in production or in materials: Producing a custom metal component from a large piece of material by grinding it down to its final shape generates a large amount of scrap metal relative to the material cost of the actual component, sometimes as much as 90 %. Although scrap metal can often be recycled, recycling typically results in material of a lower quality than the original block. An alternative manufacturing method can be to cast the structure, which might save materials compared to machining a large block of material down to a smaller component. However, developing a custom mould is, in itself, costly and time consuming, and it might not be worthwhile to produce only a few components.

Performing AM in metal is therefore a field with much interest from industry, including the industry consortium in SFI Manufacturing, which this PhD project has been a part of. The scope of this work was therefore narrowed down from working with deposition of any kind of material using robotics, to focusing on constructing *metal structures*. A demonstrated by Laarman Lab, AM in metal could be done using welding equipment [44, 45]. A thorough presentation of different welding technologies were presented in chapter 3, highlighting the main differences, advantages and drawbacks for using different methods, and section 2.3 described how WAAM can be used. Much of the work presented in this thesis concerns metals and welding technology. The hope is that metal AM can eventually help both to enable the manufacturing of components on demand, and also to perform repair work on existing components on site. Based on the research done on welding method presented in chapter 3, CMT was chosen as the preferred welding method, as it is considered very stable and spatter-free [31]. A closer description of how the method work, and how it compares to other types of arc-welding, is found in section 3.2.

Though the work presented in paper A [12] investigate how material can be deposited in a manner that is not based on layers, a layer-based approach can be easy when planning the build of a structure. The work in paper A showed that there were challenges related to the starting and stopping of material flow when working with material extrusion. As reported by [47], flame and initiation and flame-out in welding processes also tend to lead to uneven material deposition. Therefore, it could be beneficial to keep the build going as continuously as possible, which would also be more efficient. How the transition between layers happened might make a difference to

how the structure turns out, and be essential if the aim is to keep the build going as continuously as possible. Investigating how a build of thin-walled structure would react to a continuous building process was deemed a good starting point for further work.

One challenge that can arise when building thin walled structures using any kind of material deposition is how to deal with intersections within the same layer [48]. While a continuous path might be ideal in order to avoid issues related to flame initiation and flame-out [47], intersections in a robot's path within one layer while continuously depositing material will lead to double material deposition. One solution to this could be to adjust the process to make the tool deposit less material at the point of intersection, though this would require very finely tuned welding parameters. However, an alternative approach was suggested by [49]: Replacing the actual intersections with opposing corners, and ensuring that these corners were close enough together to properly melt together. This had not been done for longer, continuous builds, so whether this method with opposing corners could be combined with continuous material deposition constructing a thin-walled structure became the objective for the next work, and paper B aimed to address **RQ3** and **RQ4** [50].

4.3 Set-based control framework used in WAAM

Based on the overview of AM methods given in section 2.1, one of the benefits of using a 6 DOF manipulator to deposit material was found to be the ability to deposit material at an angle, in addition to building larger structures without being restricted by a chamber. A 6 DOF robot manipulator's end effector has the ability to reach any given point within the robot's workspace at an arbitrary orientation. For vertical material deposition, additional support structures are needed when constructing overhangs, i.e. parts of the structure that sticks out over a lower part of the structure without being supported by an preceding layer in a directly vertical direction. This indicated more materials, and a longer build time, and if the overhangs are significant for the final structure, these support structure must also be removed in post-processing [51].

By depositing fast-curing material at an angle, it could be possible to bypass this restriction, as demonstrated by Laarman Lab amongst others [43, 44, 52], described in section 4.1. This could for example be done by moving a *mobile building surface* around a fixed point of material de-

position, which at this time seemed to be the dominant approach in new research. This had been done using both plastics and metals [53, 54], though for structures at a relatively small scale. As a fixed point of material deposition would make the build less vulnerable to effects of the gravitational pull, this approach makes sense as a starting point for such research. However, as explained in section 4.1, AM in metal could be very helpful for repair work on for example ships or other constructions that cannot easily be moved, if the technology matured enough. In such events, a tool working onto a fixed, un-moving surface would be closer to a realistic scenario. This had been examined by Xiong et al. [55], using arc-welding to build metal walls with overhang on a fixed, horizontal surface. However, this was done while keeping a *fixed vertical* orientation of the torch in a AM apparatus, not using a robot manipulator or utilising a robot manipulator's flexibility to change the orientation of the tool. Another project, Kazanas et al. [56], had indeed used WAAM with non-vertical orientation of the tool to construct small, tilted wall structures. However, this had not been done during continuous builds over time, a scenario which would likely present a new set of challenges related to how the material would set on the building surface, as heat accumulation would keep the metal at a liquid stage for longer. As an approach utilising a 6 DOF robot manipulator's flexibility did not seem to be broadly investigated by actors publishing their scientific methods, building structure onto a fixed substrate using a tilted tool for material deposition became the main objective for further work.

As is further elaborated on in section 5.1, the experiments carried out in paper A were performed using a framework for set-based control developed by S. Moe, a co-supervisor for this thesis, and co-author of paper A, C and D [12, 57, 58]. Inspired by how this control method had been used to optimise spray painting in [59], the work presented in paper C focused on whether this approach could be transferred to building a thin-walled structure using WAAM. Not relying on a strictly fixed orientation of the welding gun expands the available work-space of the robot, and can help avoid obstacles in an industry or factory setting, be it external obstacles or parts of the ongoing build. A brief introduction to set-based control is given here, as not all readers of this cross-disciplinary thesis are necessarily familiar with this control method.

A robot manipulator consists of a set of joints and links: The links are the solid parts of the robot arm, and the joints are where the links meet and move relative to each other. Calculating the position of the end effector, based on knowing the characteristics and positions of each of these joints, is called

forward kinematics or *direct kinematics*. Calculation the forward kinematics can almost be compared to following a map: If you know where you start, how far you move in a given direction, and how you change direction relative to where you were going, you can calculate where you are going to end up without much difficulty. For robot control, the problem is typically the opposite: you know where you need effector of the robot arm to end up, and you know the dimensions of the joints. Then you need to calculate the necessary values in the joint space for the robot to realise this command. This calculation is called *inverse kinematics*, and is much more complicated than forward kinematics because there are often multiple valid solutions. In fact, the more joints, or DOFs, the robot has, the more solutions there are.

Parts of the robot control presented in this thesis use built-in functions from the RAPID programming language produced by ABB Robotics [60]. When such commands are used, the robot control system registers the specific, desired positions and orientations, and then performs the necessary inverse kinematics calculations for us. This is of course very helpful, but it also takes away some control over the robot's path and the process. Depending on the application, there is a risk that the calculations will take too long compared to how promptly, and how quickly, the end effector should undertake its manoeuvre. This was not a prominent problem for any of the experiments presented here, but it was one of the reasons to investigate alternatives to the RAPID commands, such as set-based control.

Control of a robot manipulator usually happens in the joint space, which means that specific positions and velocities are calculated for each of the robot manipulator's joints. The desired trajectory for the end effector of the robotic system is typically described in Cartesian space, and the trajectory needs to be mapped to a reference trajectory in the joint space [61]. Some of the robot control presented in this thesis is done using *set-based* control. This was done using a framework which had proved to work well for robotic systems with a large number of DOFs and, thus, numerous tasks that need to be solved. Set-based control is a kinematic control framework which calculates reference states based on the desired behaviour and the current state of the system. It combines set-based tasks defined by a valid interval with equality tasks defined by a desired value. An equality constraint is a constraint on the movements of the robot determined by a value having to be as close as possible to the value set for the equality constraint. A set-based constraint means that a certain variable has to stay within a given set of values. In other words, there can be one condition that must be followed precisely, such as position control of the end effector, presented by the equality

constraint, and, at the same time, a set-based task that must be followed, such as collision avoidance. A full description of the framework can be found in [59, 61].

Paper C aimed to address research question **RQ5** and **RQ6** [57], and a detailed description of the experiment carried out in paper C is found in section 5.3.

4.4 Building structures with overhang onto fixed substrate

At this point, the focus of the work had reached how non-vertical, non-layer-wise deposition of material can help build structures with overhangs by depositing the material with a moving tool. Similar work has been done on AM processes by moving a *mobile building surface* around a fixed point of material deposition. This has been done using both plastics and metals [53, 54]. This work shows promise, and should also be examined further. However, based on the research gap regarding continuous deposition of material onto a fixed surface using a non-vertical tool described in section 4.3, this was the direction in which this work should go. Also, fixed surfaces are closer to a real industry settings: If such technology, in time, is to be used for repair works on-site on ships or in factories, it is essential that the material deposition can be performed on a structure or surface that is fixed. When using a robot manipulator with an end effector that can reach any point within its workspace in an arbitrary orientation, moving and reorienting the tool will generally give more flexibility than having to move the structure under construction.

The framework for set-based control that was presented in section 4.3 and tested for WAAM in paper C [57] did not work as well with WAAM as it had with the work on spray-painting presented in [59]. It was therefore not the focus for further work, see section 5.3 for full details. At this point in the research, AM technology had come further than in 2016. Still, there limitations for the most widespread methods of AM remained much the same. Depending on the AM method, the challenges can vary from issues such as long build time or high cost [62] to issues related to structural challenges such as residual stresses or porosity within the final structure [63]. Though many path planning strategies for layer-based AM exist, layers are generally applied directly on top of each other in order to allow each now layer to be vertically attached to the previous layer [64].

Based on there still not being many available sources to work done on non-vertical material deposition onto a fixed substrate, this was to be the objective for the work carried out and presented in paper D [58]. Following the approach in [55], one structure with overhang were to be constructed onto a fixed, horizontal surface while keeping the orientation of the tool fixed as well. Material analyses of this structure were to be tested to assess the impact of the overhang compared to other parts of the structure. In addition, the objective was to construct similar structures with overhang using a non-vertical orientation of the tool to deposit material. While similar work had been done on simple wall structures in [56], as mentioned in section 4.3, these new builds would attempt to do this on a larger scale, building a complete, thin-walled structure with continuous material deposition. This would be very different than building a small wall due to the continuous heat accumulation in the build. Paper D aimed to address research question **RQ7** [58].

4.5 AM technology today — what now?

In paper A, the state of the art in large-scale AM is presented, introducing several projects that have begun working on both large-scale AM and AM using non-vertical material deposition [12]. This paper is from 2017, and as this is a rapidly evolving field, much has happened in the following years, in parallel with the work presented in this thesis. What follows is a brief outline of some similar work that has been done in the past few years focusing on metal AM and WAAM. This is not a full state-of-the art mapping, but gives some insight into the situation as of 2021.

One of the industries that have embraced the rapidly evolving metal AM technology is aviation. Producing parts for use in aircraft carries very particular challenges related to the products' structural properties and robustness. Still, some projects have come far in utilising this new technology in order to drastically lower the cost of production of, for example, titanium parts. One of these companies is Norsk Titanium [65]. Titanium's high strength makes it suitable for aerospace, but it is an expensive metal, often costing over 10 times the more common materials such as stainless steel. Saving material in the building process is, therefore, an important way to save money in production. In addition, additively building near net-shape structures can be a significantly more effective way of producing components than milling down a solid block of material or using thin-layer methods such as powder-based

Figure 4.1: **Norsk Titanium:** By building components that are near net-shape using Rapid Plasma Deposition (RPD) it is possible to save both construction time and materials. This is very beneficial when working with titanium, which is a relatively expensive building material. Photo: www.Norsktitanium.com [65]

systems.

The Norway-based company has developed its own patented technology called Rapid Plasma Deposition (RPD), where titanium is deposited layer by layer. This AM technique combines wire feeding with plasma welding, and operates with a high deposition rate and thicker wall width than most competing AM methods, and is also believed to produce fewer defects in the final structure [47, 66]. Norsk Titanium manufactures components that are near net-shape using RPD, which means that these components require little machining and post-processing to reach the desired design, as shown in Fig. 4.1. The components can be up to $900 \times 600 \times 300$ mm^3, and as each layer is approximately 3 mm to 4 mm thick, the deposition rate is about 5 kg to 10 kg per hour [65], which is quicker than many WAAM methods. From 2018, Norsk Titanium has been on Boeing's list of certified producers for the aerospace company's 3D-printed parts used in 787 Dreamliners.

The challenges of producing precisely shaped intersections and sharp edges in WAAM structures during layer by layer welding has also been investigated by, among others, Gudeljevic and Klein[67]. Their experiments were performed using CMT and continuous vertical material deposition, using an aluminium alloy as welding material. They used an adapted deposition

strategy to create smooth intersections. By manipulating the energy input from the welding equipment when the path reached intersections, the shape of the welding bead could be locally flattened by increasing the heat input. This solution should be investigated further, preferably in combination with a surveillance system with feedback for the building process.

Structures with overhangs have been explored by many projects, often focusing on material deposition from a fixed point onto a moving substrate. One example is a project using micro- laser wire deposition (µLMWD), successfully constructing overhangs with relatively sharp angles[68]. The technique was demonstrated on components only a few centimetres tall, however. Depositing the material from a fixed point onto a moving substrate or component, enables the increased contact surface described in Fig. 2.4 while keeping the material from excessive deformation under its own weight. Thus, such methods are more predictable than the the non-vertical approach presented in this thesis. However, as explained in sec. 4.3, the focus of this thesis is material deposition onto a fixed surface, as this approach might be very useful in repair work on larger and otherwise immobile structures once the technology matures.

Other projects have focused on large-scale applications of non-vertical material deposition onto a fixed surface. For example, the Relativity Space project has created what they call the world's largest 3D-printer, applying WAAM combined with a rotary table to construct a large cylindrical fuel tank [69]. Their aim is to construct a rocket with over 90 % of its parts made by AM. In 2021, their single-structure building efforts had achieved a 6.75 m tall aluminium tank with a diameter of 3 m [70]. This project also shows that overhangs can also be constructed using WAAM and a rotary table, the table reducing the movements demands upon the robot, which helps to keep the welding arc stable. The same project uses PBF direct metal laser sintering (DMLS) to build smaller parts, and hence illustrates how different AM methods can combined to build complex structures with a combination of parts. The work of the Joris Laarman Lab has also continued on from the work presented in paper A [12]: The bridge that was in its planning phase in that paper has since been printed, and more work has been done using CMT and WAAM, culminating in a market-ready, fully integrated print-on-demand system [46].

In summary, AM technology is on the rise, and many industries are interested for many reasons: AM can help to speed up production of custom parts, which is benefits both prototyping and short-run production; it can reduce costs associated with excess materials, which is especially important

for expensive materials such as titanium; it can reduce both material waste and energy use, benefiting the company's finances and the environment.

Chapter 5

Summary of publications

In this thesis, the work is presented in four published papers. These papers follow each other chronologically in conceptual advancement and methodology. This chapter will give a brief summary of the methodology and results provided by each of these papers. By highlighting which research question (descriped in chapter 4) each paper aimed to answer, this chapter show how the research progressed from a literature review and proof-of-concept experiments over to WAAM and building structures with overhang.

5.1 Additive manufacturing by robot manipulator: An overview of the state-of-the-art and proof-of-concept results

In order to outline the direction of the work of this thesis, paper A [12] presents a literature review that gives an overview of the state-of-the-art of AM by robot as of February 2017. As AM technology has evolved over the last decades, it has become an increasingly important part of prototyping, and development of new devices. The principles of building a 3D structure using for example material deposition has also been utilised on a much larger scales, constructing sculptures and even buildings. The problem addressed in paper A is whether material could be deposited using a robot arm, moving the process away from the 'in-box' methods of many of the existing and widely used AM methods, the argument being that this will remove the need for a AM machine larger than the structure that is being built (**RQ1**).

In addition to depositing material using a robot manipulator, it was desired to build a structure using a path that was not strictly layer by

layer (**RQ2**). Many widely used AM methods are based on building one 2D layer at a time, then moving straight up or down, and constructing a new 2D layer (see section 2.1). When manufacturing a structure using this approach, there are limitations to the geometries that can be constructed, especially when considering overhangs. Making the build more continuous would also be beneficial if the aim is to build larger structure. It this point in time, Joris Laarman Lab had already produced very promising results on this kind of work using a fast-curing polymers [43], but none of their algorithms or methods had been made public.

A proof-of-concept experiment was designed to map how a viscous material (STP Quickfast) with dynamic viscosity of 3.200.000 mPa·s at 25° could be used to build a cylindrical cup-structure in a continuous, non-layer-wise movement. An air-pressure drive caulking gun was connected in parallel to the end effector of a 6 DOF UR-5 robot arm. This material was deemed a good choice for a small-scale initial experiment because the materials available for the caulking gun generally had a higher velocity than for example liquid glue from a glue gun, which was one of the other options considered.

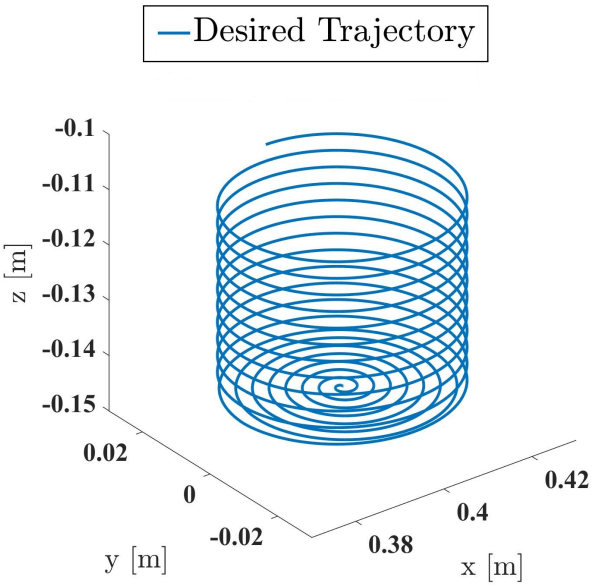

Figure 5.1: **Planned path:** A plot of the desired, continuous path of the robot's end effector. The path creates a cylindrical structure with diameter of 4 cm.

As this was meant only as a proof-of-concept build, optimising the choice of material was not a goal in itself. Compressed air was connected to the caulking gun by manually opening and closing a vent while the robot was moving along its path, thereby controlling the material flow. The structure to be built was a small cylindrical cup with bottom with a diameter of 4 cm. The simulated trajectory is shown in Fig. 5.1, and with its continuously upwards spiralling path, this deviates from strictly layer-wise methods.

The path was programmed using a framework for set-based control developed by co-author of paper A, S. Moe. An outline of the principles behind set-based control is found in section 4.3, and full details on the control method can be found in [59, 61]. In short, it combines conditions that must be followed precisely with conditions that can be followed more loosely. Tn future experiments, there could be some freedom in the orientation of the tool, not necessarily staying strictly vertical onto the building surface. This is examined further in paper C, see section 5.3. For the work in paper A, both the path and the orientation of the tool had to be followed precisely, thereby removing the set-based part of the control scheme by setting the set to be a single value instead of an interval.

Several small cup structures were built using continuous material deposition during these initial experiments, highlighting some of the challenges that had to be addressed in future work. The experiments showed that material deposition by robot using a path that was not strictly layer-wise was indeed possible. However, there were challenges related to the starting and stopping of material flow, as well as the stability of the structure compared to the contact surface between each strip of deposited material and the surface it was deposited onto. If more experiments were to be performed using the same material, it might be necessary to change the geometry of the nozzle in order to build wider layers, increasing the contact surface. The challenges related to the starting and stopping of material flow underlined the benefits of keeping a build as continuous as possible, which would also help shorten the build time.

5.2 Wire-arc additive manufacturing by robot manipulator: Towards creating complex geometries.

Many different materials can be used in AM, but constructing metal structures could be especially useful in a variety of industries: As post-processing

of metal structures is generally required even when using relatively quick methods such as casting, this reduces the required resolution of the build, which would lower the build time. As addressed in chapter 4, building end products using AM could also be beneficial when considering building custom-made parts or products, or parts that need to be produced in a low number. Machining a structure down from a larger block of metal can be an alternative, but depending on the metal, this can be costly in terms of excess materials. In the long term, the notion is that such technology could also be applied in repair work on for example ships or other structures that would benefit from on-site repairs.

Paper B [50] addresses how thin-walled structures can be built by WAAM, and which challenges need to be solved in order to perform effective manufacturing of such structures. Based on the experience from the initial experiments performed in paper A [12], it seemed that the starting and stopping of material flow could be a challenge when working with viscous materials such as glue. Whether these challenges were as prominent when working material deposition by arc-welding was therefore also of interest in these next experiments. As reported by [47], flame and initiation and flame-out tend to lead to uneven material deposition. An objective for these experiments was therefore to assess if it was possible to keep the welding process going as continuously as possible without the structure getting so hot that the accumulated heat lead to deformations (**RQ3**). Both a directly layer-based approach and an approach with a smoother transition between horizontal layers was tested for thin-walled structures. In addition, a structure with intersections was constructed, as shown in Fig. 5.3, testing how intersections can be created through opposite corners in a continuous build, as this method had been demonstrated on shorter builds by [49]. One objective was to see if this approach could be combined with a longer, continuous build, or if the accumulated heat would cause issues (**RQ4**).

The modified arc-welding method CMT is considered to be well suited for WAAM because it has a more stable arc than other types of arc welding, as examined in section 3.2. It also has a reduced heat-input which reduces residual stresses and distortions, and the stable arc reduces splattering [71]. Therefore, most of the builds presented in this paper, and in this thesis in general, are done using CMT, the exception being when the required heat input was too high for CMT, in which case pulsed MIG was used. The experimental set-up was changed to a 6 DOF ABB 2400/10 robot manipulator equipped with Fronius TPS 400i CMT welding equipment, as shown in Fig. 2.8. As the main objective of the experiments presented in paper B was

to examine the feasibility of building thin-wall structures using continuous WAAM, the choice of material was partly based on availability. Aluminium alloys were used for most of the builds, as this was an easily available material with a low cost. It became evident that some of the tests needed to be done using a material with a higher melting point, and the nickel-based alloy Inconel 625 was chosen, again partly based on availability. The objective here was to compare the end product when using materials that would react differently to accumulated heat, so these materials were deemed suitable.

The path for the robot manipulator was performed using the high-level programming language RAPID for ABB robots: The build in functions for moving in straight lines and half circles was sufficient for programming the paths for the thin-walled structures, as they were either simple rectangular or circular shapes, as shown in Fig. 5.2, or in the case of the structure with intersections shown in Fig. 5.3, a combination of these. See paper B for a more detailed descriptions and figures of the structures [50]. In order to keep the weld as continuous as possible, a smoother transition between layers of the structure spread over a few centimetres was compared to a straight, vertical movement at the end of a layer. Parts of the welding parameters, as well as the arc initiation and flame-out were controlled by RAPID functions, while the welding method, i.e. CMT, as well as the added voltage was controlled manually by a welding technician during the build. Full details

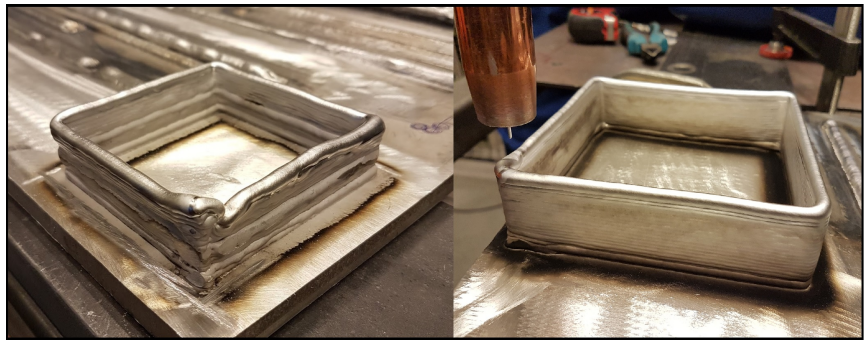

Figure 5.2: **Transition between layers:** As can be seen in the front-most corner of the structure to the left, a vertical movement of the welding gun in a single point causes deformations because the material flow is continuous, thereby depositing more material in this point than in the rest of the layer. In the structure to the right, this vertical movement is spread over 2 cm, removing the issue. More details are found in paper B [50].

on the welding parameters are found in paper B [50].

For all the builds, the first couple of layers had to be done using pulsed MIG, as this welding methods allowed for a larger heat-input. This was necessary because the substrates used were so thick that the deposited material did not adhere properly to the substrate at lower heat inputs. This makes sense for aluminium despite its relatively low melting point, because aluminium has a very low heat-emission to air and dissipates heat almost solely through conduction [72]. This means that the heat from the deposited material would very quickly spread throughout the substrate, cooling the deposited material too quickly for it to adhere properly to the substrate. As the substrate and the already welded material reached a high enough temperature due to heat accumulation, the welding method could be switched back to CMT. Detailed tables listing all relevant welding parameters for the different builds are found in paper B [50], and will not be discussed further here.

For the circular and rectangular structures built in aluminium alloys AA4043 and AA4047, the build could go on continuously with out any sign of the structure heating up enough to cause deformation. The builds were not stopped because there were any issues, but rather because the build had gone on for a long time with no sign of unwanted changes, and having to consider material costs in the experiments. Some of these final structures were 12-15 cm tall, i.e. much taller than the structures shown in Fig. 5.2. See paper B for details and images of these structures [50]. The results of these experiments indicated that continuous WAAM showed promise when building thin-walled structures. With very simple rectangular or circular structures, it was possible to build smooth structures even using a material with a relatively low melting point, such as the aluminium alloys used: The heat dissipation and heat accumulation would reach an equilibrium at a temperature low enough that the structure did not show deformations (**RQ3**).

However, for structures with intersections created by opposite corners, the structure would get clear deformations when building in the aluminium alloys. This was determined to be caused by uneven heat dissipation, and the intersections becoming areas of heat accumulation due to the thigh thermal conduction of aluminium. Another build was therefor done using the nickel-based alloy Inconel 625. This structure was built only using pulsed MIG, as the nickel-based alloy required a higher heat-input for the entire build than the aluminium alloys because of the higher melting point and the higher thermal emissivity to air [73]. For the Inconel 625 build, the intersections

Figure 5.3: **Intersections:** One of the structures with intersections after post processing, showing that the opposing corners have melted together [50].

were no longer problematic, and as can be see on the resulting structure after post-processing, shown in Fig. 5.3, the intersections would melt together completely. Another attempt to build the intersection structure in the aluminium alloy AA4043 was performed after seeing that it was possible using Inconel 625, this time using pulsed MIG instead of CMT. While CMT oscillates the filler wire itself, pulsed MIG uses pulsed current control, suing pulses to control the molten filler droplets [26, 28], allowing for a more controlled weld at higher currents than CMT. With a generally higher input, the idea was that this might lead to a more even heat distribution, making the challenges around the intersections less prominent. While this approach led to structures that were slightly less deformed than those performed using CMT, the intersections still became areas of heat accumulation, and the lower melting point of the aluminium alloy compared to the nickel alloy led to significant deformations.

The conclusion to these experiments was that the approach presented by [49] to create intersections within a layer by having a path with opposing corners can indeed be used for continuous builds, given that the building material has properties that makes it resistant to uneven heat distribution (**RQ4**). Comparing a gradual transition between layers to a vertical movement in a single point showed that the gradual transition gives a much

smoother result, while the vertical movement in a single point leads to deformations caused by the continuous material deposition, as can be seen in Fig. 5.2. It is important to note that the difference between the two structures in Fig. 5.2 is also better adjusted welding parameters, as the smooth structure to the right was built after the structure to the left showing many deformations. However, the issues shown at the front-most corner caused by the vertical layer transition in a single point would still have been there with better suited welding parameters, though less prominent.

At this point in the thesis, material analysis was not a focus, but investigating the material properties is of course important in order to decide if this is a promising method for producing end products or parts. Therefore, material analyses were later performed on one of the nickel-alloy structures with intersections to consider the properties of the materials in the intersection areas compared to other parts of the structure – see the presentation of paper D in section 5.4.

5.3 Robotised wire-arc additive manufacturing using set-based control: Experimental results

As presented in section 2.2, there are several benefits of combining material deposition with a 6 DOF robot manipulator. The first is moving the AM process away from a restricted building chamber, as is a necessity for many of the AM methods described in section 2.1. By avoiding a building chamber, the AM apparatus does not have to be larger than the structure being built, so with the large workspace of an industry size robot manipulator it is possible to build much larger structures. Though the structures built in the experiments from paper A [12] and B [50] were not very large, this set-up does have the potential for building large structures, and continuous material deposition by WAAM of thin-walled structures have been investigated (**RQ3**). The next step was to try to exploit the other great benefit of doing AM using a 6 DOF robot manipulator: The flexibility in the orientation of the end effector or tool.

The objective of paper C [57] was to build a similar thin-walled structure like those built in the experiments from paper B, but with some flexibility in the orientation of the tool. As explained in section 2.2, a 6 DOF robot can reach any point withing its workspace with an arbitrary orientation of the end effector. The notion investigated here is that the flexibility of the robot manipulator could be used to increase the flexibility of the building

process, the objective being to see how freedom in the orientation of the tool would impact the build (**RQ6**). This was done using the set-based control framework developed by co-author S. Moe, which had also been used in the experiments presented in paper A [12]. The principles behind set-based control is presented in section 4.3, and full details can be found in [59, 61]. Summarised, the set-based control framework combines strict equality constraints that must be followed precisely, such as a path, with a set-based constraints that can have some slack, for example the orientation of the tool. Using set-based control with some deviation in the orientation of the tool helps make the robot movements smoother and less demanding for the robot and may reduce the required torques, as it enables a smoother trajectory for the tool. Inspired by how this framework had been used to optimise spray painting, see [59], the aim was to investigate if this approach could be transferred to arc-welding (**RQ5**).

The experimental set-up was the same as for the experiments presented in section 5.2, i.e. a 6DOF IRB2400/10 ABB robot manipulator equipped with Fronius TPS 400i CMT welding equipment. The path was this time planned using the framework for set-based control, which generated a list of joint configurations that was then sent to the robot using the RAPID

Figure 5.4: **Set-based control:** The resulting structure built using set-based control that allowed for a slack in the orientation of the welding gun of 6°. The structure ended up having a saddle form, likely caused by the difference in gravitational pull on the deposited material, as the deviation in orientation of the welding gun was not symmetrically distributed.

function for joint control. When using joint control, RAPID did not have functions for giving commands to the welding equipment, meaning that for these experiments the welding equipment was fully controlled by the operator, even the arc initiation and flame-out, wire feed speed etc. This did not lead to a great difference when carrying out the experiment, except from a less smooth starting and stopping point of the weld, as a manual operator could not time this perfectly. Further details on this are found in paper C [57].

The structure built was a cylinder consisting of a outwards spiralling bottom layer, and walls that were an upwards spiralling helix, similar to the structure from paper A [12] shown in Fig. 5.1. This time the structure was much larger, with a radius of 60 mm, and the slack in orientation of the tool was set to 6°. The resulting structure is shown in Fig. 5.4. While the outwards spiralling bottom layer was surprisingly smooth, indicating that the welding parameters for this part of the build worked very well, the walls ended up with what looked like a saddle form. This was most likely caused by the difference in orientation of the welding gun: As shown in Fig. 5.5, the angle oscillated between 6° and closer to 0° from a strictly vertical orientation. Because of the position of the build relative to the robot, one side of the structure had the welding gun at an almost vertical orientation, i.e. a deviation from a vertical position of 0°, while the opposite side of the build had the small tilt of 6° relative to a vertical position. As gravity works on the liquid metal during deposition [55], this difference created a significant deformation to the structure that would have been avoided if there was a symmetrical distribution of the deviation in angle (**RQ6**).

This saddle form did not become very prominent until the build had gone on for a while, i.e. approx. 20+ layers. This was likely partly because the error would accumulate over time, and was not clearly visible until it had accumulated over several layers. In addition, the error would become more prominent as the structure grew hotter, because the aluminium would take longer to solidify. As it stayed liquid for longer, the difference in gravitational pull would have a stronger impact, and the error would grow in prominence. As explained, this research focused on continuous builds as a way to both reduce the building time and minimise the issues related to flame initiation and flame-out. However, in an attempt to prevent the structure from getting too hot and the error accumulating, active cooling of the aluminium build during pauses in the building process was tested. This was done by blowing cold air onto the structure to cool it down several times during the build – see the tables in paper C for a details on exactly when air-cooling was

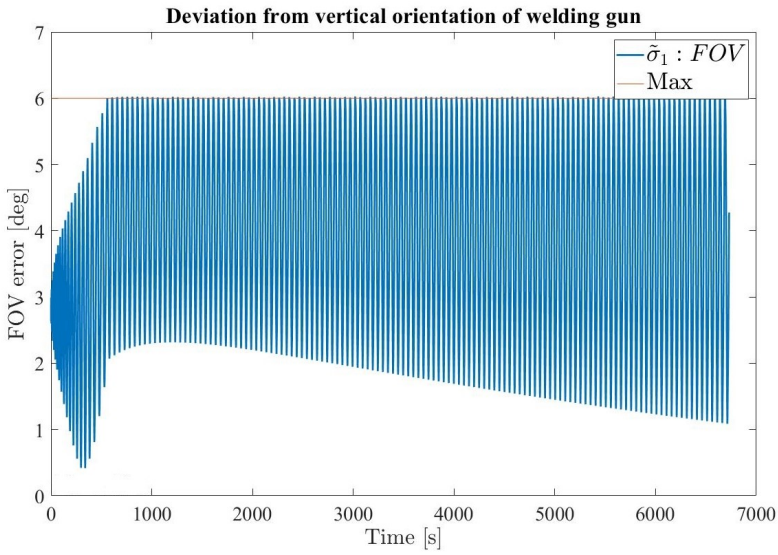

Figure 5.5: **Orientation of welding gun:** This plot shows how the orientation of the tool deviated from a strictly vertical position over time, oscillating between 6° and closer to 2°, resulting in a difference in orientation of the tool for two opposite sides of the structure. Further information is found in [58].

applied in each build. This did seem to halter the accumulation of the error, but the saddle form would return as soon as the structure grew hot again. This indicated that continuous cooling of the structure could be a solution to such challenges. However, this was not investigated further, as the focus of this thesis was continuous builds (**RQ3**).

Based on the results from these experiments, it was concluded that if the orientation of the welding gun could be more evenly distributed around a centre point, the method would be more useful, as the gravitational pull on the liquid metal would be more evenly spread out over a circular path. While this would still only benefit symmetrical structures, and this control method might not be the best way to proceed, as the main motivation of the set-based control methods is to prioritise the ease of the joint configurations (**RQ5**). Therefore, the set-based control framework was not used in the later work presented in paper D [58].

5.4 Wire-arc additive manufacturing of structures with over-hang: Experimental results depositing material onto fixed substrate

Based on the experiments performed in paper C [57], the orientation of the tool relative to the surface to be welded is not at all arbitrary, and a difference of a few degrees can make a large difference regarding how the material will set (**RQ6**). As is further investigated in section 2.1 and shown in Fig. 2.4, overhangs are challenging to build when material is only deposited orthogonally to the building surface. If the overhang grows too steep and the material is deposited strictly vertically, additional support structures must be added for the new layers to have something to adhere to. However, if fast-curing material can be deposited at an angle, the contact surface would be increased, and it would be possible to construct overhangs without support structures.

The objective of paper D is to examine if overhangs can be built using non-vertical material deposition, with the orientation of the tool following the direction of the tilt of the overhang (**RQ7**). Similar work has been done using plastic [54] and in metal [53], but while the focus has previously been to deposit material vertically onto a tilting surface, the objective in paper D is building structures by depositing material onto a fixed substrate. This difference is important if the aim is to build large structures, as tilting the platform will quickly become more challenging once the structure grows in size. It methods like this is to be used for repair work, depositing material from a tilted tool onto a fixed substrate is also much closer to a realistic environment.

As for the experiments presented in section 5.2 and 5.3, the experimental set-up was a 6DOF IRB2400/10 ABB robot manipulator equipped with Fronius TPS 400i CMT welding equipment. The path was once again programmed using the RAPID programming language's functions for linear and circular movements, as used in paper B [50]. When using these commands, the orientation of the welding gun is set using quaternions. In order to control the orientation, the desired orientation of the welding gun given in quaternions was calculated via rotation matrices and the robot's global coordinate system. As RAPID does not have mathematical functions for matrix multiplication etc., this had to be programmed manually. For the hexagonal structure shown in Fig. 5.6, the coordinates of the points had to be calculated based on the hexagon rotating 1° for each consecutive layer.

Details on all of these calculations are described in paper D [58], but will not be elaborated on here, as this is not the focus of the research.

In total, three structures with overhang were built in the work presented in paper C. The first structure, shown in Fig. 5.6 and to the left in Fig. 6.1 was built using vertical material deposition and an increasing overhang. By building a structure with slight overhang using strictly vertical deposition, the aim was to study how overhangs can be 'forced' by depositing material onto an existing part of the structure that does not fully overlap with the current path while using material that can sufficiently withstand deformations due to heat accumulation. The results from paper B [50] presented in section 5.2 showed that structures in the tested aluminium alloys were much more vulnerable to uneven heat accumulation than structures built in a nickel-alloy with a higher melting point. Therefore, the hexagonal structure was built using a Ni–Cr–Mo alloy UTP 759, as this was a similar material to Inconel 625, and easily available. As these experiments were also meant for testing new methods, an analysis of which exact material would give the best results was not considered to be a priority. In future work, this would have to be assessed further. For each approximate layer, the hexagon was

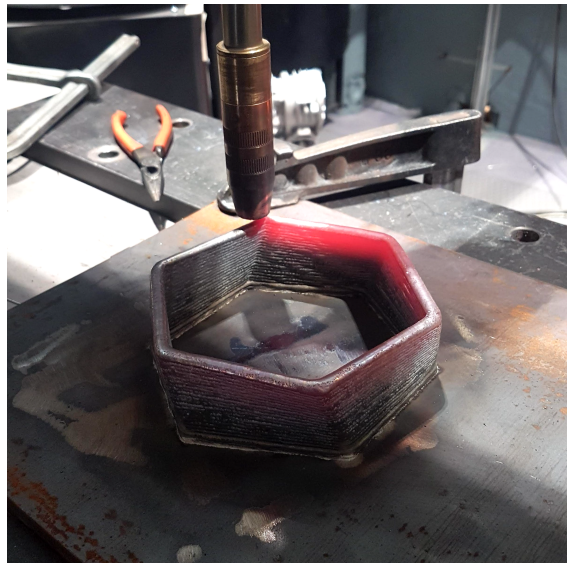

Figure 5.6: **Overhang with vertical deposition:** Using a fixed vertical orientation of the welding gun, it was possible to construct a structure with a slight overhang by rotating the hexagonal structure 1° per rotation.

Figure 5.7: **Vase with overhang:** The vase structure with outwards and inwards tilting overhang, built by having the orientation of the tool approx. follow the tilt of the overhang.

twisted 1°. This meant that by the end of the build, when the structure was approx. 45 layers tall, the structure had twisted 45°, thereby creating an overhang.

Two other builds were performed using non-vertical material deposition (**RQ7**): A shape with an overhang both outwards and inwards, seen in Fig. 5.7 and Fig. 6.1 and hereon referred to as the 'vase', and a structure with a more prominent outwards overhang, shown in the simulation in Fig. 5.8 and in Fig. 6.2, and hereon referred to as the 'bowl'. These structures are both similar to the cylinders from earlier work, though with a varying radius. The orientation of the tool was set to follow the tilt of the wall, as can be seen in the simulation in Fig. 5.7. For the vase, the overhang was at the most 25°, and the orientation of the tool only approximately followed the tilt of the wall. The exact values for the angle of the welding gun, as well as all relevant welding parameters, are listed in the tables in paper D [58].

As the vase build looked promising in the sense that it could continue without unforeseen material deformations, at least on a superficial level,

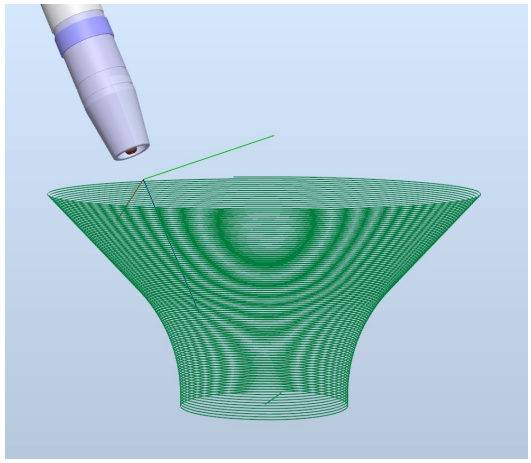

Figure 5.8: **Prominent overhang:** The simulated robot path for the bowl structure built in the work presented in paper D [58]. This structure had an overhang of 43°, and was built with the orientation of the tool closely following the tilt of the overhang.

the bowl build was performed. This time, the overhang was set to increase by 1° per approx. layer, and then keep building with this overhang when reaching 43°. This limit was set to avoid issues with the bounds of the robot's joints, as the movement grew more challenging for the robot itself. The build continued for almost another 50 layers, resulting in the structure shown in Fig. 6.2. This structure also looked good on a superficial level, without clear deformations or issues related to the non-vertical material deposition (**RQ7**). The orientation of the tool was set to follow the angle of the tilt exactly, and the increase of radius per layer as well as the layer height was set using geometry: the layer height and the increase in radius being the two short sides of a right-angled triangle, the angle being equal to the angle of the overhang, and the hypotenuse being the layer height when the tool was kept vertical. The estimated value for the layer height was based on experience from the previous builds, see details in paper D [58]. A full description on how this was calculated, as well as values for the radius, layer heights and angles throughout the vase build and bowl build are found in paper D, and will not be explained in further detail here.

The conditions for heat accumulation and heat dissipation are altered when building structures with overhangs or intersections. In order to examine the quality of the build, an optical microscopy and hardness mea-

surements were performed on one of the hexagonal structures built using vertical material deposition, as well as the structure with intersections presented in section 5.2 and paper B [50]. Both of the structures that were examined were built in the Ni–Cr–Mo alloy UTP 759. Transverse sections of stable mid-wall positions, overhang corners and intersections were examined to reveal potential process defects of fluctuations. It was evident that the micro-structure during deposition away from intersections or overhangs was different for the hexagonal structure and the structure with intersections, likely due to the difference in accumulated heat. As the structure with intersections would accumulate much more heat that the simpler, thin-walled hexagonal structure, a higher heat input suppressed the columnar dendritic growth in the material. The effects of this difference was evaluated by Vickers hardness testing, showing that the higher heat input had resulted in an increased hardness in the material. An in-depth assessment of mechanical performance of the structure, e.g. tensile strength and impact toughness was deemed out of scope for this work, but should be assessed in further work.

In conclusion, the results from the work presented in this paper showed that building structures with overhang is possible using continuous WAAM, and that good results without unforeseen deformations or complications were found when allowing the orientation of the welding gun to follow the tilt of the constructed overhang (**RQ7**). When building using a material with a relatively high melting point, such as UTP 759, it was possible to keep a build going at an angle of 43° without the building shown signs of sagging or other deformations due to accumulated heat or issues with gravitational pull on the material. Using Pythagoras to determine the increase in radius and layer height seemed an effective solution, allowing the build to continue without issues until the build was stopped by the operators. Further work should investigate if the same method would be as effective when building in for example aluminium, a material that has proven to be much more vulnerable to the gravitational pull when the structure accumulates heat as the build goes on because of its comparatively low melting point.

Chapter 6

Discussion and future work

The building techniques for three-dimensional components that are today covered by AM started out as the term 'rapid prototyping' suggests: a rapid building technique meant purely for prototyping and modelling. From there, it has evolved into being used to manufacture parts for high-specification sectors such as medicine and aviation, as well as for components at an end-product level. Still, the technology has its limitations. Many of the most common methods for AM face common challenges related to the geometry and size of the components that can be manufactured. Though some materials and techniques, such as liquid-based stereo lithography, allow for more flexibility than material extrusion, both the building rate and the in-box building methods can restrict their practicability in industrial applications. The work presented in this thesis has highlighted how robotised additive manufacturing is a useful technique that helps solves some of these challenges.

6.1 Research questions and research development

Chapter 4 gives an overview of how the research objectives and research questions were formulated and developed throughout the work on this thesis. The main research question to be answered throughout this work was investigating how robotised AM could be used to extend the areas in which AM could be useful. While initially considering many different materials, the focus was on AM in metals using wire-arc welding, as this could be an area of interest for the industry.

Firstly, the overview of AM methods presented in section 2.1 and the literature presented in section 4.1 let to the following opportunity for fur-

ther development of AM: Combining material deposition with the possibility for non-vertical and/or non-layer-wise material deposition that was not restricted by a building chamber. While several projects had used different methods for large-scale AM, most of them kept the build strictly layer-wise, and the deposition vertical. Though Laarman Lab had done much work on robotised AM [43, 44, 52], this work was not accessible by the research community. Robotised AM was therefore the aim of the work in this thesis, with an initial objective to investigate deposition methods that were not strictly layer-based. Initially, there was no specific material in focus, so a proof-of-concept experiment could be carried out using any available, suitable material.

RQ1: *How can a 6 DOF robot manipulator be combined with material deposition to perform AM in order to diverge from many of the standard methods of AM and thus avoid being restricted by a building chamber?*

RQ2: *Can a proof-of-concept build by robot be performed using a building method that is not strictly based on stacking 2D layers of material?*

The proof-of-concept experiment in paper A showed that building a thin-walled structure by continuous material deposition using a robot manipulator, and a non-layer-wise path, was indeed possible (**RQ1, RQ2**). A continuous build like the one performed in the experiments in paper A is beneficial for its high material deposition rate: fewer pauses in the building process shortens the build time, which is, in itself, financially beneficial. When working with different forms of material deposition, fewer stops in the building process can in addition help keep the quality of the build high. These initial experiments also helped highlight some of the main challenges with robotised AM: Already in the preliminary experiments using viscous glue it became evident that the beginning and end phases of material deposition are challenging. A continuous build is hence more predictable, and less vulnerable to unwanted variations in the build.

Further literature studies, as well as input from the industry, led the work towards AM in metals, as described in section 4.2. One method for metal deposition by robot was WAAM, and the possibility to build metal structure using robot manipulators combined with welding equipment had already been demonstrated [44, 52]. Robotised WAAM can also be more accessible to the industry because a robot manipulator can often be used for a series of tasks, meaning that the equipment can be of value even when

not used for WAAM. A industry robot manipulator will generally also be possible to sell if no longer needed, making the investment less of a risk. The presentation of welding technology given in chapter 2 gives a more thorough introduction to different welding methods, and explains how the main focus ended up being on CMT welding.

The initial experiments in paper A had shown that the beginning and ending of material deposition could lead to uneven material deposition and deformations. The same applies to arc welding processes: arc initiation and flame-out both lead to uneven material deposition, as reported by [47]. This is unfortunate because deformations and inaccuracies often accumulates during these kinds of open-loop builds. Therefore, one of the main objectives going forward was keeping the build as continuous as possible. To investigate how robotised AM using arc-welding could be used, and if the building process could be continuous, new test experiments were carried out. The literature, presented in chapter 4, showed that one challenge for layer-based material deposition was intersections within each layers, so this was also an objective for these initial welding experiments.

RQ3: *Is it possible to build thin-walled metal structures in one continuous process using WAAM, thereby avoiding additional issues related to flame-initiation and flame-out?*

RQ4: *When the structure requires intersections within a layer, can an alternative approach using opposing corners to avoid intersections within layers be used on a build with continuous material deposition over several layers?*

Several thin-walled structures were built using continuous WAAM in the work presented in paper B, thereby avoiding the issues related to flame-initiation and flame-out. For very generic aluminium structures, without any areas that could lead to uneven heat-accumulation, the build could keep going continuously without the structure showing signs of deformations (**RQ3**). It was also possible to perform continuous builds with intersections using the approach presented in [49]. However, these structures had some issues when built with aluminium, as the uneven heat distribution throughout the structure led to an accumulative error in the intersections. However, the method worker well for builds when switching to a nickel-based alloy with a higher melting point and higher heat emission to air than aluminium [73], in the sense that the opposing corners melted together completely without visible deformations (**RQ4**). This highlighted the difference in building with

materials depending on their melting point and other properties.

As presented in section 5.3, the main focus of the work from this point came to be continuous builds that could deviate from the strictly layer-wise building methods, focusing on the possibility of non-vertical material deposition. Now that the feasibility of continuous WAAM builds was shown (**RQ3**), the next step was to utilise the freedom in orientation given by the 6 DOF robot manipulator. Based on the experience with the framework for set-based control presented in [59, 61], the idea was to see if this approach could be transferred to WAAM in order to ease the joint configuration for the robot. Not relying on a strictly fixed orientation of the welding gun expands the available work-space of the robot, and can help avoid obstacles in the area.

RQ5: *Can the suggested framework for set-based control be suited to build a thin-walled, symmetrical structure using WAAM?*

RQ6: *Does freedom in the orientation of the tool significantly affect the build?*

Based on the resulting structures, and the building process described in paper C [57], the framework for set-based control presented in [59, 61] did not work well for building a symmetrical structure using WAAM: The orientation of the welding gun seemed to impact the process a great deal compared to for spray painting, leading to unwanted deformations of the build, as the deviation in the orientation of the tool was not symmetrically distributed, as explained further in section 5.3 (**RQ5, RQ6**). Therefore, this set-based solution was not considered for further work in its current state. Instead, the focus was turned to material deposition by robot in order to create structures with overhangs, i.e. parts of the structure that sticks out over a lower part of the structure without being supported by an preceding layer in a directly vertical direction. Because, even though the orientation of the welding gun was deemed to have a large significant impact on the build, this might not necessarily be negative if used the right way: The literature showed that Xiong et al. had build a structure with overhang on a fixed substrate using vertical material deposition [55], while Kazanas et al. had created quite steep, simple wall structures using an orientation of the tool which followed the direction of the tilt of the overhang [56]. Significant overhangs had been built the orientation of the tool was used in a strategic way. The main objective of paper D was therefore to build structures with

a significant overhang onto a fixed substrate sing continuous material deposition, and an orientation of the tool that followed the tilt of the overhang.

RQ7: *Can an overhang be constructed by depositing material continuously while letting the orientation of the tool follow the tilt of the overhang?*

Building structures with overhang using an orientation of the tool which followed the tilt of the overhang worked well in the sense that the final structure showed few signs of deformation, and the build could continue without interruption caused by unforeseen build defects (**RQ7**). A full description of these experiments are found in paper D [58], and a full discussion of the different elements of this work and its indications is found in chapter 6. The ability to build overhanging structures was one of the main motivations to use robotised AM, as overhangs significantly expands the range of geometries that can be manufactured beyond those possible with the most common in-box AM methods. Even methods that do allow for overhangs, such as PFB and VP, are very limited when it comes to the size of the component. This is due not only to the build having to take place within a chamber limiting the product's size, but also because the layers need to be so thin that the building time is impracticably long, whereas material extrusion or WAAM methods can deposit several kg of material per hour. In this work, structures with overhangs were built using WAAM and a Ni–Cr–Mo alloy, using both a strictly vertical and a non-vertical welding gun orientation. It was possible to manufacture a structure with less prominent overhangs using a vertical orientation of the welding gun, as long as the contact surface between consecutive layers was quite large relative to the width of the welding bead (**RQ7**).

Builds done using a tilted gun orientation, which followed the tilt of the constructed overhang as shown in Fig. 2.6, showed great promise. Building a structure with such a large overhang proved unsuccessful when the gun was oriented vertically, as explained in paper C when using the set-based control method [57]. However, when the orientation of the welding gun was tilted tangentially to the vase wall as shown in Fig. 6.1, the build was much more successful, see paper D fro details [58]. Another build was done in the same Ni–Cr–Mo alloy to create a structure with an even larger overhang, almost 45°, as shown in Fig. 6.2, and the build still showed few malformations. Details on this build is also found in paper D [58]. The heat input and accumulated heat in the structure will affect an overhang more than a vertical wall, even for materials with higher melting points such as the

Figure 6.1: **Overhangs:** Two of the structures with overhangs built using the Ni–Cr–Mo alloy UTP759. For further details on these builds, see paper D [58].

Ni–Cr–Mo alloy used in these builds, so this should be investigated further in future work.

Future work on this topic should focus both on how prominent the overhang can get before the structure shows significant deformation, and on how the choice of building material impacts upon the final structure. Experiments performed on intersections in paths when manufacturing structures in a semi-layer-wise manner, presented in paper B, show that the properties of the building material are indeed important [50]. Softer materials with a lower melting point, such as aluminium alloys, are more vulnerable to deformations. Inaccuracies and flaws that are biased in its distribution will accumulate as the build progresses, and become problematic for the continued material deposition. For example: If heat accumulation in parts of the structure causes the metal to spread out more before becoming solid, leading to a lower layer height, this will not necessarily even itself out as the build progresses, but rather accumulate over time. Harder metals, such as nickel-based alloys, with higher melting points can withstand such deformations more easily, which leaves more room for inaccuracies without compromising the building process in a significant way. For further details, see paper D [58].

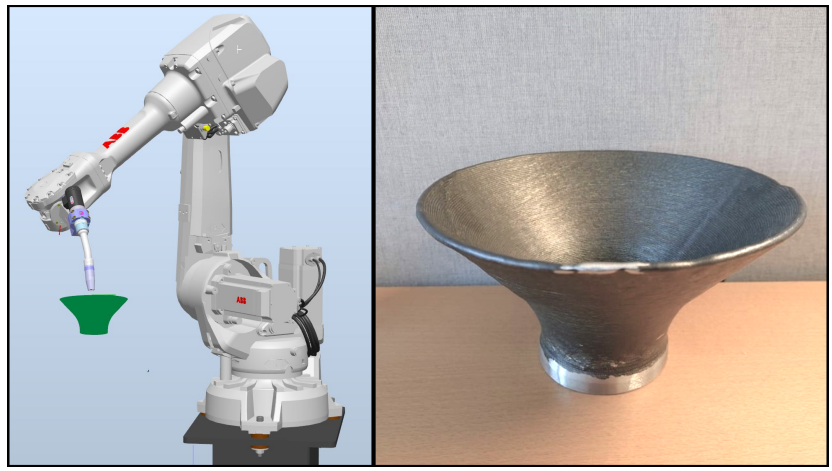

Figure 6.2: **Significant overhang:** A bowl structure with an overhang of 43° was built using material deposition from a welding gun that followed the was tilted tangentially to the bowl walls. Simulation of the path shown to the left was tested using ABB's simulation software Robot Studio. See paper D for full details on this build [58].

6.2 Further discussions and future work

The work presented in this thesis has focused on a building process that is as continuous as possible. In the preliminary experiments (paper A [12]), a viscous glue was tested as a building material for a robotised AM process. The ensuing work and experiments all focused on the construction of metal structures using WAAM and CMT, as presented in papers B, C and D [50, 57, 58]. When building thin-walled structures using WAAM, it was generally possible to keep the building process going for a long time once the welding parameters were adjusted so that the heat input and heat dissipation reached an equilibrium. Depending somewhat on the building material, it was generally pauses and interruptions in the building process that lead to deformations: such an interruption could, for example, occur when pausing to adjust the distance from the welding gun to the surface to be welded because the layer height estimation turned out to be too high or too low. Such situations clearly illustrates the need to include feedback and closed-loop control of the manufacturing process in future work. This would help avoid unnecessary interruptions and arc terminations.

The distance from the feed wire to the building surface, i.e. between the electrodes, was one of the parameters that needed the most adjustment throughout the builds in this work. This distance determines the length of the welding arc, which impacts upon the voltage and heat input, as explained in chapter 3. Based on experience, it is possible to give an acceptable approximation of both a good starting distance between the welding gun and the substrate, and also the layer height, i.e. how far the welding gun has to move in the z-direction. When running the build using off-line scripts, this approximated layer height was set in the beginning of the build, and determined the height increase as the build progresses. Both over- and under-estimating the layer height will impact upon the voltage and material deposition during the build, as the distance between the electrode and the substrate will deviate from the desired distance, affecting both the welding arc length and the heat input.

To some extent, the process tries to 'correct itself', returning the electrode spacing to the desired value. This can be explained as follows: If the estimated layer height is *too low* and the welding arc *too short*, the heat input *increases*, along with the depth of the welding pool. The temperature hence rises, and the deposited material takes longer to cool down and harden, and therefore spends more time in its gravity-vulnerable liquid state. Under its own weight, the welding bead thus becomes *wider and lower*, which thus *increases* the distance between the welding gun and the surface to be welded again. This occurs both in vertical material deposition, as shown in papers B and C [50, 57], and also in non-vertical material deposition, as presented in papers C and D [57, 58]. Although a welding arc is not as predictable as a traditional resistor regarding the relationship between voltage and current, an over-approximation of the layer height will generally lead to the opposite results as under-approximation, i.e. a lower heat input. This means that, if the approximated layer height is *too big*, the heat input goes down. The material will then cool faster, resulting a narrower welding bead with an *increase* in height [74], and the distance to the welding gun thus decreases again. This effect can help to regulate small deviations in the arc length, though, as the associated arc instabilities will affect the properties of the deposited material, this is still not an ideal solution for the manufacturing process.

For the experiments presented in this thesis, the deviation in approximated layer height turned out, in several cases, to accumulate significantly over time. An example is the build of a hexagonal structure with overhang, built using vertical material deposition, as presented in paper D [58]. This

build had to be terminated because the distance between the consumable electrode and the substrate grew too wide: a small over-approximation of the layer height accumulated over the 45 layers until the arc became so unstable that the build had to be interrupted. This build shows how much the building material matters when the welding parameters are not optimally tuned. A large portion of the build was performed with a significant shift away from an ideal arc length, even though the finished structure showed few superficial signs of this. Optical microscopy showed that the structure was not compromised by the high porosity that one might expect from a WAAM process with a very long and unstable welding arc, due to the stretched arc resulting in reduced gas shielding.

Combining GMAW welding and a 6-DOF robot manipulator shows that manufacturing of metal structures with overhangs is possible using non-vertical deposition of material by WAAM, even for DED AM methods that are not done within a volume of excess material (such as PBF or VP). The builds done using the Ni–Cr–Mo alloy UTP759 show that the orientation of the welding gun greatly affects the width and height of the welding bead, which is as expected from the work in [55]. This effect became challenging when trying to implement additional freedom in the gun orientation using set-based control. Having increased freedom in the tool orientation as introduced by this approach has shown promising results in spray painting [59]. However, this set-based framework does not require the orientation to be symmetrical around the constructed structure. The experiments presented in paper D [58] show that symmetry is much more important for arc welding than for spray painting, even when using relatively hard materials with a high melting point. The conclusion is that, in its current form, the set-based framework presented in [59, 61] is not suitable for WAAM: the freedom in gun orientation has too great an impact on the resulting build, and the a-symmetry leads to an unpredictable result, as shown in paper D [58].

The research presented in this thesis is based on open-loop, offline robot control. The path of the robot's end effector is pre-programmed, both for the WAAM experiments and the preliminary experiment using a UR-5 robot and viscous glue. This programming is done either using commands from ABB's RAPID programming language, or by using the set-based framework from [59, 61] to determine configurations for each of the robot's joints based on the desired path. What this means is that the robot will continue along the pre-defined path, regardless of whether the structure shows significant geometric discrepancies, and even if these discrepancies might block its path.

In future work, the system needs feedback in the system to improve and adapt to the building process.

The welding processes in the experiments are partly controlled by the control system of the welding equipment, which adjusts the welding parameters described in section 3.1 relative to each other. In addition, the supply current was adjusted manually during the welding process, and tables with all of the relevant welding parameters can be found in papers B, C and D [50, 57, 58]. As experience accrued during testing, each successive task required fewer manual adjustments compared with the one before because less unplanned tuning of the welding parameters was necessary during the build. This, in turn, led to increasingly successful builds with fewer visible malformations, as more accurately adjusted welding parameters gave a more even and predictable deposition of welding material.

Still, several of the WAAM processes had to be interrupted or terminated because the approximated layer height was wrong, or because malformations due to uneven heat dissipation accumulated over time. The challenges related to the layer height and the length of the welding arc can perhaps be solved by ensuring a more stable layer height by careful design of the building process, as shown in [74]. The build can potentially also benefit greatly from feedback or surveillance of the building process, and the possibility to adjust the robot path during the build using closed-loop control. A visual surveillance system should hence be considered in future work. This could be done, for example, by installing a set of static cameras or laser scanners around the build area or on one or more dedicated robots involved in the building process, as suggested by [75]. This could enable the three-dimensional geometry to be calculated photogrametrically from the multiple views. However, this poses its own challenges if it is going to enable the avoidance of blind spots and collisions. Also, depending on the building material, it can be challenging to get an accurate mapping of the structure if the surface is, for example, too reflective. In addition, 3D imaging techniques designed for improved imaging of reflective surfaces generally require a long exposure time, for example 50 ms, which makes it challenging to get a good mapping of an active welding process [76].

Surveillance could alternatively be done using a heat-monitoring camera. This might also be challenging because the metal structure potentially has a reflective surface, or low emissivity, which makes such readings inaccurate. Objects with low emissivity emit very little thermal energy compared to how much thermal energy they reflect, so the radiant heat picked up by a thermal camera might not describe the surface temperature of the structure

itself, but instead the reflected thermal radiation from the environment [77]. The surface's reflectivity depends on the welding metal, and on the extent of oxidation or contamination creating a film over its surface. For an active welding process, this can partly be solved by filtering out the strongest radiation from the molten pool, for example by using a band-pass filter as done in [78]. Heat surveillance can also be done using non-contact infrared sensors to monitor the heat development in, for example, the welding pool, as done by Alfaro and Franco in 2010 [79]: Because the welding pool temperature is directly connected to the penetration depth of the weld, monitoring the welding pool's surface temperature can help approximate the penetration depth, taking advantage of this correlation between different parameters of the welding process.

In general, closer monitoring of the manufacturing process and the possibility of closed-loop control of the robot's path are essential, and needs to be addressed in future work before this approach can be used in production or for repair work in industry. If such an approach is to be used in an environment such as a ship which exhibits heaving and swaying, closed-loop control is essential, as external influences will most likely impact upon an open-loop system in ways that cannot be predicted accurately.

This thesis has focused on continuous WAAM, while other projects have focused on metal AM using spot welding, or robotised AM using other fast-curing materials. Once this technology matures, robotised AM will, hopefully, enable on-site production of a new range of custom components with a relatively low production time. This will help to save materials compared to, for example, machining, and will reduce the costs of unique parts compared with mass production. On-site production of components can also lessen the need to store extra parts. Hopefully it will also be possible to use robotised AM to perform repairs on existing constructions, such as ships or other formations that are costly or difficult to move.

References

[1] Ingrid Fjordheim Onstein, Linn Danielsen Evjemo, and Jan Tommy Gravdahl. Additive manufacturing path generation for robot manipulators based on CAD models. *IFAC-PapersOnLine*, 53(2):10037–10043, 2020. https://doi.org/10.1016/j.ifacol.2020.12.2724.

[2] Linn D Evjemo, Tone Gjerstad, Esten I Grøtli, and Gabor Sziebig. Trends in smart manufacturing: Role of humans and industrial robots in smart factories. *Current Robotics Reports*, 1(2):35–41, 2020. https://doi.org/10.1007/s43154-020-00006-5.

[3] Ian Gibson, David W Rosen, Brent Stucker, et al. *Additive manufacturing technologies*, volume 238. Springer, 2010.

[4] Pranjal Jain and AM Kuthe. Feasibility study of manufacturing using rapid prototyping: FDM approach. *Procedia Engineering*, 63:4–11, 2013. https://doi.org/10.1016/j.proeng.2013.08.275.

[5] Ian Gibson, David W Rosen, Brent Stucker, and Mahyar Khorasani. *Additive manufacturing technologies*, volume 17. Springer, 2021.

[6] Anton Wiberg. *Towards Design Automation for Additive Manufacturing: A Multidisciplinary Optimization approach*, volume 1854. Linköping University Electronic Press, 2019. https://doi.org/10.3384/lic.diva-160888.

[7] David Rosen Ian Gibson and Brent Stucker. Additive manufacturing technologies 3D printing, rapid prototyping, and direct digital manufacturing, 2015. https://doi.org/10.1007/978-1-4939-2113-3.

[8] Fabrizia Caiazzo, Vittorio Alfieri, Gaetano Corrado, and Paolo Argenio. Laser powder-bed fusion of Inconel 718 to manufacture turbine

blades. *The International Journal of Advanced Manufacturing Technology*, 93(9):4023–4031, 2017. https://doi.org/10.1007/s00170-017-0839-3.

[9] Benjamin Graf, Stefan Ammer, Andrey Gumenyuk, and Michael Rethmeier. Design of experiments for laser metal deposition in maintenance, repair and overhaul applications. *Procedia CIrP*, 11:245–248, 2013. https://doi.org/10.1016/j.procir.2013.07.031.

[10] Make.3dexperience.3ds.com. Introduction to 3D printing - additive processes, 2020-2021. https://make.3dexperience.3ds.com/processes/3D-printing. Accessed 2021-09-28.

[11] H Bikas, AK Lianos, and P Stavropoulos. A design framework for additive manufacturing. *The International Journal of Advanced Manufacturing Technology*, 103(9):3769–3783, 2019. https://doi.org/10.1007/s00170-019-03627-z.

[12] Linn Danielsen Evjemo, Signe Moe, Jan Tommy Gravdahl, Olivier Roulet-Dubonnet, and Brøtan Vegard Gellein, Lars Tore. Additive manufacturing by robot manipulator: An overview of the state-of-the-art and proof-of-concept results. In *2017 22nd IEEE International Conference on Emerging Technologies and Factory Automation (ETFA)*, pages 1–8. IEEE, 2017. https://doi.org/10.1109/ETFA.2017.8247617.

[13] ABB.com. IRB 2400, 2016-2021. https://new.abb.com/products/robotics/industrial-robots/irb-2400. Accessed 2021-09-03.

[14] Markus Korpela, Niko Riikonen, Heidi Piili, Antti Salminen, and Olli Nyrhilä. Additive manufacturing — past, present, and the future. In *Technical, Economic and Societal Effects of Manufacturing 4.0*, pages 17–41. Palgrave Macmillan, Cham, 2020. https://doi.org/10.1007/978-3-030-46103-4_2.

[15] Amagoia Paskual, Pedro Álvarez, Alfredo Suárez, et al. Study on arc welding processes for high deposition rate additive manufacturing. *Procedia Cirp*, 68:358–362, 2018. https://doi.org/10.1016/j.procir.2017.12.095.

[16] Geir Langelandsvik. Wire arc additive manufacturing of aluminium alloys. 2021. https://hdl.handle.net/11250/2780782.

[17] Stewart W Williams, Filomeno Martina, Adrian C Addison, Jialuo Ding, Goncalo Pardal, and P Colegrove. *Materials Science and Technology*, 32(7):641–647, 2016. https://doi.org/10.1179/1743284715Y.0000000073.

[18] Bintao Wu, Zengxi Pan, Donghong Ding, Dominic Cuiuri, Huijun Li, Jing Xu, and John Norrish. A review of the wire arc additive manufacturing of metals: properties, defects and quality improvement. *Journal of Manufacturing Processes*, 35:127–139, 2018. https://doi.org/10.1016/j.jmapro.2018.08.001.

[19] Baker Ralph. Method of making decorative articles, April 14 1925. US Patent 1,533,300.

[20] Geir Langelandsvik, Olav Ragnvaldsen, Jan Eskil Flåm, Odd Magne Akselsen, and Hans Jørgen Roven. Wire and arc additive manufacturing with TiC-nanoparticle reinforced AA5183 alloy. 2020. https://doi.org/10.1051/matecconf/202032607002.

[21] John Frederick Lancaster. The physics of welding. *Physics in technology*, 15(2):73, 1984.

[22] Kenneth Easterling. *Introduction to the physical metallurgy of welding*. Elsevier, 2013. https://doi.org/10.1016/C2013-0-04524-0.

[23] Klas Weman and Gunnar Lindén. *MIG welding guide*. Woodhead Publishing, 2006.

[24] Einar Halmøy. *Sveiseteknikk*, volume 4th edition. 1991.

[25] The Lincoln Electric Company. Constant current vs. constant voltage output, 1999-2022. https://www.lincolnelectric.com/en-gb/support/process-and-theory/Pages/constant-current-vs-constant-coltage-output.aspx. Accessed 2021-12-22.

[26] Ramesh Singh. Chapter 3 - welding and joining processes. In Ramesh Singh, editor, *Applied Welding Engineering*, pages 147–170. Butterworth-Heinemann, Boston, 2012. https://doi.org/10.1016/B978-0-12-391916-8.00015-7.

[27] Nabeel Arif, Jae Hak Lee, and Choong Don Yoo. Modelling of globular transfer considering momentum flux in GMAW. *Journal of Physics*

D: Applied Physics, 41(19):195503, 2008. https://doi.org/10.1088/0022-3727/41/19/195503.

[28] Changwen Dong, Jiaxiang Xue, and Yu Hu. Control study of pulsed MIG high-speed welding power source based on single neuron adaptive PID model. In *2018 10th International Conference on Intelligent Human-Machine Systems and Cybernetics (IHMSC)*, volume 02, pages 381–385, 2018. https://doi.org/10.1109/IHMSC.2018.10192.

[29] Jie Pang, Shengsun Hu, Junqi Shen, Peng Wang, and Ying Liang. Arc characteristics and metal transfer behavior of CMT+ P welding process. *Journal of Materials Processing Technology*, 238:212–217, 2016. https://doi.org/10.1016/j.jmatprotec.2016.07.033.

[30] Jair Carlos Dutra, Régis Henrique Gonçalves e Silva, and Cleber Marques. Melting and welding power characteristics of MIG – CMT versus conventional MIG for aluminium 5183. *Welding International*, 29(3):181–186, 2015. https://doi.org/10.1080/09507116.2014.932974.

[31] Fronius.com. CMT - cold metal transfer: The cold welding process for premium quality, 2019-2021. https://www.fronius.com/en/welding-technology/world-of-welding/fronius-welding-processes/cmt. Accessed 2021-10-29.

[32] J Słania, R Krawczyk, and Sz Wójcik. Quality requirements put on the inconel 625 austenite layer used on the sheet pile walls of the boiler's evaporator to utilize waste thermally. *Archives of Metallurgy and Materials*, 60, 2015. https://doi.org/10.1515/amm-2015-0192.

[33] rooiejoris.nl/"3D Elephant Petition". 3D elephant petition, 2015. http://www.rooiejoris.nl/3d-elephant-petition/. Accessed 2017-03-23.

[34] totalkustom.com/"News". Total kustom news, 2014-2017. http://www.totalkustom.com/news.html. Accessed 2017-03-26.

[35] mx3d.com/"Dragon Benches". MX3D - dragon benches, 2015. http://mx3d.com/projects-2/. Accessed: 2022-05-24.

[36] rooiejoris.nl/"Z Unlimited". Z-unlimited, 2015. http://www.rooiejoris.nl/z-unlimited/. Accessed 2017-03-23.

[37] 3dprint.com/"3D-printed hotel suite". 3D-printed hotel suite, 2015. https://3dprint.com/94558/3d-printed-hotel-lewis-grand/. Accessed 2017-03-27.

[38] apis-cor.com/"ApisCor Bookbuyer". Apis cor we print buildings, 2016. http://apis-cor.com/files/ApisCor_BookBuyer_en.pdf. Accessed 2017-04-02.

[39] apis-cor.com/"The first on-site house has been printed in Russia". The first on-site house has been printed in russia, 2017. http://apis-cor.com/en/about/news/first-house. Accessed 2017-04-02.

[40] ICON Team. Icon delivers series of 3d-printed homes for homeless in austin, 2020. https://www.iconbuild.com/updates/icon-delivers-series-of-3d-printed-homes-for-homeless. Accessed 2022-05-24.

[41] Kampc.be. 3D-printing in the construction world, 2018-2021. https://www.kampc.be/c3po_eng. Accessed 2021-11-04.

[42] peri.com/"Germany´s first printed house officially openend". Germany´s first printed house officially openend, 2021. https://www.peri.com/en/media/press-releases/germanys-first-printed-house-officially-openend.html. Accessed 2022-05-24.

[43] Joris Laarman, Sasa Jokic, Petr Novikov, Luis E Fraguada, and Areti Markopoulou. Anti-gravity additive manufacturing. *Fabricate: Negotiating Design & Making*, pages 192–197, 2014.

[44] designbook.com/"3D printing welder by joris laarman creates gravity-defying sculptures". 3D printing welder by joris laarman creates gravity-defying sculptures, 2014. https://www.designboom.com/technology/metal-3d-printer-by-joris-laarman-lab-creates-gravity-defying-sculptures-02-21-2014/. Accessed: 2022-05-24.

[45] jorislaarman.com/"Butterfly Screen". Butterfly screen, 2016. http://www.jorislaarman.com/work/butterfly-screen/. Accessed 2033-05-24.

[46] MX3D.com. M1 system - full solution for WAAM, 2019-2021. https://mx3d.com/services/m1-systems/. Accessed 2021-12-10.

[47] Filomeno Martina, Jorn Mehnen, Stewart W Williams, Paul Colegrove, and Frank Wang. Investigation of the benefits of plasma deposition for the additive layer manufacture of Ti–6Al–4V. *Journal of Materials Processing Technology*, 212(6):1377–1386, 2012. https://doi.org/10.1016/j.jmatprotec.2012.02.002.

[48] Donghong Ding, Chen Shen, Zengxi Pan, Dominic Cuiuri, Huijun Li, Nathan Larkin, and Stephen van Duin. Towards an automated robotic arc-welding-based additive manufacturing system from CAD to finished part. *Comput. Aided Des.*, 73:66–75, 2016. https://doi.org/10.1016/j.cad.2015.12.003.

[49] Jorn Mehnen, J Ding, H Lockett, and P Kazanas. Design for wire and arc additive layer manufacture. In *Global Product Development*, pages 721–727. Springer, 2011. https://doi.org/10.1007/978-3-642-15973-2_73.

[50] Linn Danielsen Evjemo, Geir Langelandsvik, and Jan Tommy Gravdahl. Wire arc additive manufacturing by robot manipulator: towards creating complex geometries. *IFAC-PapersOnLine*, 52(11):103–109, 2019. https://doi.org/10.1016/j.ifacol.2019.09.125.

[51] Jingchao Jiang, Xun Xu, and Jonathan Stringer. Support structures for additive manufacturing: a review. *Journal of Manufacturing and Materials Processing*, 2(4):64, 2018. https://doi.org/10.3390/jmmp2040064.

[52] Jorislaarman.com. Joris laarman lab: Work, 2013-2021. https://www.jorislaarman.com/. Accessed 2021-11-13.

[53] Jayaprakash Sharma Panchagnula and Suryakumar Simhambhatla. Manufacture of complex thin-walled metallic objects using weld-deposition based additive manufacturing. *Robotics and Computer-Integrated Manufacturing*, 49:194–203, 2018. https://doi.org/10.1016/j.rcim.2017.06.003.

[54] Chengkai Dai, Charlie CL Wang, Chenming Wu, Sylvain Lefebvre, Guoxin Fang, and Yong-Jin Liu. Support-free volume printing by multi-axis motion. *ACM Transactions on Graphics (TOG)*, 37(4):1–14, 2018. https://doi.org/10.1145/3197517.3201342.

[55] Jun Xiong, Yangyang Lei, Hui Chen, and Guangjun Zhang. Fabrication of inclined thin-walled parts in multi-layer single-pass GMAW-based additive manufacturing with flat position deposition. *Journal of Materials Processing Technology*, 240:397–403, 2017. https://doi.org/10.1016/j.jmatprotec.2016.10.019.

[56] Panagiotis Kazanas, Preetam Deherkar, Pedro Almeida, Helen Lockett, and Stewart Williams. Fabrication of geometrical features using wire and arc additive manufacture. *Proceedings of the Institution of Mechanical Engineers, Part B: Journal of Engineering Manufacture*, 226(6):1042–1051, 2012. https://doi.org/10.1177/0954405412437126.

[57] Linn Danielsen Evjemo, Signe Moe, and Jan Tommy Gravdahl. Robotised wire arc additive manufacturing using set-based control: experimental results. *IFAC-PapersOnLine*, 53(2):10044–10051, 2020. https://doi.org/10.1016/j.ifacol.2020.12.2725.

[58] Linn Danielsen Evjemo, Geir Langelandsvik, Signe Moe, Morten Høgseth Danielsen, and Jan Tommy Gravdahl. Wire-arc additive manufacturing of structures with overhang: Experimental results depositing material onto fixed substrate. *CIRP Journal of Manufacturing Science and Technology*, 38:186–203, 2022. https://doi.org/10.1016/j.cirpj.2022.04.006.

[59] Signe Moe, Jan Tommy Gravdahl, and Kristin Y Pettersen. Set-based control for autonomous spray painting. *IEEE Transactions on Automation Science and Engineering*, 15(4):1785–1796, 2018. https://doi.org/10.1109/TASE.2018.2801382.

[60] ABB Robotics. Technical reference manual: RAPID Instructions, Functions and Data types, 2004-2010.

[61] Signe Moe, Gianluca Antonelli, Andrew R Teel, Kristin Y Pettersen, and Johannes Schrimpf. Set-based tasks within the singularity-robust multiple task-priority inverse kinematics framework: General formulation, stability analysis, and experimental results. *Frontiers in Robotics and AI*, 3:16, 2016. https://doi.org/10.3389/frobt.2016.00016.

[62] Osama Abdulhameed, Abdulrahman Al-Ahmari, Wadea Ameen, and Syed Hammad Mian. Additive manufacturing: Challenges,

trends, and applications. *Advances in Mechanical Engineering*, 11(2):1687814018822880, 2019. https://doi.org/10.1177/1687814018822880.

[63] J.P. Oliveira, A.D. LaLonde, and J. Ma. Processing parameters in laser powder bed fusion metal additive manufacturing. *Materials Design*, 193:108762, 2020. https://doi.org/10.1016/j.matdes.2020.108762.

[64] Jingchao Jiang and Yongsheng Ma. Path planning strategies to optimize accuracy, quality, build time and material use in additive manufacturing: a review. *Micromachines*, 11(7):633, 2020. https://doi.org/10.3390/mi11070633.

[65] Norsktitanium.com. Norsk titanium, 2021. https://www.norsktitanium.com. Accessed 2021-12-03.

[66] Xi Zhang and Enquan Liang. Metal additive manufacturing in aircraft: current application, opportunities and challenges. In *IOP Conference Series: Materials Science and Engineering*, volume 493, page 012032. IOP Publishing, 2019. https://doi.org/10.1088/1757-899X/493/1/012032.

[67] Manuela Gudeljevic and Thomas Klein. Investigation of material characteristics of intersections built by wire and arc additive manufacturing using locally varying deposition parameters. *The International Journal of Advanced Manufacturing Technology*, 116(5), 2021. https://doi.org/10.1007/s00170-021-07548-8.

[68] Ali Gökhan Demir. Micro laser metal wire deposition for additive manufacturing of thin-walled structures. *Optics and Lasers in Engineering*, 100:9–17, 2018. https://doi.org/10.1016/j.optlaseng.2017.07.003.

[69] Relativityspace.com. World's largest 3D metal printers, 2019-2021. https://www.relativityspace.com/stargate. Accessed 2021-12-10.

[70] Suwat Kuntanapreeda and Drew Hess. Opening access to space by maximizing utilization of 3d printing in launch vehicle design and production. *Applied Science and Engineering Progress*, 14(2):143–145, 2021. https://doi.org/10.14416/j.asep.2020.12.002.

[71] Baoqiang Cong, Ruijie Ouyang, Bojin Qi, and Jialuo Ding. Influence of cold metal transfer process and its heat input on weld bead

geometry and porosity of aluminum-copper alloy welds. *Rare Metal Mat. Eng.*, 45(3):606–611, 2016. https://doi.org/10.1016/S1875-5372(16)30080-7.

[72] Haibin Geng, Jinglong Li, Jiangtao Xiong, and Xin Lin. Optimisation of interpass temperature and heat input for wire and arc additive manufacturing 5A06 aluminium alloy. *Sci. Technol. Weld. Joi.*, 22(6):472–483, 2017. https://doi.org/10.1080/13621718.2016.1259031.

[73] Masanobu Kobayashi, Miki Otsuki, Hiroaki Sakate, F Sakuma, and A Ono. System for measuring the spectral distribution of normal emissivity of metals with direct current heating. *Int. J. Thermophys.*, 20(1):289–298, 1999. https://doi.org/10.1023/A:1021415305603.

[74] Hongyao Shen, Rongxin Deng, Bing Liu, Sheng Tang, and Shun Li. Study of the mechanism of a stable deposited height during GMAW-based additive manufacturing. *Applied Sciences*, 10(12):4322, 2020. https://doi.org/10.3390/app10124322.

[75] Andreas Hanssen Moltumyr, Mathias Hauan Arbo, and Jan Tommy Gravdahl. Towards vision-based closed-loop additive manufacturing: A review. In *2020 3rd International Symposium on Small-scale Intelligent Manufacturing Systems (SIMS)*, pages 1–6. IEEE, 2020. https://doi.org/10.1109/SIMS49386.2020.9121578.

[76] Jianhua Wang, Yuguo Zhou, and Yanxi Yang. 3-D measurement method for nonuniform reflective objects. *IEEE Transactions on Instrumentation and Measurement*, 69(11):9132–9143, 2020. https://doi.org/10.1109/TIM.2020.3001413.

[77] Rikke Gade and Thomas B Moeslund. Thermal cameras and applications: a survey. *Machine vision and applications*, 25(1):245–262, 2014. https://doi.org/10.1007/s00138-013-0570-5.

[78] Shigeru Takushima, Daiji Morita, Nobuhiro Shinohara, Hiroyuki Kawano, Yasuhiro Mizutani, and Yasuhiro Takaya. Optical in-process height measurement system for process control of laser metal-wire deposition. *Precision Engineering*, 62:23–29, 2020. https://doi.org/10.1016/j.precisioneng.2019.11.007.

[79] Sadek CA Alfaro and Fernand Díaz Franco. Exploring infrared sensoring for real time welding defects monitoring in GTAW. *Sensors*, 10(6):5962–5974, 2010. https://doi.org/10.3390/s100605962.

Publications

Additive manufacturing by robot manipulator: An overview of the state-of-the-art and proof-of-concept results

L. D. Evjemo, S. Moe, J. T. Gravdahl, O. Roulet-Dubonnet, L. T. Gellein, and V. Brøtan. Additive manufacturing by robot manipulator: An overview of the state-of-the-art and proof-of-concept results. In 22nd IEEE ETFA, Cyprus, pages 1-8, 2017.

ADDITIVE MANUFACTURING BY ROBOT MANIPULATOR: AN OVERVIEW OF THE STATE-OF-THE-ART AND PROOF-OF-CONCEPT RESULTS

Linn Danielsen Evjemo[1], Signe Moe[1], Jan Tommy Gravdahl[1], Olivier Roulet-Dubonnet[2], Lars Tore Gellein[2], and Vegard Brøtan[3].

***Abstract*— For the last decades, additive manufacturing (AM) has become an ever increasing part of the development of new technology and devices. However, it is still challenging to use this technology on a larger scale. This paper presents the state-of-the-art of large-scale AM, looking into some of the projects that have come furthest in utilising AM technology on large structures such as buildings or sculptures. The background for this research is to consider the possibility of large-scale AM by robot manipulator using the welding method cold metal transfer (CMT). After outlining the the necessary algorithms and components for such an AM system, a proof-of-concept experiment using a UR5 robot is presented. This initial experiment will clarify some of the challenges that need to be addressed in future work.**

I. INTRODUCTION

Additive manufacturing (AM) is an umbrella term for several specific techniques that primarily build up structures layer by layer, and which often go by names such as free-form fabrication, rapid prototyping (RP), or 3D-printing [1]. AM is the most general term, and will be used throughout this article. AM technology has made it easier for small companies and individual developers to make custom made parts at a reasonable price, and it has also made prototyping easier and less expensive. While AM has mostly been used for creating smaller parts for larger products or processes, the process has also been used to create small end products.

Typically, AM is time demanding for larger components. This is because the production layer size affects the roughness and accuracy of the constructed surfaces. With low layer thicknesses, the AM-machines are often restricted to small build volumes, as larger volumes tend to take an unreasonable amount of time. However, in many cases machining or other surface treatments are necessary to get the desired surface properties for the end product. In such parts where surface quality and detail are less important, it is possible to build quicker and bigger. For traditional AM-processes, this implies that the machines need to grow to a larger scale than the produced parts, which in any case would limit the build volume.

One way of enabling additive manufacturing of large-scale products "outside the box", is to combine AM with robotics. By using a robot manipulator to extrude a fast-curing material, gradually building up a larger structure, the workspace for the build would be massively expanded. Most of the flexibility for the shape and form of the final product that traditional AM-methods allows for should be kept or even improved, as parameters like build speed, layer thickness, and even nozzle size would allow for changing build speed between the general production and finer details. If the build material is metal, or some other very fast-curing material, the need for support structures could also decrease to the point of only relying on anchoring and stabilising. If necessary, it would also be possible to increase the flexibility of the building process itself, because the structure would no longer have to be built layer by layer from the bottom-up or top-down - which is necessary for most existing forms of AM. Several robot manipulators could potentially also work simultaneously, building with several different materials.

In this paper, we will present an overview of current approaches to AM by robot, as well as a novel concept of using an industrial robotic manipulator as a means for 3D-printing or AM. We will outline the necessary algorithms and components needed to realise such a system. The paper is organized as follows: In section II, an overview of the current approaches to large-scale AM by robot will be presented. In section III, we will explain our novel idea of AM by robot manipulator. A proof-of-concept experiment is presented in section IV, and the results as well as plans for future work are summarized in section V.

II. AN OVERVIEW OF CURRENT TECHNOLOGY

Several projects are already working on realising robotised AM, both with generic materials like plastic or cement, and with metal. Most of these projects are initiated by private businesses, but there are also a few universities working on this kind of technology.

One way of creating large structures through AM methods is by splitting the final product into smaller parts that can be 3D-printed, and then assemble the pieces afterwards. This has been done for example for the 3D Elephant Petition [2], Total Kustom's concrete castle [3], and to some extent the Dragon Bench from Joris Laarman Lab [4].

[1]Linn Danielsen Evjemo, Signe Moe, and Jan Tommy Gravdahl are with the Department of Engineering Cybernetics, NTNU, Trondheim, Norway {linn.d.evjemo, signe.moe, jan.tommy.gravdahl}@ntnu.no

[2]Olivier Roulet-Dubonnet and Lars Tore Gellein are with SINTEF Raufoss Manufacturing AS, Trondheim, Norway {Olivier.Roulet-Dubonnet, Lars.Tore.Gellein}@sintef.no

[1]Vegard Brøtan is with the Department of Mechanical and Industrial Engineering, NTNU, Trondheim, Norway {vegard.brotan}@ntnu.no

Fig. 1. **3D Elephant Petition:** The pieces that make up the 3D-printed elephant sculpture were made by five traditional Ultimaker 3D-printers. Each of these printers were given an extended degree of freedom by connecting them to a rail that moved vertically, which made it possible to print pieces that were up to 2.5 meters tall. Photo: www.rooiejoris.nl [2].

Fig. 2. **Concrete Castle:** This castle was built in cement in 2014 using Total Kustom's AM technology. This was their first large project, and the structure was therefore built piece by piece, and then assembled afterward. Photo: www.totalkustom.com [12].

Fig. 3. **Apis Cor House:** The robot manipulator used in their project is similar to a tower crane, with a workspace in a circular area around its base. Photo: www.totalkustom.com [14].

The 3D Elephant Petition, created by Joris van Tubergen in 2014, took traditional 3D-printing one step further in the process of 3D-printing large structures "outside-the-box". As part of an art project, he created a life-scale 3D-printed elephant sculpture over the course of two weeks. He did this by combining five Ultimaker 3D printers with his own add-on called Z-Unlimited [5]. This add-on allowed each printer to move over 2.5 meters vertically while printing horizontally. This extended degree of freedom enabled the system to print structures that were over 2.5 meters tall. The remaining dimensions for each piece were still limited to the dimensions of the Ultimaker 3D-printer's original workspace. Even though the 3D-printed pieces were larger than what what a standard Ultimaker 3D-printer can produce, the final structure shown in figure 1 had to be assembled manually.

In 2006, two researchers from Cornell University developed and released an open-source, low-cost print-at-home system called Fab@Home [6]. This was done in an effort to make AM technology more available for developers, and encourage the invention of new technology. This was a three-axis gantry positioning system that used a syringe-based extrusion tool to do material extrusion along a translation-only path. The printer was designed so that it was possible to use a great variety of materials, for instance RTV silicone rubber, epoxy, and even chocolate. Model 2 was released in 2009, with improvements like a more versatile material extrusion system, as well as a price reduction due to changes in the electronics and mechanics [7].

The company Total Kustom are working on large-scale 3D-printing of houses, as part of an effort to help the construction of more affordable housing. They have 3D-printed large structures of cement with their own 3D Concrete Printing Technology, like the concrete castle that was built in 2014 [3], shown in figure 2. Their first construction was printed piece by piece, and then assembled manually. The castle was build using a cement mix, and the layers were 10 mm in height and 30 mm in width [8]. The project later 3D-printed an entire hotel suite, this time in one piece [9]. According to their website, they are now going into production of the first commercially available 3D Concrete Printers [10]. The largest models will have a workspace of approximately 150 m^2, and build structures that are up to 12 m tall, with an average printing speed of 100 m^2 in area and 3 m height in 48 hours [11].

Apis Cor company recently managed to 3D-print a complete house in Moscow Region, using a self-developed mobile system for AM. They used a concrete mixture as building material, and built using a robot manipulator similar to a tower crane, as shown in figure 3. Their printer weighs around 2 tonns, has a maximum working area of 132m^2 in a circular area around the base, and can build structures that are up to 3300 mm tall [13]. The printer uses the traditional bottom-up approach, and deposits material layer by layer. The printed house was 38 m^2, and built in 24 hours of machine printing time [14].

Large-scale AM with a cable-suspended robot has also been tested, with promising results. In 2015, researchers from the University of Laval in Canada used AM to build a life-size foam statue of Sir Wilfrid Laurier, the seventh Prime Minister of Canada [15]. They used a 6 degrees of freedom (DOF) cable-suspended robot in the process, a type of robot that is attached to a mobile platform or end effector by

multiple cables. The final statue was about $215 \times 550 \times 620$ mm large, printed with material laid out in a path that was 10 mm tall and 12 mm wide. The whole print was done with the end-effector pointing in the same direction, making this a translation-only build. For traditional 3D-printers, this type of print would be possible with only 3 DOFs, because the end-effector's orientation never changes. However, for a cable-suspended robot, 6 DOFs are necessary to keep the orientation of the end effector unchanged. This project was inspired by the work done by researchers from Ohio University in 2007, who created a cable-suspended contour crafting system. Their motivation was that building large structures with a gantry robot, a large overhanging system covering the whole work area, is difficult because the robot must be extremely large, heavy, and difficult to move around. A cable-suspended system also has to be larger than the structure it is building [16], but it is more mobile because the cable frame is much lighter than a complete gantry robot system. Still, a gantry robot-system is much more accurate than a cable-system.

The Norwegian company Norsk Titanium (NTi) has developed a method for cost-efficient AM of titanium airplane parts. Traditionally, titanium parts are created by subtracting material from a large, wrought titanium block until the desired shape is achieved using a 3 axis manipulator in a confined box with inert gas. Components that require a lot of machining becomes more costly and produces much more waste compared to NTis method. By fusing titanium wire together in an atmosphere of argon gas, NTi are able to build up titanium parts layer by layer [17]. Even though this process demands that the AM parts are machined afterwards, this process saves both time and material. NTi's system currently has a workspace of $120 \times 120 \times 180$ cm [18], which is quite large compared to traditional 3D-printers.

One of the projects that has come furthest in combining AM and robotics, is the work done by Joris Laarman Lab. They have moved, step by step, from using AM as a design tool and over to building structures directly with AM methods. Early projects like the Bone Chair from 2006 [19] used AM to create complex molds for design furniture that were to be casted in one piece [20].

The MX3D Metal printer must be the most exciting thing to come out of Joris Laarman Lab yet. This was a further development of the Mataerial project from 2012 [21], where a 6 DOF industrial robot manipulator was used to deposit material along a pre-designed trajectory. The Mataerial project was a collaboration between Joris Laarman Lab and the Institute of Advanced Architecture of Catalonia (IAAC), and resulted in a patented AM method for building fast-curing thermoplastic in any direction: no longer limited to the top-down or bottom-up approach. This made it possible to build almost any kind of structure, with no need for support or underlying layers, like shown in figure 4.

By combining the industrial robot manipulator as used in the first Mataerial project with an advanced welding machine, Joris Laarman Lab were able to build structures in metals such as steel, aluminium, bronze, stainless steel, and copper.

Fig. 4. **Mataerial project:** Combining an industrial manipulator with a fast-curing plastic makes it possible to "print" double curved lines in mid-air. Photo: www.mataerial.com [21].

Fig. 5. **Butterfly Screen:** This 2×3 meter large double-curved bronze screen is built by an industrial robot manipulator using the MX3D AM technology. Photo: www.jorislaarman.com [23].

This robot is able to build double-curved lines in midair by depositing small amounts of molten metal at a time. The Dragon bench from 2014 was built piece by piece, and later welded together manually [4]. The Butterfly Screen on the other hand, shown in figure 5, is a 2×3 meter large double curved bronze structure that was built as a whole using the MX3D AM technology. Joris Laarman Lab are aiming to create an AM system that can eventually print structures directly from Computer Aided Design (CAD). MX3D have announced that they plan to use their AM method to build a one-piece, fully functional steel bridge sometime in 2017. The structure will be built at a work-site near their offices in Amsterdam, and will be placed across the Oudezijds Achterburgwal Canal [22].

III. AM USING CMT BY 6 DOF ROBOT MANIPULATOR

Our research plan on using a robot manipulator to do AM in metal. More specifically, the aim is to use the welding

method Cold Metal Transfer (CMT) to deposit metal along a given trajectory, building the final metal structure gradually as the manipulator tracks this reference trajectory. CMT is a metal inert gas (MIG) process which is modified so that the motions of the wire is integrated in the welding process. The need of an extra electromagnetic force is removed by using a wire retraction motion to help the metal droplet detachment. This means that both heat input and spatter can be decreased compared to other MIG methods [24]. CMT was chosen over other welding methods due to its high quality string, which is expected to be a decisive factor in additive manufacturing based on welding.

Mounting it on an industrial 6 DOF robot was a logical choice to enable building large objects. Combining CMT welding with robotised AM has the potential to build metal structures from scratch, not just perform robotised welding. However, this technology could also be useful in repair work, for example when needing to close holes and tears in large metal surfaces on ships or other large structures. The usual argument against industrial robots for AM is their limited precision, but metal welding is a comparatively rough process, so robot precision is not expected to be the limiting factor for product quality. AM by robot manipulator would free us from having to build structures layer by layer, which makes it possible to print more complex geometries. Being able to print in any direction may also make it possible to design more efficient path planning algorithms, which can potentially save both time and money.

In order to create a system for CMT-focused robotised AM, there are several problems that need to be solved. Path planning algorithms must be designed, planning the path the robot should follow while depositing material. These should be designed so that they can be used for a number of different building materials, as it will be useful to run tests with materials that are easier to deposit than metal. Control algorithms for the robot manipulator should be improved to account for feedback from the build process and the deposited material. The control algorithms will have to rely upon the properties of the given material, the thickness of the material line that is deposited, and on how fast the material hardens. It is therefore necessary to consider the time aspect, i.e. how fast it is possible to deposit the material, and how long it will take to build the complete structure.

Methods for collision avoidance must also be included in the system, something that might prove especially challenging if the system is to deviate from the standard bottom-up or top-down building approach. Throughout the process, it will be necessary to create experiment(s) with robot manipulator and deposition of material in order to test the control algorithms that are designed.

IV. PROOF OF CONCEPT EXPERIMENT

Building on our previous experience with robotic set ups [25], a small-scale proof-of-concept experiment was designed. After considering alternatives like a glue gun, or even the print head of a traditional 3D-printer, a caulking gun of the type *Juniorfix* from Würth was chosen to deposit material.

Fig. 6. **Experiment set-up:** A caulking gun driven by compressed air is connected in parallel to the end effector of a UR-5 robot arm.

This alternative was deemed the best choice for a small-scale, initial experiment like this. In addition, the different materials that were available for the caulking gun had properties that made them better suited than for instance hot glue. These materials were typically less liquid than hot glue, and would behave in a more manageable way. The layers of hot glue would for instance just blend into each other if the layers were deposited too close together, and too quickly. The idea of using the print head of a 3D-printer was discarded partly because it would complicate the experimental set-up, and partly because it was necessary to have the opportunity to extrude more material at once than what one can expect with a traditional 3D-printer. A 3D-printer would almost certainly have been able to build a more accurate structure, but the main requirement of this experiment was build-time and simplicity, not accuracy.

The caulking gun was driven by compressed air, which created a smooth and constant flow of material once the pressure was turned on. The flow of compressed air was controlled by a valve that had to be operated manually. The material used was STP Quickfast from Würth, which is a type of fast-hardening, viscous glue. The caulking gun was fastened to the end of a UR-5 robot as shown in figure 6, with the nozzle parallel to the end effector of the robot arm. The trigger button of the caulking gun was strapped in place so that the extrusion of material was controlled directly by supplying compressed air. Because the nozzle was circular, the extruded material also had a circular cross-section, and the diameter was set by changing the diameter of the nozzle.

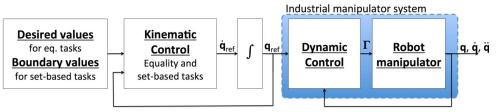

Fig. 7. **Control structure of the system:** The control algorithm is implemented in the block for kinematic control. Figure from [25].

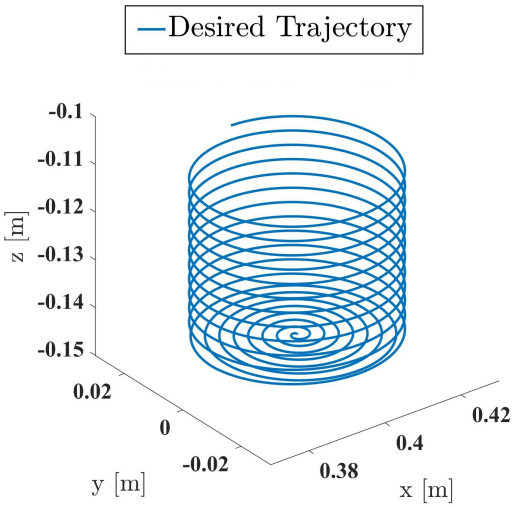

Fig. 8. **UR5 Trajectory:** Here we see a plot of the trajectory the robot's end effector should follow while depositing material along its path.

A. TRAJECTORY DESIGN

The goal of the experiment was to construct a small cup, and the trajectory was designed such that the robot motion was continuous also as the nozzle moved upwards while printing the sides of the cup. This already deviates from traditional AM methods, which as a norm build one layer at a time and then move up (or down) a certain height before printing the next layer. This added flexibility can potentially allow for a more efficient building process in terms of both time and energy.

Each point on the spiral trajectory is expressed in cylindrical coordinates θ, r, and z. We define h as the height difference between each layer of the cup size, and r_1 as the horizontal distance between each layer of the bottom. H is the desired final height of the structure, and R is the desired radius of the final structure. All of these variables are given in meters. r and z are defined as functions of θ:

$$r(\theta) = \begin{cases} \frac{r_1}{2\pi}\theta & \theta \leq \frac{R}{r_1}2\pi \\ R & \theta > \frac{R}{r_1}2\pi \end{cases} \tag{1}$$

$$z(\theta) = \begin{cases} 0 & \theta \leq \frac{R}{r_1}2\pi \\ \frac{h}{2\pi}(\theta - \frac{R}{r_1}2\pi) & \theta > \frac{R}{r_1}2\pi \end{cases} \tag{2}$$

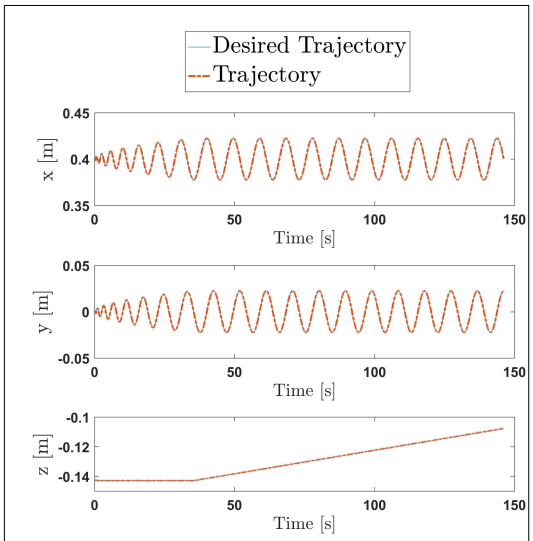

Fig. 9. **Translation error:** Here we see the desired x-, y-, and z-position plotted together with the actual position of the robot manipulator's end effector during one of the builds. The Cartesian coordinates are given in the robot frame.

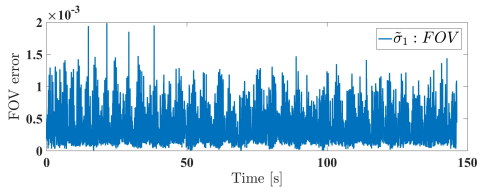

Fig. 10. **Field-of-view error:** The registered error between the actual field-of-view and the desired field-of-view is less than 2×10^{-3}.

Thus, the time-derivatives of r_1 and z are given by:

$$\dot{r}(\theta) = \begin{cases} \frac{r_1}{2\pi}\dot{\theta} & \theta \leq \frac{R}{r_1}2\pi \\ 0 & \theta > \frac{R}{r_1}2\pi \end{cases} \tag{3}$$

$$\dot{z}(\theta) = \begin{cases} 0 & \theta \leq \frac{R}{r_1}2\pi \\ \frac{h}{2\pi}\dot{\theta} & \theta > \frac{R}{r_1}2\pi \end{cases} \tag{4}$$

where $\dot{\theta}$ is defined as:

$$\dot{\theta} = \begin{cases} \frac{2\pi U}{r_1\sqrt{\theta^2+1}} & \theta \leq \frac{R}{r_1}2\pi \\ \frac{U}{\sqrt{R^2+\frac{h}{2\pi}^2}} & \theta > \frac{R}{r_1}2\pi \end{cases} \tag{5}$$

$\dot{\theta}$ is chosen such that the end effector velocity along the trajectory is constant and equal to the desired velocity U, which is necessary for even deposition of the printing

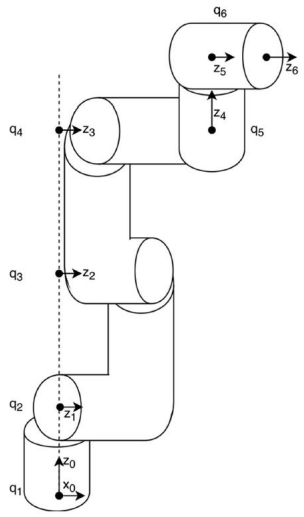

Fig. 11. **UR 5 Manipulator:** Here we see the coordinate frames assigned to the robot's joints, which is the foundation for the Denavit-Hartenberg parameters presented in table I. Figure from [25].

TABLE I
DENAVIT-HARTENBERG PARAMETERS FOR UR5, FOUND IN [26].

Joint	$\mathbf{a}_i$ **[m]**	α_i **[rad]**	$\mathbf{d}_i$ **[m]**	θ_i **[rad]**
1	0	$\frac{\pi}{2}$	0.089	q_1
2	-0.425	0	0	q_2
3	-0.392	0	0	q_3
4	0	$\frac{\pi}{2}$	0.109	q_4
5	0	$-\frac{\pi}{2}$	0.095	q_5
6	0	0	0.082	q_6

material.

Figure 8 shows the designed trajectory the robot's end effector should follow. In figure 9 we see the desired x-, y-, and z-coordinates plotted together with the actual coordinates from the robot, and in figure 10 we see the error of the field-of-view σ_{fov}, defined in (14).

B. ROBOT CONTROL

In this experiment, a UR-5 robot with 6 DOFs was used. Its configuration is given by $q = [q_1, q_2, q_3, q_4, q_5, q_6]^T$, q_i being the joint variables. The Denavit-Hartenberg parameters are shown in table I, and the coordinate frame can be seen in figure 11. It was necessary to control the end effector position to track the desired trajectory and the direction of the end effector to deposit material at a constant orientation. This can be formalised as a task variable $\sigma \in \mathbb{R}^n$, which is defined as:

$$\sigma(t) = \begin{bmatrix} x \\ y \\ z \\ \sigma_{fov} \end{bmatrix} = f(q(t)) \tag{6}$$

The variable σ_{fov} is the error in the *field-of-view*, the vector pointing straight out of the end effector (z_6-axis in figure 11). The task variable differentiated with respect to time is given by:

$$\dot{\sigma}(t) = \frac{\delta f(q(t))}{\delta q}\dot{q}(t) = J(q(t))\dot{q}(t) \tag{7}$$

where $J(q(t)) = \frac{\delta f}{\delta q}$ is the Jacobian, and $\dot{q}(t)$ is the system velocity. The desired behavior of the robot is defined by σ_{des}. However, the robot is controlled in joint space, so an inverse kinematics approach is necessary to find the corresponding movement in joint space. It is proven that if the joint velocities track $\dot{q}_{des}$ as defined below, the task variable σ will converge asymptotically to σ_{des} [27]:

$$\dot{q}_{des} = J^{\dagger}\dot{\sigma}_{des} = J^{\dagger}(\dot{\sigma}_{des} + \Lambda\tilde{\sigma}) \tag{8}$$

where $\tilde{\sigma}$ is the task error, defined as:

$$\tilde{\sigma} = \sigma_{des} - \sigma \tag{9}$$

and Λ is a positive definite matrix of gains. $J^{\dagger}$ is the right psudoinverse of J, which is the matrix satisfying the four Moore-Penrose conditions [28], J^* being the complex conjugate of J:

$$JJ^{\dagger}J = J \tag{10}$$

$$J^{\dagger}JJ^{\dagger} = J^{\dagger} \tag{11}$$

$$(JJ^{\dagger})^* = JJ^{\dagger} \tag{12}$$

$$(J^{\dagger}J)^* = J^{\dagger}J \tag{13}$$

The desired geometric trajectory that the end effector should follow, are given by the Cartesian coordinates that make up the first part of (6): $[x_{des}, y_{des}, z_{des}]^T$.

For the last element of (6), $\sigma_{fov,des}$, we control the *error* of the field-of-view, which is defined as:

$$\sigma_{fov} = \sqrt{(a_{des} - a)^T(a_{des} - a)} \tag{14}$$

where a is the current orientation of the end effector, which corresponds to the vector z_6 in figure 11, and a_{des} is the desired orientation. Because the field of view should be straight downwards, $a_{fov,des}$ is:

$$a_{fov,des} = \begin{bmatrix} 0 \\ 0 \\ -1 \end{bmatrix} \tag{15}$$

We wish for the error between the actual and the desired orientation to be zero:

$$\sigma_{fov,des} \equiv 0$$

$$\dot{\sigma}_{fov,des} \equiv 0$$

To express the desired end effector position in Cartesian coordinates, we rewrite the trajectory given in cylindrical coordinates (1)-(2) through the following transformation:

$$\begin{aligned} x_{des} &= r(\theta)\cos\theta \\ y_{des} &= r(\theta)\sin\theta \\ z_{des} &= z(\theta) \end{aligned} \tag{16}$$

Thus, the time derivatives are given as:

$$\begin{aligned} \dot{x}_{des} &= \dot{r}(\theta)\cos\theta - r(\theta)\sin\theta\dot{\theta}(\theta) \\ \dot{y}_{des} &= \dot{r}(\theta)\sin\theta + r(\theta)\cos\theta\dot{\theta}(\theta) \\ \dot{z}_{des} &= \dot{z}(\theta) \end{aligned} \tag{17}$$

where $\dot{r}$, $\dot{z}$, and $\dot{\theta}$ are defined in (3)-(5). Thus, the commanded joint velocity is defined in (8) with $\sigma_{des} = [x_{des}, y_{des}, z_{des}, 0]^T$ and $\dot{\sigma}_{des} = [\dot{x}_{des}, \dot{y}_{des}, \dot{z}_{des}, 0]^T$. We find the desired joint configuration q_{des} by numerically integrating $\dot{q}_{des}$, and send this to the UR-5 dynamic controller via TCP-IP. This built-in controller ensures that the reference is tracked.

C. Results

Material properties such as viscosity and density of the material used in this initial experiment put a height constraint on the structure to be built. In fact, the structure would collapse in on itself if it was built much taller than a critical height of a few centimetres. It was also necessary to adjust the vertical velocity of the nozzle. By reducing the height difference between layers, thereby making the nozzle press each layer down slightly while moving along the trajectory, the area of the contact surface between each layer was increased. This made the structure more stable, and less likely to collapse in on itself. This coincides with the approach chosen by Total Kustom, who also built layers that were three times wider than they were tall when printing the Concrete Castle [8]. Even with this modification, it was difficult to build steady structures that were taller than approximately 4 cm with the material that was used in our proof-of-concept experiment.

The beginning and end of the build was the most challenging part of the experiment. As mentioned, the extrusion of material was controlled by supplying compressed air to the caulking gun. Because the compressed air was controlled by a valve that had to be turned manually, turning the air on and off was a continuous process. The dynamics of this process greatly influence the flow of material. When turning the compressed air on, this meant that it was necessary to begin turning the valve approximately 10 seconds before the caulking gun would actually begin extruding material. In addition, the extrusion of material would change gradually, first extruding a small amount of material quite slowly, and then extruding more material quite quickly, depending on how much compressed air that was added. It seems reasonable that this extrusion process could be modelled by a time delay in series with a first or second order process.

When the build reached its end, it was also challenging to stop the extrusion of material. Naturally, the stopping process was also continuous, so it was necessary to time when to start closing the valve. If the valve was turned too early, so that the amount of material that was extruded was reduced while the robot was still following the build trajectory, the material would not adhere properly to the previous layer. Instead, it would be dragged after the manipulators end effector, pulling on the walls of the built structure, and this way increase the chances of the structure collapsing. When the valve was turned later, the caulking gun would still be depositing material when the end effector moved away from the build. Still, this was considered the best approach. The excess material was removed manually from the final structure straight after the build was done.

Fig. 12. **Test results:** The experimental work resulted in these small cups. It is evident that the width of the printed material, along with the height of the structure and the speed of the material deposition, are all important elements for the final result.

In summary, there are a number of parameters that was found to greatly influence the end result. Material properties such as density, viscosity and adhesiveness are important, but also the properties of the reference trajectory and the dynamics of the actuator, in this case the pressure controlled caulking gun, play a major role.

V. CONCLUDING REMARKS

The initial proof-of-concept experiment along with the state-of-the-art review presented in this paper has shown that large-scale AM by robot manipulator is indeed possible, and has helped show some of the problem areas that need to be addressed in future work. Increasing the contact surface between each layer proved to be very helpful in order to increase the stability of the structure, and this will be necessary to include in later experiments. In the initial experiment, we achieved a larger contact surface by decreasing the height of each layer to make the nozzle press each layer down. A larger contact surface can also be achieved by changing the geometry of the nozzle, for example making it flat and elliptic, or even rectangular. Which approach to go for should be based on the material that is used, and on what kind of structure one is trying to build.

The starting and stopping point of the build will be challenging, especially when the extrusion of material is not controlled by a simple on/off-mechanism. It should therefore be a goal to create a better control mechanism for the flow of material. Even if it is not possible to stop or start the material flow momentarily, it might be possible to adjust the movement of the robot manipulator so that it works better with the material flow, for example making it slow down when it is close to the end.

In future work, a complete, full-scale system for AM by robot manipulator needs to have some way of monitoring the process, and to give feedback on whether or not the build is

going as planned. What is expected to be a decisive aspect for robotised AM using CMT is the ability to compensate in real time for local welding defects such as local string collapse, and geometrical deviations from the building plan. In order to create an efficient system it will be necessary to design the control algorithms so that the system is able to compensate and correct weaknesses due to inaccuracies earlier in the build process. This initial experiment had a translation-only based trajectory, but in future experiment there should be more focus on the fact that the orientation of the robot's end effector can be controlled. The UR5 robot has 6 DOFs, which means that the manipulator can reach every point in its workspace with arbitrary orientation.

ACKNOWLEDGMENTS

The work reported in this paper was based on activities within centre for research based innovation SFI Manufacturing in Norway, and is partially funded by the Research Council of Norway under contract number 237900.

REFERENCES

[1] I. Gibson, D. W. Rosen, B. Stucker, *et al.*, *Additive manufacturing technologies*. Springer, 2010, vol. 238.

[2] rooiejoris.nl/"3D Elephant Petition", "3d elephant petition," 2015, accessed 2017-03-23. [Online]. Available: http://www.rooiejoris.nl/3d-elephant-petition/

[3] totalkustom.com/"News", "Total kustom news," 2014-2017, accessed 2017-03-26. [Online]. Available: http://www.totalkustom.com/news.html

[4] mx3d.xom/"Dragon Benches", "Mx3d - dragon benches," 2015, accessed: 2017-03-22. [Online]. Available: http://mx3d.com/projects-2/

[5] rooiejoris.nl/"Z Unlimited", "Z-unlimited," 2015, accessed 2017-03-23. [Online]. Available: http://www.rooiejoris.nl/z-unlimited/

[6] E. Malone and H. Lipson, "Fab@ home: the personal desktop fabricator kit," *Rapid Prototyping Journal*, vol. 13, no. 4, pp. 245–255, 2007.

[7] J. I. Lipton, D. Cohen, M. Heinz, M. Lobovsky, W. Parad, G. Bernstien, T. Li, J. Quartiere, K. Washington, A. Umaru, *et al.*, "Fab@ home model 2: Towards ubiquitous personal fabrication devices," in *Solid Freeform Fabrciation Symposium*, 2009.

[8] totalkustom.com/"3D Castle Completed", "Total kustom 3d castle completed," 2014-2017, accessed 2017-04-03. [Online]. Available: http://www.totalkustom.com/3d-castle-completed.html

[9] 3dprint.com/"3D-printed hotel suite", "3d-printed hotel suite," 2015, accessed 2017-03-27. [Online]. Available: https://3dprint.com/94558/3d-printed-hotel-lewis-grand/

[10] totalkustom.com/"Business Opportunities", "Total kustom business opportunities," 2014-2017, accessed 2017-03-26. [Online]. Available: http://www.totalkustom.com/business-opportunities.html

[11] 3dprint.com/"3D Concrete House Printer", "3d printer pre-order," 2017, accessed 2017-04-03. [Online]. Available: http://www.totalkustom.com/pre-order.html

[12] totalkustom.com/"Rudenko's 3D Printer", "Total kustom rudenko's 3d-printer," 2014-2017, accessed 2017-03-27. [Online]. Available: http://www.totalkustom.com/rudenko-s-3d-printer.html

[13] apis-cor.com/"ApisCor Bookbuyer", "Apis cor we print buildings," 2016, accessed 2017-04-02. [Online]. Available: http://apis-cor.com/files/ApisCor_BookBuyer_en.pdf

[14] apis-cor.com/"The first on-site house has been printed in Russia", "The first on-site house has been printed in russia," 2017, accessed 2017-04-02. [Online]. Available: http://apis-cor.com/en/about/news/first-house

[15] E. Barnett and C. Gosselin, "Large-scale 3d printing with a cable-suspended robot," *Additive Manufacturing*, vol. 7, pp. 27–44, 2015.

[16] P. Bosscher, R. L. Williams, L. S. Bryson, and D. Castro-Lacouture, "Cable-suspended robotic contour crafting system," *Automation in Construction*, vol. 17, no. 1, pp. 45–55, 2007.

[17] norsktitanium.com/"Norsk Titanium Technology", "Norsk titanium technology," 2015, accessed 2017-03-29. [Online]. Available: http://www.norsktitanium.com/wp-content/uploads/2016/07/Norsk_Titanium_Technology.mp4?_=1

[18] 3dprintingindustry.com/"US to Open Large-Scale Metal 3D-Printing Facility with Norsk Titanium", "Us to open large-scale metal 3d-printing facility with norsk titanium," 2015, accessed 2017-03-29. [Online]. Available: https://3dprintingindustry.com/news/us-to-open-large-scale-metal-3d-printing-facility-with-norsk-titanium-54236/

[19] Marcus Fairs, "Joris laarman works with opel," 2006, accessed: 23-06-2017. [Online]. Available: https://www.dezeen.com/2006/12/27/joris-laarman-works-with-open/

[20] jorislaarman.com/"Arm Chair", "Arm chair," 2015, accessed: 23-06-2017. [Online]. Available: http://www.jorislaarman.com/work/arm-chair/

[21] mataerial.com/"Gravity-Neutral 3D Printing", "Mataerial," 2013-2016, accessed 2016-12-13. [Online]. Available: http://www.mataerial.com/

[22] mx3d.com/"Bridge", "Mx3d bridge," 2015, accessed 2017-03-27. [Online]. Available: http://mx3d.com/projects/bridge/

[23] jorislaarman.com/"Butterfly Screen", "Butterfly screen," 2016, accessed 2017-03-27. [Online]. Available: http://www.jorislaarman.com/work/butterfly-screen/

[24] H. Zhang, J. Feng, P. He, B. Zhang, J. Chen, and L. Wang, "The arc characteristics and metal transfer behaviour of cold metal transfer and its use in joining aluminium to zinc-coated steel," *Materials Science and Engineering: A*, vol. 499, no. 1, pp. 111–113, 2009.

[25] S. Moe, G. Antonelli, A. R. Teel, K. Y. Pettersen, and J. Schrimpf, "Set-based tasks within the singularity-robust multiple task-priority inverse kinematics framework: General formulation, stability analysis, and experimental results," *Frontiers in Robotics and AI*, vol. 3, p. 16, 2016.

[26] Universal Robots, "Actual centre of mass for robot," 2016, accessed 2017-04-06. [Online]. Available: https://www.universal-robots.com/how-tos-and-faqs/faq/ur-faq/actual-center-of-mass-for-robot-17264/

[27] G. Antonelli, G. Indiveri, and S. Chiaverini, "Prioritized closed-loop inverse kinematic algorithms for redundant robotic systems with velocity saturations," in *Intelligent Robots and Systems, 2009. IROS 2009. IEEE/RSJ International Conference on*. IEEE, 2009, pp. 5892–5897.

[28] G. H. Golub and C. F. Van Loan, *Matrix computations*. JHU Press, 2012, vol. 3.

Wire arc additive manufacturing by robot manipulator: Towards creating complex geometries

L. D. Evjemo, G. Langelandsvik, and J. T. Gravdahl. Wire arc additive manufacturing by robot manipulator: Towards creating complex geometries. In 5th IFAC ICONS, Belfast, pages 103-109, 2019.

Available online at www.sciencedirect.com

ScienceDirect

IFAC PapersOnLine 52-11 (2019) 103–109

IFAC Papers Online CONFERENCE PAPER ARCHIVE

Wire Arc Additive Manufacturing by Robot Manipulator: Towards Creating Complex Geometries

Linn Danielsen Evjemo *, **Geir Langelandsvik** **, **Jan Tommy Gravdahl** ***

* *Department of Engineering Cybernetics, NTNU, Trondheim, Norway (e-mail: linn.d.evjemo@ntnu.no)*

** *SINTEF Industry, Trondheim, Norway (e-mail: geir.langelandsvik@sintef.no)*

*** *Department of Engineering Cybernetics, NTNU, Trondheim, Norway (e-mail: jan.tommy.gravdahl@ntnu.no)*

Abstract: Additive manufacturing (AM) is the umbrella term that covers a variety of techniques that build up structures layer-by-layer as opposed to machining and other subtracting methods. It keeps evolving as an important technology in prototyping and the development of new devices. However, using AM on a larger scale is still challenging, as traditional methods require the AM machines to be larger than the manufactured structure. The research presented in this paper is a continuation of our work on assessing the possibility of large-scale robotic AM. The focus in this paper is the feasibility of large-scale AM of metallic materials by arc welding. A series of experiments with robotic arc welding using an ABB IRB2400/10 robot are presented and discussed. These experiment will help map some of the challenges that need to be addressed in future work.

Keywords: Additive manufacturing, manufacturing systems, robot programming, wire arc additive manufacturing, aluminium alloys, Inconel alloys

1. INTRODUCTION

Traditional methods for additive manufacturing (AM) require the AM apparatus to be larger than the component it is producing. This puts great limitations on the volume of the structures that can be built, as it is only practical to extend the size of the machine up to a point. These AM techniques also mainly use a strictly layer by layer approach in the building process, either top-down or bottom-up, making it impossible to build overhangs without including additional support structures that must later be removed. Combining deposition of material with the flexibility of a 6 degrees-of-freedom (DOF) robot manipulator could drastically increase the workspace. If the material was fast-curing, like that of the MX3D Resin project (Jorislaarman.com, 2015-2018), a 6 DOF robot manipulator could deposit material in almost any direction. This would make it possible to move away from the layer-wise approach, and thereby remove the need for support structures when building more complex shapes, which could potentially help save both time and money.

The experiments presented in this paper build on our earlier work with AM by robot manipulators (Evjemo et al., 2017), where necessary algorithms and components for a system combining AM methods and a robot manipulator were outlined. Some initial experiments were done, using a 6 DOF UR-5 robot combined with an air-pressure driven caulking gun and a relatively fast-curing adhesive. This apparatus was used to build a simple cup-structure in a spiralling trajectory, moving away from the layer-wise approach. This work showed that AM by robot manipulator is indeed possible, and mapped some of the challenges that had to be addressed in future work. A state-of-the-art review of large-scale AM was also presented in this paper (Evjemo et al., 2017), showing the increased interest in different forms of large-scale AM: Spanning from how AM technology can be used to construct buildings (Apiscor.com, 2017) or bridges (Mx3d.com/"Bridge", 2017), to how the technology can be used creatively in art and design.

AM of metallic materials by arc welding could be useful in a variety of industries, and has the potential to not only perform robotised welding but to build metal structures from scratch. In this paper the focus is therefore on wire arc additive manufacturing (WAAM), with a special focus on the modified metal inert gas welding method cold metal transfer (CMT). CMT is well-suited for WAAM due to a more stable arc reducing metal splattering (so-called 'fireworks'), and a reduced heat input refining the deposited micro-structure and reducing residual stresses and distortion (Cong et al., 2016). Two sets of experiments are presented in this paper: Building a thin-walled, quadratic box, and building a more complex box-shape with challenges related to intersections within layers. An important objective for the experiments was to make the build as continuous as possible, as this could both save time and make the structure less prone to deformations. As with the experiment in (Evjemo et al., 2017), the robot

10.1016/j.ifacol.2019.09.125

Fig. 1. **Experimental set-up:** ABB IRB2400/10 robot manipulator with welding equipment from Fronius.

path is based on translation-only motions, the orientation of the welding gun staying fixed.

2. AM WELDING EXPERIMENTS BY 6 DOF ROBOT MANIPULATOR

In collaboration with SINTEF Industry, experiments were done using a 6 DOF IRB 2400/10 robot manipulator from ABB Robotics (Abb.com, 2016-2018). Attached to the robot's end effector was a metal inert gas (MIG) weld gun using the CMT technology developed by Fronius. This was partially controlled by the program running on the robot, though some settings had to be adjusted manually. The experimental set-up is shown in fig. 1. The robot path could be programmed manually with the robot control pad, or using the programming language RAPID. Testing was done in the simulation software RobotStudio from ABB.

2.1 Experiment 1: Thin-walled, quadratic box

AM of larger components is traditionally very time consuming due to slow deposition of material relative to the size of the final component. To make AM by robot as efficient as possible, it was of interest to assess the effects of a continuous build, and to avoid a strictly layer-wise build with a wait time between each layer. The structure in the initial welding experiment was geometrically very simple: A 10×10 cm^2 square-box built on a horizontal surface, as shown to the left in fig. 2. The aim was initially to test how a structure built by continuous welding would correspond to the heat development during prolonged deposition, and examine the visual appearance after deposition in terms of irregularities and distortions. Arc initiation and termination create uneven material deposition during WAAM, as reported by (Martina et al., 2012). Therefore, it was desirable not to have breaks during the welding process.

Manual programming: The first welding experiments were done by manually programming the path using the robot's control pad. The structure was welded onto a metal surface of AA6082 T6 rolled aluminium plate, from hereon referred to as the base, and the welding material was the aluminium-silicon alloy AA4047 in Ø1.2 mm wire form. The path was created by manually jogging the robot to each of the four corners of a square with the correct dimensions and saving these corner positions. Using a variation of the RAPID-function MoveL (ABB Robotics, 2004-2010), the robot was programmed to move linearly between these corners.

Fig. 2. **Square-box:** Smoother layer transitions, blunter corners and longer sides clearly improved the visual appearance of the structure.

The distance from the tip of the welding gun to the base was approximately 12 mm. The estimated height of each deposited welding bead, from hereon referred to as the layer height, was set to 1.8 mm. The robot's end effector would move vertically one layer height at the end of each layer. The amount of deposited material was determined by the wire-feed speed, as well as the welding gun's travel speed along its path. The travel speed was set to 9 mm/second, and this value was kept throughout the experiments. The first square-box build was done welding with a current of 62 A. The resulting structure is shown to the left in fig. 2, where the corner closest to the camera is the starting point, and the transition point between layers.

RobotStudio: In the second experiment, the path was programmed using the programming language RAPID, and simulated in RobotStudio. The square-box dimensions were changed from 10×10 cm^2 to 12×12 cm^2, which implied a longer deposition distance in each layer, yielding a longer cooling time of the deposited material. This could in turn reduce distorting and overheating in the built components.

In the first experiment there was an issue with accumulation of material in the point of the vertical height increase, as can be seen in fig. 2. The transition between layers were therefore modified: Instead for a vertical movement in a single point, the height increase was spread over a slope of two centimetres at the end of each layer, as shown in fig. 3.

The square-box was designed with sharp corners. However, the first experiment showed that this made the end effector stay slightly longer in the corner points while changing direction, which lead to unwanted material accumulation. The corners were therefore made blunter in the following experiments by changing the *zone data* variable in the code so that the corner points worked as fly-by points instead of stop points: The robot's end effector would never actually reach the corner point on its path, but instead start changing directions when it was within a certain distance

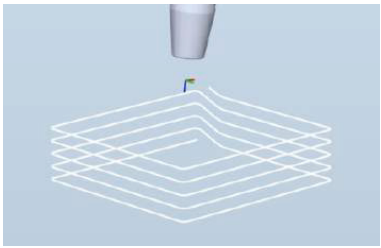

Fig. 3. **Slope between layers:** To avoid material accumulation, a smoother transition between layers was introduced, and the effect can be seen in fig. 2.

Fig. 4. **Continuous build:** Square-box structures with rounded corners and a smooth transition between layers.

of the corner point (ABB Robotics, 2004-2010). A value of *z1* meant that the tool centre point (TCP) could start changing directions 1 mm away from the fly-by point, while *z5* meant that the TCP could start changing direction 5 mm away from the point, and so on (Robotstudio.com, 2016). In this experiment, the zone data was set to *z5*. The initial build with these adjustments is shown to the right in fig. 2, and later builds with the same dimensions are shown in fig. 4.

2.2 Experiment 2: Flower-shape with opposing angles

One of the challenges that arise when building a thin-walled structure in a layer-wise manner is how to deal with intersections within the same layer (Ding et al., 2016). Continuous material deposition is desired for efficiency, but intersections in the robot's path within the same layer will then lead to deposition of material in the same point twice. Starting and stopping the welding process at each side of an existing bead is not considered to be a good solution due to the mentioned challenges regarding uneven material deposition at arc initiation and flame-out (Martina et al., 2012).

One solution to this problem is to altogether avoid crossings within the same layer. If the path within each layer can be traversed without passing the same point twice, it could be possible to design the path so that two opposite corner angles pass close enough together that they remelt and merge together, thereby creating what looks and works like an intersection. The method of opposite

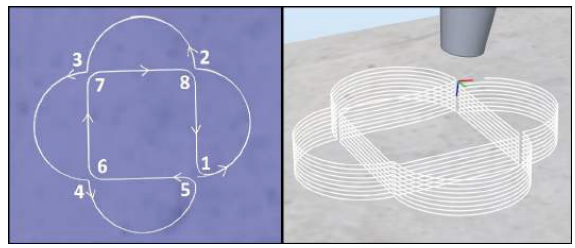

Fig. 5. **Opposite corners:** To avoid crossings within the same layer, the path was designed so that opposing corners merged together to create intersections in the final structure (Mehnen et al., 2011).

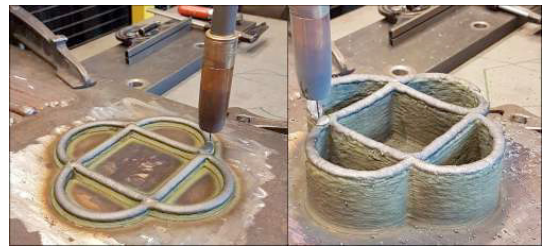

Fig. 6. **Inconel 625:** The flower structure built in Inconel 625 (4 layers to the left, 25 layers to the right). Fig. 10 shows the same structure after post processing.

angles described in (Mehnen et al., 2011) was tested for the thin-walled "flower"-shape, shown in the RobotStudio simulation in fig. 5. The pattern was repeated continuously for several layers. As with the box shown in fig. 2, the height increase between layers were done gradually over a slope of 2 cm at the end of each layer.

Three different materials were examined for the flower geometry. Tests were first done with the aluminium-silicon alloy AA4047 previously used to build the square-box. Further, the nickel-based alloy Inconel 625 was utilised, and some tests were done using another aluminium-silicon alloy, AA4043. The results from the former experiments were used to adjust the welding parameters in order to improve the final build.

The nickel- and aluminium-based alloys were used to assess the dependence of the physical properties of the welding metal when building. Compared to aluminium, Inconel 625 possess a much higher melting point (1350 °C) and higher thermal emissivity to air (Kobayashi et al., 1999). Welding with Inconel 625 requires higher energy input. Therefore, a pulsed MIG weld gun was preferred over CMT for this build, and the base plate was changed to black carbon steel. The as-deposited structure is shown in fig. 6, and the welding parameters are listed in table 2.

Lastly, a set of experiments were done trying to build the flower-shape in aluminium AA4043, using the experience from the previous experiments to attempt a successful build with a softer metal than the nickel-alloy. We wanted to weld the first few layers with an even higher heat input than before, so the last experiments with aluminium were done with pulsed metal inert gas (MIG) welding. This will be explained further in section 3. The welding parameters

Fig. 7. **Pulsed MIG:** The final flower structure built in aluminium AA4043. This build has 65 layers, and some grinding were performed to reduce material accumulation in the intersections.

are listed in table 3, and fig. 7 shows the most successful attempt.

3. RESULTS

Throughout these experiments, the accumulated experience regarding heat input and path design was implemented to help improve the following tests.

3.1 Experiment 1: Thin-walled square-box

Transitioning between layers by moving the welding gun vertically in a single point led to some unwanted material accumulation, as seen in fig. 2. As the aim was to see how feasible it was to build a structure by continuous welding, it was not an option to interrupt the welding procedure. This would in any case have lead to additional challenges related to the starting and stopping of the weld due to the difference in material deposition at the beginning and end of a welding bead (Mehnen et al., 2011). The gradual height increase over a slope introduced in the second square-box build, shown in the simulation in fig. 3, seemed to work well and was kept for the following experiments. Rounding off the corners seemed to solve the material accumulation problem there as well, as can be seen by comparing the corners of the structures in fig. 2.

The first, manual test with CMT with a current of 62 A seemed to overheat the structure, making the metal so hot and liquid that each layer became almost flat. The problem increased over time, making the walls of the structure uneven, as seen in fig. 2. Therefore, the heat input was reduced for the next builds, and the length of the walls was increased from 10 cm to 12 cm to allow for a longer cool-down period, resulting in the structure to the right in fig. 2. Fig. 4 shows additional builds of the square-box, where the material deposition could go on continuously until the structures were significantly taller than the first attempts.

3.2 Experiment 2: Flower-shape with opposing angles

Several experiments were done in order to build the structure shown in fig. 5, both in the aluminium alloys AA4047 and AA4043, and the nickel-based alloy Inconel 625.

Fig. 8. **Intersections:** First attempts at merging opposite corners together.

Opposing Angles: One challenge was to find an optimal distance between the corners in the path that needed to melt together, e.g. corner 3 and 7 in fig. 5. These corner parts of the path had the same fly-by point, but used different zone data, as explained in section 2.1. By changing how close to the fly-by point the end effector would move, it was possible to control the distance between the corners.

Two different builds in aluminium AA4047 are shown in fig. 8. The structure on the left had corners that ended up too close together, i.e. were too sharp. The material deposited in the opposing corners would slightly overlap, and this would accumulate over time, resulting in a height difference. The variation in the contact distance between the welding gun and the deposited structure due to the height difference in turn affected the material deposition, and the result was that the inner walls of the structure became slopes instead of straight walls. For the structure shown to the right in fig. 8, the corners were too blunt and far apart, so that the metal did not melt together as intended.

The flower-shape built in Inconel 625 (fig. 6) did not show the same issues related to the opposing corners as the aluminium structures in fig. 8. The material did not accumulate in the same way, and there were no clear signs of surface artefacts as the structure got hotter, and the build could go on continuously for 25 layers. The build was interrupted because the layer-height had been overestimated in the program. This meant that the distance between the welding gun and the welding surface increased for every layer. Thus, the Inconel 625 build was stopped after 25 layers when welding fireworks indicated that there were too long contact distance between the welding gun and the surface.

Three structures were built in the last experiment with aluminium AA4043. Height regulation was included in the program for the last test (3^{rd} test table 3), so that the build could go on for much longer than any of the other tests. This last structure is shown in fig. 7.

Welding current and temperature: To make the weld adhere properly to the base, the first few layers of every structure had to be welded with a relatively high heat input. If not, the deposited material would just clump together in droplets, as shown in fig. 9, as the temperature was too low for the base metal and the deposited metal to properly melt together. To avoid deterioration of the structure due to excessive heat build-up, the heat input was reduced after the first few layers.

Fig. 9. **Low heat input:** Welding the first layers with a heat input that was too low made the deposited material clump together and not adhere properly to the base.

The welding parameters for the flower-shape experiments are listed in tables 1, 2 and 3. The changes in currents were done manually on the welding apparatus, not as part of the program running on the robot manipulator. To change the current, the program was interrupted by releasing the hold-to-run control, and then started again where it left off. This meant that there was a short break of 30-45 seconds between each layer with different currents.

Table 1. Welding param. for the tests building the flower-shape in aluminium AA4047.

Aluminium flower-shape (CMT welding)				
Layer	**Current**	**Wire feed sp.**	**Voltage**	**Layer h.**
1st test (approx. 12 × 12 cm)				
1-2	90 A	4.1 m/min	16.6 V	2 mm
2nd test (approx 16 × 16 cm)				
1-2	160 A	7.0 m/min	19.2 V	2 mm
3+	80	3.7 m/min	16.4 V	2 mm
3rd test (approx 16 × 16 cm)				
1-2	90 A	4.1 m/min	16.6 V	2 mm
3-10	60 A	2.9 m/min	16.1 V	2 mm
4th test (approx 16 × 16 cm)				
1-2	150 A	6.6 m/min	18.7 V	2 mm
3	100 A	4.5 m/min	16.9 V	2 mm
4-10	75 A	3.5 m/min	16.3 V	2 mm
8	100 A	4.5 m/min	16.9 V	2 mm
9-20	75 A	3.5 m/min	16.3 V	2 mm

4. DISCUSSION

Manually programming the welding process worked well enough for the simple square-box structure. However, it was inaccurate in the sense that the placement of the corners of the path was decided by how well the operator was able to aim manually. Editing existing scripts was tedious with this manual approach, e.g. moving the structure to another part of the base meant reprogramming

Table 2. Welding param. for the flower-shape build with Inconel 625.

Inconel 625 flower-shape (fig. 6 and 10)				
Layer	**Current**	**Wire feed sp.**	**Voltage**	**Layer h.**
1	185 A	7.9 m/min	15.3 V	2 mm
2	130 A	5.0 m/min	12.9 V	2 mm
3-4	120 A	4.4 m/min	12.6 V	2 mm
5-25	105 A	3.6 m/min	12.1 V	2 mm

Table 3. Welding param. for the tests building the flower-shape in aluminium AA4043.

Aluminium flower-shape (MIG pulsed welding)				
Layer	**Current**	**Wire feed sp.**	**Voltage**	**Layer h.**
1st test (approx. 16 × 16 cm)				
1-3	205 A	9.6 m/min	24.0 V	1.8 mm
4	149 A	6.8 m/min	20.7 V	1.8 mm
5	102 A	4.7 m/min	19.1 V	1.8 mm
6-25	72 A	3.5 m/min	18.4 V	1.8 mm
2nd test (approx. 20 × 20 cm)				
1	211 A	9.9 m/min	23.9 V	1.65 mm
2	151 A	6.9 m/min	20.9 V	1.65 mm
3	102 A	4.7 m/min	19.1 V	1.65 mm
4-30	72 A	3.5 m/min	18.4 V	1.65 mm
3rd test (With height reduction, approx. 20 × 20 cm)				
1	211 A	9.9 m/min	23.8 V	1.2 mm
2	151 A	6.9 m/min	20.9 V	1.2 mm
3	102 A	4.7 m/min	19.1 V	1.2 mm
4-65	72 A	3.5 m/min	18.4 V	1.2 mm

the entire path. It was therefore necessary to change to the more flexible way of programming the robot path in RAPID, which also made it simpler to create paths for more complicated structures. Furthermore, this made it possible to simulate and test the paths in RobotStudio.

Spreading the height increase between layers out over a short slope of a few centimetres seems like a good solution when working with a layer-by-layer approach. Because there is some slack in the optimal distance between the structure and the tip of the welding gun, this should work for any layer-wise structure as long as the layer height is relatively small compared to the length of the slope.

The solution for intersections used in these experiments, based on the work of (Mehnen et al., 2011), would of course demand that it is possible to traverse the entire path of one layer without the need for actual crossings. The flower-shape is so simple that one can see this path quite easily. More complex shapes would demand that we have an algorithm to help calculate the tool-path, e.g. the Medial Axis Transformation algorithm proposed by (Ding et al., 2014).

WAAM with aluminium AA4047 was challenging. The alloy's low melting temperature of 577 °C and high melt fluidity makes it vulnerable to overheating with prolonged deposition. The temperature vulnerability of building with aluminium proved more significant for smaller structures, which is to be expected as a larger area enable more heat dissipation to the base plate. In addition, a larger structure means that there is a longer cool-down period between each time material is deposited in the same point. Aluminium's inherent properties imply heat dissipation almost solely through conduction, and very low heat emission to air (Geng et al., 2017). In thin-wall building with an increasing number of layers, the heat dissipation gradually decreases due to longer conduction distance and decreasing temperature gradient through the thickness. Consequently, aluminium is especially vulnerable to overheating during prolonged deposition.

For the simple square-box structure with a large enough base area, continuous material deposition was possible for many layers without deterioration of the structure due to excessive heat build-up, as can be seen in fig. 4. It was

Fig. 10. **Post processing:** The Inconel 625 structure shown in fig. 6 after post processing. The opposing corners within each layer have merged together.

Fig. 11. **Grinding:** In the last test with aluminium AA4043 (fig. 7) some grinding was done every 10 layers or so in an attempt to avoid material accumulation in the intersection points.

more challenging to build the flower-shape. As explained in section 3.2, the inner walls of the flower structure became slopes instead of straight walls when welding with an aluminium-alloy. The inner walls are surrounded by heat, hampering heat dissipation. In addition, due to the high thermal conduction of aluminium, intersections become areas of heat accumulation. When a new layer is deposited in this high-temperature area, the cooling rate of the deposited metal goes down (i.e. solidification takes longer). Gravitational forces will flatten the liquid metal creating a wide, flat layer upon solidification. Further away from the intersection, deposited metal will solidify faster, creating a higher layer height. The discrepancy in layer height will accumulate over several layers, creating the slope seen in the flower component in fig. 7.

To avoid the poor surface appearance of the flower profile, a change of welding material from aluminium to Inconel 625 was performed. The nickel material had both higher melting point and thermal emissivity (Kobayashi et al., 1999). Consequently, more heat was dissipated to air creating a stable inter-pass temperature of the deposit. Without inter-sectional heat accumulation as with aluminium, the sloped wall phenomenon was avoided. Post processing shows that the corners did indeed melt together well enough to function as crossings within each layer, see fig. 10.

Different solutions were tested in order to successfully build the flower-shape without too much unwanted material accumulation in the opposite corners. There seemed to be a very fine balance between building the opposite corners too close together and too far apart, especially when working aluminium. Even the slightest accumulation of material in these intersection points had a large impact on the final result. In the test shown in fig. 7, some grinding was done to try and even this out, but the inner walls would still slope slightly.

With more experiments, it should be possible to optimise the distance between these kinds of opposite corners based on the structure's shape, size and material. The optimal distance varies a lot with the material and the welding parameters, because they determine the dimensions of the welding bead, which again determines how close together the opposite corners must be placed for them to merge. What worked best was a combination of rounded and sharp corners: Corner 5-8 in fig. 5 had zone data set to *z5*, while corner 2-4 had zone data set to *z1*. The merge between corner 1 and 5 was particularly challenging due to how the path was designed: The robot would stay longer in the same area, depositing more material, so the zone data in corner 1 was increased from *z1* to *z5*.

In the last aluminium build of the flower-shape, done with pulsed MIG welding, the path was altered so that the inner walls were built *before* the outer walls. The idea was that this should allow the heat to dissipate more quickly, as the inner walls would have time to cool down slightly before being enclosed by the heat from the outer walls. This might have had some effect on the first few layers, but as the structure grew taller, the height difference became negligible when considering heat flow.

The layer height for the Inconel 625 build was initially set to 2.0 mm, but as explained in section 3.2, this was too big, and the experiment had to be interrupted. The layer height should have been closer to 1.7 mm or thereabout. The program was adjusted so that the welding gun could be lowered during the last aluminium build, compensating for inaccuracies in assumed layer height. For the aluminium AA4043 build, the welding gun was lowered 21 mm over 65 layers, which is about 0.3 mm per layer. This implies that the layer height should be set to 0.9-1.0 mm instead of 1.2 mm for future experiments with pulsed MIG welding in aluminium for the given experimental setup.

5. CONCLUDING REMARKS

The work presented in this paper has shown that continuous WAAM shows promise when trying to build structures in this scale, though the results greatly depend on the building material. A smooth and gradual transition between layers works well to avoid deformations, and this solution could be kept for future experiments. Even so, building with a continuous height increase throughout the path should be considered, like what was done in the initial experiments described in (Evjemo et al., 2017). This would mean moving away from the layer-by-layer approach, avoiding the need for support structures.

If a layer can be built without actual crossings within the robot's path, intersections can be created through opposite corners (Mehnen et al., 2011), though it is clear that this is more challenging for aluminium than for harder materials such as Inconel 625. More research needs to be done to see how material properties can be used to calculate how close together such opposite corners should be placed, as this is

related to the dimensions of the welding bead at a given heat input, and the metal's melt fluidity and cooling rate.

As with the experiments presented in earlier work (Evjemo et al., 2017), these latest tests have all been done using translation-only robot paths with the welding gun placed perpendicular to a horizontal surface. Because each layer has to be vertically attached to the previous layer, these methods are limited when it comes to building structures with overhang, which will depend on support structures. The ABB IRB2400/10 robot manipulator has 6 DOFs, and can thereby reach every point in its workspace in an arbitrary orientation, so one of the next steps should be to use this flexibility to build more complex structures.

One way of doing this could be to change the orientation of the welded structure by rotating and tilting the welding surface, as shown in the work of (Panchagnula and Simhambhatla, 2018). The overlying objective of our research is to find methods that can be used to build larger structures, or to modify existing structures in industry. In such cases, having to change the orientation of the structure itself could be very limiting, so future work will therefore focus on controlling the orientation of the welding gun itself. When the welding gun is not placed vertically on the surface, it will be necessary to address challenges related to gravitational effects on the welding bead.

Monitoring the building process and designing control algorithms to correct for geometrical deviations in the structure should also be addressed in future work.

ACKNOWLEDGEMENTS

The work reported in this paper was based on activities within centre for research based innovation SFI Manufacturing in Norway, and is partially funded by the Research Council of Norway under contract number 237900. Mr. Morten H. Danielsen is acknowledged for his experimental guidance related to arc welding.

REFERENCES

ABB Robotics (2004-2010). Technical reference manual: RAPID Instructions, Functions and Data types.

Abb.com (2016-2018). IRB 2400. URL `https://new.abb.com/products/robotics/industrial-robots/irb-2400`. Accessed 2018-10-22.

Apis-cor.com (2017). Robotics in construction. URL `http://apis-cor.com`. Accessed 2019-06-07.

Cong, B., Ouyang, R., Qi, B., and Ding, J. (2016). Influence of cold metal transfer process and its heat input on weld bead geometry and porosity of aluminum-copper alloy welds. *Rare Metal Mat. Eng.*, 45(3), 606–611.

Ding, D., Pan, Z.S., Cuiuri, D., and Li, H. (2014). A tool-path generation strategy for wire and arc additive manufacturing. *Int. J. Adv. Manuf. Tech.*, 73(1-4), 173–183.

Ding, D., Shen, C., Pan, Z., Cuiuri, D., Li, H., Larkin, N., and van Duin, S. (2016). Towards an automated robotic arc-welding-based additive manufacturing system from CAD to finished part. *Comput. Aided Des.*, 73, 66–75.

Evjemo, L.D., Moe, S., Gravdahl, J.T., Roulet-Dubonnet, O., Gellein, L.T., and Brøtan, V. (2017). Additive manufacturing by robot manipulator: An overview of the state-of-the-art and proof-of-concept results. In *22nd IEEE ETFA, Cyprus*, 1–8.

Geng, H., Li, J., Xiong, J., and Lin, X. (2017). Optimisation of interpass temperature and heat input for wire and arc additive manufacturing 5A06 aluminium alloy. *Sci. Technol. Weld. Joi.*, 22(6), 472–483.

Jorislaarman.com (2015-2018). MX3D resin. URL `http://www.jorislaarman.com/work/mx3d-resin/`. Accessed 2018-10-22.

Kobayashi, M., Otsuki, M., Sakate, H., Sakuma, F., and Ono, A. (1999). System for measuring the spectral distribution of normal emissivity of metals with direct current heating. *Int. J. Thermophys.*, 20(1), 289–298.

Martina, F., Mehnen, J., Williams, S.W., Colegrove, P., and Wang, F. (2012). Investigation of the benefits of plasma deposition for the additive layer manufacture of Ti–6Al–4V. *J. Mater. Process Tech.*, 212(6), 1377–1386.

Mehnen, J., Ding, J., Lockett, H., and Kazanas, P. (2011). Design for wire and arc additive layer manufacture. In *Global Product Development*, 721–727. Springer.

Mx3d.com/"Bridge" (2017). Mx3d bridge. URL `https://mx3d.com/projects/bridge-2/`. Accessed 2019-06-07.

Panchagnula, J.S. and Simhambhatla, S. (2018). Manufacture of complex thin-walled metallic objects using weld-deposition based additive manufacturing. *Robot. Com.-Int. Manuf.*, 49, 194–203.

Robotstudio.com (2016). Rapid-ifdtechrefmanual: Zone data. URL `http://developercenter.robotstudio.com/BlobProxy/manuals/Rapid-IFDTechRefManual/doc576.html`. Accessed 2019-01-18.

Robotised wire arc additive manufacturing using set-based control: Experimental results

L. D. Evjemo, S. Moe, and J. T. Gravdahl. Robotised wire arc additive manufacturing using set-based control: Experimental results. In 21st IFAC World Congress, Berlin, pages 1-8, 2020.

Available online at www.sciencedirect.com

ScienceDirect

IFAC PapersOnLine 53-2 (2020) 10044–10051

IFAC Papers Online CONFERENCE PAPER ARCHIVE

Robotised Wire Arc Additive Manufacturing Using Set-based Control: Experimental Results

Linn Danielsen Evjemo *, **Signe Moe** *,**, **Jan Tommy Gravdahl** *

* *Department of Engineering Cybernetics, NTNU, Trondheim, Norway (e-mail: linn.d.evjemo@ntnu.no, signe.moe@ntnu.no, jan.tommy.gravdahl@ntnu.no)*

** *Department of Mathematics and Cybernetics, SINTEF Digital, Oslo, Norway*

Abstract: Additive manufacturing (AM) is a term that covers a variety of techniques for building custom-made, three dimensional structures. Such methods have moved from initially being used for creating simplified models to enable visualising of a product in a developing process, to creating structures that are suitable as end-products (Gibson et al., 2010). This has made prototyping and the production of custom made parts more accessible to small companies and developers, and AM technologies are still gaining momentum. However, traditional methods for AM are limited to building structures that are smaller than the AM apparatus itself, and bound to building structures layer by layer. The motivation for combining AM with a robot manipulator is to increase the workspace of the build, making it possible to build much larger structures, and to deposit material in any direction. The focus of this research is large-scale AM in metal, so the work presented in this paper focuses on a set-based control method for wire-arc additive manufacturing (WAAM) of a cylindrical, thin-walled structure. The set-based control method used to control the robot manipulator allows for some freedom in the orientation of the tool, so that the material is not necessarily deposited strictly vertically. Evaluating how this impacts the structure helps map how feasible this solution is for building more complex structures in future work.

Keywords: Additive Manufacturing, manufacturing systems, robot programming, set-based control. wire arc additive manufacturing

1. INTRODUCTION

Additive manufacturing (AM) is more commonly spoken of as 3D-printing, rapid prototyping (RP), or free-form fabrication. Most well-established methods for AM have strict limitations on size and geometry of the structures that is produced. Motivated by an aim to circumvent the main limitations that traditional AM methods face today, our research combine wire arc additive manufacturing (WAAM) with a 6 degrees-of-freedom (DOF) robot manipulator, and a set-based control method that allows for some freedom in the orientation of the welding gun. This freedom means that throughout the build, material is deposited in a mostly non-vertical manner, which differ strongly from traditional methods. Combining metal AM with freedom in orientation of the material deposition, and a non-layer-by-layer approach to the building process itself, makes this a novel idea.

1.1 Robotised WAAM

For traditional AM methods, the building process is in most cases done in-box, enclosed in an AM machine that must be larger than the structure it is building. It is only practical to expand the size of such an apparatus up to a certain point, which greatly limits the size of any structure that can be produced. Furthermore, traditional methods for AM methods primarily use a layer-by-layer approach, either building the structure strictly bottom-up or top-down. Since each layer has to be vertically attached to either the previous layer or some other means of support, the production of structures with overhangs depend upon additional support structures being built, which must again be removed post-build. A 6 DOF robot manipulator can move a tool attached to its end effector, e.g. a welding gun, to any point in its workspace with an arbitrary orientation, making it possible to deposit fast solidifying material in any direction. Moving away from the layer-wise approach could thereby remove the need for support structures, saving both time and material.

A focus of this research is to build metal structures using WAAM. The modified metal inert gas welding method cold metal transfer (CMT) is well suited for WAAM because is has a more stable arc which reduces metal splattering, and has a reduced heat-input which reduces residual stresses and distortions by refining the deposited microstructure (Cong et al., 2016). There is therefore an extra

10.1016/j.ifacol.2020.12.2725

Fig. 1. **Proof-of-concept:** Structure built with helix-path, but with a strictly vertical orientation of the tool (Evjemo et al., 2017).

focus on CMT in our research.

Building large components can be quite time consuming, with or without a strictly layer-wise approach: The height of each deposited welding bead affects the roughness of the finished surface, as well as the accuracy of the build compared to the model. If the surface is to be post-processed, and the level of detail in the build is therefore less important, one can increase how much material is deposited at a time, thereby making it possible to build quicker and bigger. It is still necessary to make such a build as effective as possible, so an objective for our research is to build continuously, both to save time and to make the structure less vulnerable to deformations due to flame-out and arc initiation when pausing the welding process (Evjemo et al., 2019).

1.2 Orientation of welding gun

The structures manufactured in the experiments presented here are built in aluminium, which has very low heat-emission to air and dissipates heat almost solely through conduction (Geng et al., 2017). Earlier tests have shown that accumulation of heat in structures built in materials as soft as aluminium will more easily lead to deformations compared to structures build in harder metals such as nickel (Evjemo et al., 2019). All the experiments presented in (Evjemo et al., 2017) and (Evjemo et al., 2019) were conducted with a fixed, vertical orientation of the welding gun on a horizontal surface. If the flexibility of the robot manipulator can be used in such a way that it is no longer necessary to keep a strictly vertical orientation of the welding gun, it might be possible to gain more flexibility in the building process. This could allow for a longer cool-down period in parts of the structure that require it, without the need to pause the build.

This paper presents how a thoroughly tested method for set-based control was used to program the robot's path, including some freedom in the orientation of the tool, thereby increasing the flexibility of the build. Others have worked on making AM more flexible by building on a tilting surface, with a fixed point of material deposition. This has been performed both in plastic using a 6 DOF robot manipulator (Dai et al., 2018), and in metal (Panchagnula and Simhambhatla, 2018). However, the focus of our research is to see how a robot manipulator can deposit material on a fixed surface with a not strictly vertical orientation of the tool. Joris Laarbman Lab have produced very promising results on similar work, using both a fast-curing polymer (Laarman et al., 2014) and stainless steel (Jorislaarman.com, 2015-2019), but none of their algorithms or methods have been made public.

The aim was to build a cup structure similar to the one built in viscous glue in the proof-of-concept experiments from 2017 (Evjemo et al., 2017), seen in Figure 1. As a consequence of using a soft building material, the original glue cup was built very small, with a radius of 2 cm. These new structures in aluminium are built much larger: The radius was set to 8 cm, in the hopes that heat would dissipate quickly enough to enable a continuous build. The method for set-based control, presented in Section 2, allowed for additional freedom in the orientation of the welding gun. The aim of these experiments was to show how robotised WAAM can better take advantage of the flexibility of a 6 DOF robot manipulator. An objective was also to investigate how additional freedom in the orientation of the welding gun will affected the build, and if this is a promising method going forward.

The rest of this paper is organized as follows: In Section 2, the theory behind the set-based control method used in these experiments is explained. The results and data from the experiments are presented in Section 3. The results are then evaluated and discussed in Section 4. Finally, some concluding remarks are discussed in Section 5.

2. THEORY: SET-BASED CONTROL

The aim of the experiment was to construct a large, cylindrical shape built with the same path as the cup from the initial experiments presented in (Evjemo et al., 2017). This path already deviates from traditional AM methods in the sense that the structure is not built layer-wise, but with a continuous vertical motion creating a helix, see Figure 2. As with the glue cup shown in Figure 1, a bottom layer was included by depositing material in an outwards spiral.

To allow some freedom in the orientation of the welding gun, a set-based framework was used to control the joints of the robot manipulator. This framework is particularly suited for robotic systems with a large number of DOFs and several tasks to solve. Furthermore, it allows for set-based tasks defined by a valid interval (such as collision avoidance) in addition to equality tasks defined by an exact desired value (e.g. position control). For an extensive description of the framework and its properties, the interested reader is referred to (Moe et al., 2016; Moe et al., 2018).

Typically, the desired behaviour of a robot is described in task space, whereas the robot is actually controlled in the joint space. Set-based control is a kinematic control

framework which calculates reference states based on the desired behaviour and the current state of the system.

A general robotic system has n DOFs and its configuration is given by the joint values $\boldsymbol{q} = [q_1, q_2, \ldots, q_n]^T$. The system tasks and task velocities are described through forward kinematics and the Jacobian matrix. For instance, a task $\boldsymbol{\sigma}(t) \in R^m$ can be expressed as

$$\boldsymbol{\sigma}(t) = \boldsymbol{f}(\boldsymbol{q}(t)), \tag{1}$$

where $\boldsymbol{f}(\boldsymbol{q}(t))$ is the forward kinematics, which can be derived for instance through the Denavit-Hartenberg convention (Spong and Hutchinson, 2005). The time-derivative of the task is given as

$$\dot{\boldsymbol{\sigma}}(t) = \frac{\partial \boldsymbol{f}(\boldsymbol{q}(t))}{\partial \boldsymbol{q}} \dot{\boldsymbol{q}}(t) = \boldsymbol{J}(\boldsymbol{q}(t)) \dot{\boldsymbol{q}}(t), \tag{2}$$

where $\boldsymbol{J}(\boldsymbol{q}(t)) \in R^{m \times n}$ is the Jacobian matrix and $\dot{\boldsymbol{q}}(t) \in R^n$ is the system velocity. For compactness, the argument $\boldsymbol{q}$ of tasks and Jacobians are omitted from the equations for the remainder of this section.

Consider a single m-dimensional equality task with a defined desired trajectory $\boldsymbol{\sigma}_{\text{des}}(t) \in R^m$. The corresponding joint references $\boldsymbol{q}_{\text{des}}(t) \in R^n$ may be computed by integrating

$$\dot{\boldsymbol{q}}_{\text{des}} = \boldsymbol{J}^{\dagger} \Big(\dot{\boldsymbol{\sigma}}_{\text{des}} + \boldsymbol{\Lambda} \tilde{\boldsymbol{\sigma}} \Big), \tag{3}$$

where $\boldsymbol{J}^{\dagger}$ is the pseudoinverse of $\boldsymbol{J}$, $\tilde{\boldsymbol{\sigma}} = \boldsymbol{\sigma}_{\text{des}} - \boldsymbol{\sigma}$ is the task error and $\boldsymbol{\Lambda} \in R^{m \times m}$ is a positive-definite matrix of gains.

In these experiments, we consider two tasks to achieve welding: Position control $\boldsymbol{\sigma}_{\text{pos}}(\boldsymbol{q}) \in R^3$ of the end effector to follow the defined welding trajectory and field of view (FOV) $\sigma_{\text{FOV}} \in R$. The latter is defined as the angle between the outgoing unit vector of the end effector, i.e. the direction it is pointing when depositing material, and a vertical vector. In traditional welding and in previous experiments conducted by the authors, σ_{FOV} is defined as en equality task with $\sigma_{\text{FOV, des}} = 0°$, corresponding to maintaining a constant orientation of the end effector normally to the welding surface. However, to allow some freedom in the orientation when depositing materials, σ_{FOV} is considered a set-based task in these experiments. This approach has shown promising results in similar applications such as spray painting (Moe et al., 2018).

For a set-based task $\sigma \in R$, the desired behaviour is not defined by an explicit σ_{des}, but $\sigma \in [\sigma_{\min}, \sigma_{\max}] \ \forall \ t \geq t_0$. The set-based control framework handles a set-based task by ignoring them and letting the motion be controlled only by the equality tasks until such a time this would result in the set-based task leaving its valid set. This is considered mode 1 of the system. However, should mode 1 result in the set-based task leaving its valid set, it is actively inserted into the kinematic controller with the goal of keeping it on the limit of the valid set. This is mode 2 of the system, which is active until such a time that controlling only the equality tasks will naturally bring the set-based task into the valid set. Since the set-based task σ_{FOV} in these experiments is defined as the angle between the FOV of the end effector and a vertical vector, the valid set is defined as $C_{\text{FOV}} = \left[0°, \sigma^{\circ}_{\text{FOV, max}}\right]$. In mode 1, σ_{FOV} is ignored and the desired motion of the robot is determined based on position control and the desired welding trajectory. In mode 2, σ_{FOV} is actively controlled to its maximum limit to prevent the task from being violated. Thus, the two modes are defined as

$$\begin{aligned} \dot{\boldsymbol{q}}_{1,\text{des}} &= \boldsymbol{J}^{\dagger}_{\text{pos}} \left(\dot{\boldsymbol{\sigma}}_{\text{pos, des}} + \boldsymbol{\Lambda}_1 \tilde{\boldsymbol{\sigma}}_{\text{pos}} \right), \\ \dot{\boldsymbol{q}}_{2,\text{des}} &= \begin{bmatrix} \boldsymbol{J}_{\text{pos}} \\ \boldsymbol{J}_{\text{FOV}} \end{bmatrix}^{\dagger} \left(\begin{bmatrix} \dot{\boldsymbol{\sigma}}_{\text{pos, des}} \\ 0 \end{bmatrix} + \boldsymbol{\Lambda}_2 \begin{bmatrix} \boldsymbol{\sigma}_{\text{pos, des}} - \boldsymbol{\sigma}_{\text{pos}} \\ \sigma_{\text{FOV, max}} - \sigma_{\text{FOV}} \end{bmatrix} \right). \end{aligned} \tag{4}$$

The switching between modes is determined in Algorithm 2 using the tangent cone (Algorithm 1). In general, the tangent cone algorithm returns True 1) if the task is in its valid interval or 2) if it is outside the valid interval but moving towards it. Algorithm 2 evaluates whether or not this is the case for σ_{FOV} given Mode 1, i.e. if controlling the joints based only on the position task ($\dot{\boldsymbol{q}}_{1,\text{des}}$) will lead σ_{FOV} out of its valid interval. For further details, see (Moe et al., 2016; Moe et al., 2018).

.

Algorithm 1 The boolean function in_T_C.

Input: σ, $\dot{\sigma}$, $\sigma_{\min}$, $\sigma_{\max}$
if $\sigma_{\min} < \sigma < \sigma_{\max}$ **then**
  return True
else if $\sigma \leq \sigma_{\min}$ *and* $\dot{\sigma} \geq 0$ **OR** $\sigma \geq \sigma_{\max}$ *and* $\dot{\sigma} \leq 0$ **then**
  return True
else
  return False
end

.

Algorithm 2 Activation of modes.

a = in_T_C(σ_{FOV},$\boldsymbol{J}_{\text{FOV}}\dot{\boldsymbol{q}}_{1,\text{des}}$,0,$\sigma_{\text{FOV,max}}$)
if *a is True* **then**
  $\dot{\boldsymbol{q}}_{\text{des}} = \dot{\boldsymbol{q}}_{1,\text{des}}$
else
  $\dot{\boldsymbol{q}}_{\text{des}} = \dot{\boldsymbol{q}}_{2,\text{des}}$
end

The trajectory consists of an outwards spiralling bottom which moves over to an upwards helix when the desired radius for the bottom is reached, shown in Figure 2. As in (Evjemo et al., 2017), each point on the spiral trajectory is expressed in cylindrical coordinates θ, r, and z. We define h as the height difference between each bead or layer in the wall, and r_1 as the horizontal distance between each bead in the bottom. H is the desired final height of the structure, and R is the desired radius. All of these variables are given in meters. r and z are defined as functions of θ:

$$r(\theta) = \begin{cases} \frac{r_1}{2\pi}\theta & \theta \leq \frac{R}{r_1} 2\pi \\ R & \theta > \frac{R}{r_1} 2\pi \end{cases} \tag{5}$$

$$z(\theta) = \begin{cases} 0 & \theta \leq \frac{R}{r_1} 2\pi \\ \frac{h}{2\pi}(\theta - \frac{R}{r_1} 2\pi) & \theta > \frac{R}{r_1} 2\pi \end{cases} \tag{6}$$

Thus, the time-derivatives of r and z are given by:

$$\dot{r}(\theta) = \begin{cases} \frac{r_1}{2\pi}\dot{\theta} & \theta \leq \frac{R}{r_1} 2\pi \\ 0 & \theta > \frac{R}{r_1} 2\pi \end{cases} \tag{7}$$

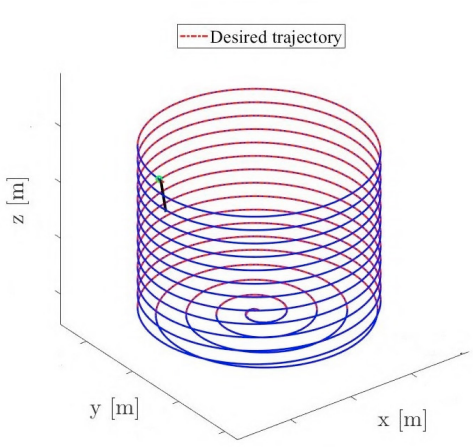

Fig. 2. **Helix path:** The dimensions in this plot is exaggerated in order to more easily illustrate the path.

$$\dot{z}(\theta) = \begin{cases} 0 & \theta \leq \frac{R}{r_1} 2\pi \\ \frac{h}{2\pi}\dot{\theta} & \theta > \frac{R}{r_1} 2\pi \end{cases} \tag{8}$$

where $\dot{\theta}$ is defined as:

$$\dot{\theta} = \begin{cases} \frac{2\pi U}{r_1\sqrt{\theta^2+1}} & \theta \leq \frac{R}{r_1} 2\pi \\ \frac{U}{\sqrt{R^2+\frac{h}{2\pi}^2}} & \theta > \frac{R}{r_1} 2\pi \end{cases} \tag{9}$$

$\dot{\theta}$ is chosen such that the end effector velocity along the trajectory is constant and equal to the desired velocity U, which is necessary for even deposition of metal.

To express the desired end effector position in Cartesian coordinates, we rewrite the trajectory given in cylindrical coordinates (5)-(6) through the following transformation:

$$\begin{aligned} x_{des} &= r(\theta)\cos\theta \\ y_{des} &= r(\theta)\sin\theta \\ z_{des} &= z(\theta) \end{aligned} \tag{10}$$

Thus, the time derivatives are given as:

$$\begin{aligned} \dot{x}_{des} &= \dot{r}(\theta)\cos\theta - r(\theta)\sin\theta\dot{\theta}(\theta) \\ \dot{y}_{des} &= \dot{r}(\theta)\sin\theta + r(\theta)\cos\theta\dot{\theta}(\theta) \\ \dot{z}_{des} &= \dot{z}(\theta) \end{aligned} \tag{11}$$

where $\dot{r}$, $\dot{z}$, and $\dot{\theta}$ are defined in (7)-(9). Thus, the commanded joint velocity is defined in (3) with $\boldsymbol{\sigma}_{\text{pos}} = [x_{des}, y_{des}, z_{des}]^T$ and $\dot{\boldsymbol{\sigma}}_{\text{pos}} = [\dot{x}_{des}, \dot{y}_{des}, \dot{z}_{des}]^T$.

In the experiments presented in this paper, the following numeric values are used:

- U is 0.10 m/s, based on tests in (Evjemo et al., 2019).
- R is 0.08 m
- r_1 is between 4.0 mm and 4.5 mm, see Tables 1-4
- h is between 12 mm and 14 mm, see Tables 1-4

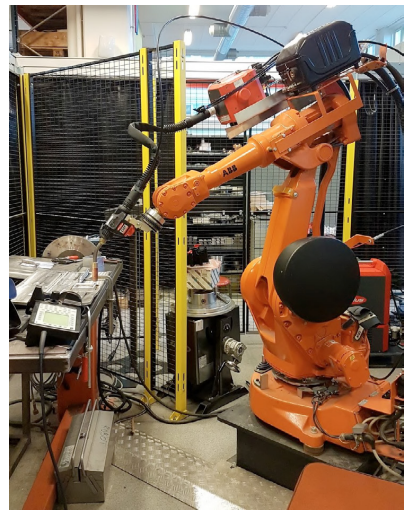

Fig. 3. **Experimental set-up:** 6 DOF ABB IRB2400/10 robot manipulator with welding equipment from Fronius.

- The freedom in orientation $\sigma^{\circ}_{\text{FOV, max}}$ is between 0 and 10

3. EXPERIMENTAL RESULTS

These experiments were performed in collaboration with SINTEF Industry using a 6 DOF IRB 2400/10 robot manipulator from ABB Robotics (Abb.com, 2016-2018) with an attached metal inert gas (MIG) welding gun with CMT technology developed by Fronius, see Figure 3. The metal cylinder structure shown in Figure 4 was built in order to have some grounds of comparison between a build done with and without deviations in the orientation of the welding gun. It was built using the RAPID programming language from ABB, just as the structures referenced in (Evjemo et al., 2019). The vertical position of the welding gun was increased continuously throughout the build, creating a helix path, thereby avoiding traditional layers.

The base plate for all the builds presented here was made of the aluminium alloy 6082-T6, and was approx. 15 mm thick. The welding wire was of the aluminium alloy AlMg4.5Mn. For the purpose of documenting the experiments presented in this paper, the welding parameters are given for each *approximate* layer in Table 1 to 4. This should be interpreted as that the current etc. was adjusted after approx. this number of full rotations in the upwards helix path from Figure 2.

3.1 Test 1: Pulsed MIG, fixed orientation of welding gun

Because of the before-mentioned benefits of using CMT, such as reduced metal splattering and less residual stresses, the aim was to use this method for as much of the building process as possible. On the other hand, work presented in (Evjemo et al., 2017) and (Evjemo et al., 2019) show

Fig. 4. **Vertical welding gun:** Cylindrical structure built with fixed, vertical orientation of the welding gun, with continuous height increase like that shown in Figure 2.

that there are significant benefits to building as continuously as possible, ideally avoiding breaks in the welding process altogether. The metal plate used as base in these experiments was thicker than the base used in earlier tests, which meant that the distortions of the base plate due to the heating and cooling of the metal should be less prominent. However, this also meant that the first part of the build, the spiralling bottom, had to be welded with a higher heat-input than the rest of the structure in order for the weld to adhere properly to the base (Evjemo et al., 2019). The heat-input available when using CMT technology was not sufficient, so the bottom part of the cup instead had to be welded using pulsed MIG welding, which allows for a scientifically higher heat-input than CMT.

In our experimental set-up, it was not possible to change welding methods without pausing the welding process. This was not ideal, and made it necessary to make the choice between an uninterrupted build and the very controlled welding process that CMT could provide. Focusing on doing a continuous build, test 1 was done without interruption using only pulsed MIG welding. Based on experience from earlier experiments presented in (Evjemo et al., 2019), the layer height was set to 1.2 mm, and the radius of the cylinder was set to 60 mm. As the thickness of the thin-walled structure shown in Figure 4 was approx. 4 mm, the horizontal distance between layers in the spiralling bottom layer was also set to 4 mm.

Test 1 stopped after 4-5 layers after with the error message "Wire buffer full" on the welding equipment. This was due to over heating of the soft aluminium wire when using Pulsed MIG over time, a problem that had not been encountered when working with harder metals with a higher melting point such as the nickel alloy Inconel625 (Evjemo et al., 2019). The build from test 1 is shown to the top left of Figure 5.

Table 1. Welding param. for test 1: Pulsed MIG welding and fixed orientation of welding gun.

Test 1: Pulsed MIG				
Layer number	**Current** (A)	**Wire feed sp.** (m/min)	**Voltage** (V)	**Bead w.** (mm)
bottom	180	10.5	22.0	4.0
bottom	165	9.5	21.5	4.0
≈ **1**	120	7.0	18.7	1.2
≈ **2**	100	5.9	17.9	1.2
≈ **3**	85	5.0	17.2	1.2
≈ **4-5**	71	4.3	16.4	1.2

Fig. 5. **Set-based control:** The structures built in the first three tests, and close-up of the bottom.

3.2 Test 2: Pulsed MIG + CMT, fixed orientation of welding gun

As test 1 was interrupted, the second test was also done with a fixed orientation of the welding gun. The estimated bead width in the spiralling bottom was increased from 4.0 mm to 4.5 mm, as the overlap between the beads in the spiral was slightly too large. In order to avoid the wire feed issue from test 1, which seemed to be caused by overheating, the second test was performed using CMT welding. The thick metal base still made it necessary to weld the bottom with a higher heat-input, and the welding parameters from test 1 had seemingly worked well for this part of the build. The combination of pulsed MIG and CMT welding was introduced: When the robot moved from the part of the path that was the spiralling bottom layer on to the helix walls, the process was manually interrupted and paused. The settings for welding method was changed manually from pulsed MIG to CMT, before the welding process continued.

The welding parameters for this test are listed in Table 2. Test 2 was interrupted after completing the bottom and building approx. 14 rotations of wall because the tip of the welding gun ended up too close to the surface.

Table 2. Welding param. for test 2: Pulsed MIG + CMT welding and fixed orientation of welding gun.

Test 2: Pulsed MIG + CMT				
Pulsed MIG on bottom layer				
Layer number	**Current** (A)	**Wire feed sp.** (m/min)	**Voltage** (V)	**Bead w.** (mm)
bottom	180	10.5	22.0	4.5
bottom	160	9.2	21.3	4.5
Beginning of walls, changed to CMT				
≈ **1**	135	9.0	15.0	1.2
≈ **2**	115	8.2	14.3	1.2
≈ **3-4**	80	5.2	11.8	1.2
≈ **5-14**	75	4.8	11.7	1.2

The estimated height of each layer of deposited material was set to 1.2 mm based on previous builds, but the decreasing distance between the structure and the welding gun indicated that this should be increased for the next tests. In addition, the metal base contracted more than anticipated, so the welding gun was placed slightly higher above the base at the beginning of the welding process to counteract this.

3.3 Test 3: Pulsed MIG + CMT, set-based control of welding gun orientation

Because tests 1 and 2 had shown how much the metal base would bend and contract when heating up, the welding gun was placed approx. 16 mm above the base, as opposed to approx 11 mm for tests 1 and 2. In addition, the estimated height of each layer of deposited material was increased from 1.2 mm to 1.4 mm. The estimated width of the welding bead was kept to 4.5 mm, as the bottom layer from test 2 was smoother than that from test 1. Freedom for the orientation of the welding gun was included, which allowed for up to 10° deviation in angle relative to a vertical orientation.

The large heat-input from the pulsed MIG welding used when building the bottom lead the whole structure to heat up in a way that seemed to make the ensuing deposition of material uneven. As can be seen to the top right of Figure 5, the walls became quite uneven compared to earlier experiments (Evjemo et al., 2019) or the reference structure shown in Figure 4. Therefore, some active cooling was added to the process: When the welding was paused in order to change from pulsed MIG to CMT, cool air was blown onto the structure for approx. 30 seconds in order for it to cool down.

This build was only programmed to be 4 cm tall, and completed without complications. The result can be seen to the bottom left of Figure 5.

3.4 Test 4: Pulsed MIG + CMT, set-based control of welding gun orientation

Test 3 was overall successful, but the complete structure was only 4 cm tall. The aim of test 4 was therefore to keep most of the parameters from test 3, including the manual interruption in order to change welding methods, and build a taller structure. The estimated bead width in the bottom layer was kept at 4.5 mm, and the estimated height of each layer of deposited material was kept at 1.4 mm. The freedom in orientation angle was set to 6°. The build completed without complications. The welding parameters are listed in Table 4, and the final structure is shown in Figure 6. The active cooling when swapping from pulsed MIG to CMT was also included for this build.

Table 3. Welding param. for test 3: Pulsed MIG + CMT welding and set-based control of orientation of welding gun.

Test 3: Pulsed MIG + CMT				
Pulsed MIG on bottom layer				
Layer number	**Current** (A)	**Wire feed sp.** (m/min)	**Voltage** (V)	**Bead w.** (mm)
bottom	180	10.5	22.0	4.5
bottom	168	9.7	21.6	4.5
Beginning of walls, changed to CMT. Some active cooling.				
≈ **1**	135	9.0	15.0	1.4
≈ **2**	116	8.9	14.3	1.4
≈ **3**	100	7.0	13.8	1.4
≈ **4-5**	85	5.5	11.9	1.4
≈ **6-7**	80	5.2	11.8	1.4
≈ **8-28**	75	4.8	11.7	1.4

Table 4. Welding param. for test 4: Pulsed MIG + CMT welding and set-based control of orientation of welding gun.

Test 4: Pulsed MIG + CMT				
Pulsed MIG on bottom layer				
Layer number	**Current** (A)	**Wire feed sp.** (m/min)	**Voltage** (V)	**Bead w.** (mm)
bottom	180	10.5	22.0	4.5 mm
bottom	168	9.7	21.6	4.5
Beginning of walls, changed to CMT. Some active cooling.				
≈ **1**	135	9.0	15.0	1.4
≈ **2**	116	8.9	14.3	1.4
≈ **3**	100	7.0	13.8	1.4
≈ **4-5**	85	5.5	11.9	1.4
≈ **6-105**	80	5.2	11.8	1.4

Fig. 6. **Set-based:** The tallest cylinder structure.

4. DISCUSSION

The spiral making out the bottom of the cup was very smooth, with few deformations, as shown to the bottom right in Figure 5. This was somewhat surprising, as earlier welding experiments had shown that the arc initiation could easily be a source for distortions in the structure (Evjemo et al., 2019). Building the same shape

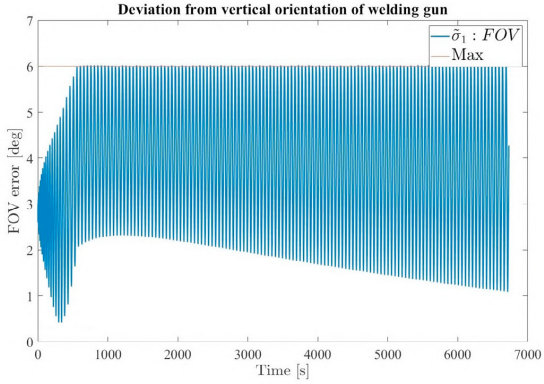

Fig. 7. **Orientation:** This is the $\sigma^{\circ}_{\text{FOV}}$ along the 4^{th} build. It ends up going back and forth from approx. 1° and 6°.

in a smaller version made out of viscous glue had also shown that material would easily heap up in the centre of the spiral, due to continuous material deposition in a very small area (Evjemo et al., 2017). The reason why this worked much better in these latest builds is likely that the high heat-input provided by the use of pulsed MIG welding meant that the metal was hot enough to properly melt together with the metal base, and subsequently the already deposited metal bead.

The method for set-based control is meant to simplify the movements of the robot by defining the position control of the end effector a set to stay within rather than a strict value to follow, as explained in Section 2. As can be seen in Figure 6, the tallest build ended up having a slight saddle form, even though the robot's path was meant to result in a cylinder with a flat top. This is likely due to the difference in orientation of the welding gun on the right side of the build compared to the left side. The build was done on a base that was not placed directly in front of the robot's base, but about 20 cm to the left. The result was therefore that the welding gun was more orthogonal to the surface on the side of the structure closest to the central axis of the robot, and had more of an angle on the side of the structure furthest away from the base. The deviation from a vertical orientation of the welding gun during the 4^{th} test is plotted in Figure 7: On one side of the structure, the limit of 6° is reached but not broken. On the other side, the deviation reaches a maximum of 2°, before slowly decreasing, almost coming back to 1° at the end of the build.

The difference in orientation of the welding gun was decided by the metal base's placement relative to the robot. The orientation of the welding gun determines how the material is deposited, and how the metal spreads out on the existing build, as gravity works on the liquid metal during deposition (Xiong et al., 2017). If the difference in the orientation of the welding gun could be more evenly distributed around some kind of centre point of the structure, so that the additional gravitational pull on the liquid metal would be evenly spread out over the circular path, it seems likely that the result would be more even. It should therefore be considered if the set-based control method can somehow be manipulated to prioritise a condition of moving around a centre point for the orientation over the freedom of the robot's movements.

The program used for controlling the robot in these experiments did not itself separate between building the bottom and the walls. The robot was given a list of joint angles generated by the set-based control system presented in Section 2, and moved between these configurations with a provided speed. Because the welding method had to be changed between the bottom and the walls in tests 2 to 4, the process had to be paused manually by the human operator when the bottom was built. It was somewhat challenging to evaluate in real-time when the bottom was completed by looking at the welding process while wearing a protective welding helmet. In one of the tests, the program was in fact paused too early, changing the welding method to CMT before the two final beads of the bottom layer was deposited. This did not change the resulting build dramatically, as the structure was already hot enough for the deposited metal to adhere properly to the base even when using CMT and a lower current.

During test 2 (Section 3.2), the build had to be interrupted due to an increasing distance between the welding gun and the surface. The height of each welding bead is determined by both the welding current, the temperature of the existing structure, and the gravitational pull when welding with a non-vertical orientation of the welding gun. This makes it difficult to accurately anticipate what the height difference h each bead in the walls should be, even with experience from previous builds. Actively adjusting this value during the build could help solve this, and keep the building process going. This was done in (Evjemo et al., 2019), but that solution meant that the welding process had to be paused shortly while the adjustments were made. Even though the manual changing of welding methods in the most recent experiments also required a short pause in the welding process during the build, continuity was an important objective. Adjusting h this way was therefore not considered a viable solution, and not used in the latest tests.

5. CONCLUDING REMARKS

The work presented in this paper has shown that continuous WAAM with some freedom in the orientation of the welding gun is possible, but that the deviation in orientation should to some extend be evenly distributed over the structure. If not, gravity can lead to unexpected deviations, such as the saddle form in the structure built in test 4 (Figure 6). If the set-based control method could be manipulated to distribute the deviation in orientation around a structural centre point, that might help solve this issue. However, this is not necessarily straight forward, as the main motivation of the set-based method is to prioritise the ease of the joint configurations.

The structures built in these experiments have taken advantage of the robot's manipulator's freedom in orientation as well as in position, unlike the work presented

in (Evjemo et al., 2017) and (Evjemo et al., 2019). Not relying on a strictly fixed orientation of the welding gun expands the available workspace for the build when performing WAAM by robot. If the build is done near the limits of the robot's workspace, introducing some freedom in orientation could help make a path feasible. Considering a lab or factory situation, a non-vertical orientation of the tool could make it possible to build around obstacles, either external ones or existing parts of the build. The next step of this research should be to build a more complex structure with overhang, which traditional AM methods cannot construct without adding additional support structures that must be removed in post-processing.

Manually pausing the build to change welding methods when necessary was challenging, because it was difficult to accurately determine when the bottom was finished just by observing the welding process thorough a welding mask. Even though pausing the program a bit early did not change the resulting build dramatically, the manual changing of welding methods was something that made it difficult to accurately re-produce an experiment. An important part of future work would be to remove the need for manually interrupting the welding process in order to change welding method. It might still be necessary to pause the welding process in order for the metal to cool down after the intense heat input provided by pulsed MIG welding, either naturally or through active cooling. If this could be included in the programming, it would still remove some of the inconsistencies that might arise when a human operator tries to manually pause the process at a given point, and thereby help create a build that is easier to re-produce.

Some way of monitoring the build should also be addressed in future work. This could either be external monitoring, such as cameras, or monitoring of the welding process itself by monitoring the currents and other welding parameters. A change in distance between the wire in the welding gun and the surface of the structure will impact the current, so monitoring this can help tell a lot about how smooth the structure is, if the distance between the welding gun and surface is increasing or decreasing, etc. Future work should also include designing and/or implementing control algorithms to help adjust the robot's path in order to correct for geometrical deviations based on the monitoring data. Implementing a way to actively adjust the height increase h between each bead in the walls should be included in this work, to help keep the build going even if the estimated h deviates from how the physical result.

ACKNOWLEDGEMENTS

The work reported in this paper was based on activities within centre for research based innovation SFI Manufacturing in Norway, and is partially funded by the Research Council of Norway under contract number 237900. Mr. Morten H. Danielsen is acknowledged for his experimental guidance related to arc welding.

REFERENCES

Abb.com (2016-2018). IRB 2400. URL `https://new.abb.com/products/robotics/industrial-robots/irb-2400`. Accessed 2018-10-22.

Cong, B., Ouyang, R., Qi, B., and Ding, J. (2016). Influence of cold metal transfer process and its heat input on weld bead geometry and porosity of aluminum-copper alloy welds. *Rare Metal Mat. Eng.*, 45(3), 606–611.

Dai, C., Wang, C.C., Wu, C., Lefebvre, S., Fang, G., and Liu, Y.J. (2018). Support-free volume printing by multi-axis motion. *ACM Transactions on Graphics (TOG)*, 37(4), 134.

Evjemo, L.D., Langelandsvik, G., and Gravdahl, J.T. (2019). Wire arc additive manufacturing by robot manipulator: Towards creating complex geometries. In *5th IFAC ICONS, Belfast*, 103–109. Elsevier.

Evjemo, L.D., Moe, S., Gravdahl, J.T., Roulet-Dubonnet, O., Gellein, L.T., and Brøtan, V. (2017). Additive manufacturing by robot manipulator: An overview of the state-of-the-art and proof-of-concept results. In *22nd IEEE ETFA, Cyprus*, 1–8.

Geng, H., Li, J., Xiong, J., and Lin, X. (2017). Optimisation of interpass temperature and heat input for wire and arc additive manufacturing 5A06 aluminium alloy. *Sci. Technol. Weld. Joi.*, 22(6), 472–483.

Gibson, I., Rosen, D.W., and Stucker, B. (2010). *Additive manufacturing technologies*, volume 238. Springer.

Jorislaarman.com (2015-2019). MX3D bridge. URL `https://www.jorislaarman.com/work/mx3d-bridge/`. Accessed 2019-11-11.

Laarman, J., Jokic, S., Novikov, P., Fraguada, L.E., and Markopoulou, A. (2014). Anti-gravity additive manufacturing. *Fabricate: Negotiating Design & Making*, 192–197.

Moe, S., Antonelli, G., Teel, A.R., Pettersen, K.Y., and Schrimpf, J. (2016). Set-Based Tasks within the Singularity-Robust Multiple Task-Priority Inverse Kinematics Framework: General Formulation, Stability Analysis, and Experimental Results. *Frontiers in Robotics and AI*, 3(April), 1–18. URL `http://journal.frontiersin.org/article/10.3389/frobt.2016.00016`.

Moe, S., Gravdahl, J.T., and Pettersen, K.Y. (2018). Set-based control for autonomous spray painting. *IEEE Transactions on Automation Science and Engineering*, 15(4), 1785–1796. doi:10.1109/TASE.2018.2801382.

Panchagnula, J.S. and Simhambhatla, S. (2018). Manufacture of complex thin-walled metallic objects using weld-deposition based additive manufacturing. *Robot. Com.-Int. Manuf.*, 49, 194–203.

Spong, M.W. and Hutchinson, S. (2005). *Robot Modeling and Control*. Wiley.

Xiong, J., Lei, Y., Chen, H., and Zhang, G. (2017). Fabrication of inclined thin-walled parts in multi-layer single-pass gmaw-based additive manufacturing with flat position deposition. *Journal of Materials Processing Technology*, 240, 397–403.

Wire-arc additive manufacturing of structures with overhang: Experimental results depositing material onto fixed substrate

L. D. Evjemo, G. Langelandsvik, S. Moe, M. H. Danielsen, and J. T. Gravdahl. Wire-arc additive manufacturing of structures with overhang: Experimental results depositing material onto fixed substrate. *CIRP Journal of Manufacturing Science and Technology*, 38, 186-203 (2022).

CIRP Journal of Manufacturing Science and Technology 38 (2022) 186–203

Contents lists available at ScienceDirect

CIRP Journal of Manufacturing Science and Technology

journal homepage: www.elsevier.com/locate/cirpj

Wire-arc additive manufacturing of structures with overhang: Experimental results depositing material onto fixed substrate

Linn Danielsen Evjemo[a,*], Geir Langelandsvik[b], Signe Moe[c], Morten Høgseth Danielsen[b], Jan Tommy Gravdahl[a]

[a] Norwegian University of Science and Technology, O. S. Bragstads plass 2D, Gløshaugen, Trondheim, Norway
[b] Department of Materials and Nanotechnology, SINTEF Industry, Trondheim, Norway
[c] SINTEF Digital/Sopra Steria, Oslo, Norway

ARTICLE INFO

Available online xxxx

Keywords:
Additive manufacturing
Wire arc additive manufacturing
Cold metal transfer
Arc Welding
Robotics

ABSTRACT

As additive manufacturing (AM) technology grows both more advanced and more available, the challenges and limitations are also made more evident. Most existing solutions for AM build structures layer by layer using strictly vertical material deposition. As each layer must vertically adhere to the previous layer, support structures must be added if there are to be any kinds of overhangs. For methods requiring the build to be performed within a chamber, the size of the structure is also very limited. The research presented in this paper explores possible solutions to these challenges, focusing on wire-arc additive manufacturing in order to effectively build structures that can not easily be constructed using in-box, layer-based methods for AM. By non-vertical material deposition using an industrial robot manipulator, metal structures with overhangs are built onto a fixed, horizontal surface without any support structures. Cross sections of two different structures are examined by optical microscopy and hardness measurements to reveal potential differences between the areas with and without intersections or overhang.

Introduction

Over the last decades, additive manufacturing (AM) has become increasingly important for low-cost prototyping and customisation. AM is the umbrella term that covers many different techniques for building up a 3D structure, such as 3D-printing, rapid prototyping (RP) and free-form fabrication [1]. Out of these, 3D printing is perhaps the most available method, as desktop 3D-printers have become both affordable and easier to use for both professionals and enthusiasts. Even if AM technology has made prototyping and modelling easier, there are still some major limitations for most traditional methods of AM. Depending on the AM method, the challenges can vary from issues such as long build time or high cost [2] to issues related to structural challenges such as residual stresses or porosity within the final structure [3]. This research aims to address how to get around two of the most pronounced challenges: limitations on geometrical design and size.

Many widely used methods for AM require the AM process to be done 'in-box', such as powder bed fusion (PBF) or vat polymerisation (VP). In other words, the build must be conducted inside a chamber filled with powder or liquid material that is hardened layer by layer, gradually building up the structure [1]. Other methods use localised material feeding in some form, such as powder based direct energy deposition (DED) or material jetting (MJT), but are still limited by the size of the AM apparatus because the material extrusion happens strictly vertically in a 3 DOF gantry-like machine. This means that for AM techniques that require a build chamber or a basin, the AM machine must be larger than the structure being constructed, which greatly limits the build volume. This is generally not the case with some methods for DED such as AM done by arc welding, where material deposition is made without the limitations of an enclosed space. In addition, some projects have over the last years scaled up extrusion based AM systems in order to build full-size houses [4,5]. These set-ups prove useful in construction, but they are tailored for this purpose, and deposit material faster and with lower accuracy compared to smaller 3D printers. They are therefore not suited for producing metal parts at a low scale, etc.

Even though commercial 3D-printers more suited for building prototypes or end-products are growing in scale, a large 3D-printer is still in most cases limited to a chamber of less than one-by-one

* Corresponding author.
E-mail addresses: linn.d.evjemo@ntnu.no (L.D. Evjemo), geir.langelandsvik@sintef.no (G. Langelandsvik), signe.moe@soprasteria.com (S. Moe), morten.danielsen@sintef.no (M.H. Danielsen), jan.tommy.gravdahl@ntnu.no (J.T. Gravdahl).

https://doi.org/10.1016/j.cirpj.2022.04.006
1755-5817/

metre. This is why AM has mostly been used for creating relatively small end products, or smaller parts for larger products. With AM by material deposition, there is no excess material that needs to be contained, so it is not necessary to do the build in-box. If material deposition can be combined with for example an industrial robot manipulator, the work-space will increase dramatically. Attaching the robot manipulator to an actuator rail can increase the work-space even further.

AM methods based on vertical material deposition and a layer-by-layer building process are also somewhat limited with respects to the obtainable geometry of the structure. Most AM methods execute the build strictly layer by layer, either bottom-up or top-down, and the material is deposited or set using a tool which is limited to Cartesian movements. Though many path planning strategies exist, layers are generally applied directly on top of each other, as all material must be vertically attached to the previous layer [6]. Building any kind of overhang may therefore require additional support structures to be included in the build, which means more materials and a longer build time [7]. If the cavities or overhangs are significant for the final product, the support structures must be removed in post-processing. Different AM technologies demand different kinds of support structures with their own advantages and disadvantages, and minimising side effects such as extended build time or additional material cost is important as AM technology becomes more commonly used in industry [7]. Some AM methods with a relatively low building rate due to thin layer heights, such as PBF or VP, allow for overhangs because the otherwise unsupported parts of the structure can rest on underlying excess material, such as a powder bed. Still, if overhangs could be built without the need for such support structures or other kinds of additional support for methods with a higher material deposition rate, such as DED or material extrusion, this could save both time and materials.

A 6 degrees-of-freedom (DOF) robot manipulator can move its end effector with an attached tool to any point within its workspace and with an arbitrary orientation. If fast-curing material was deposited using such a 6 DOF robot arm, material could be deposited non-vertically, removing the need for support structures. The building material would still have to be attached to previously deposited material, but if this could be done at an angle, support structures might be superfluous.

The research presented here will focus on depositing material onto a *fixed* surface using a 6 DOF robot arm. Similar work have been done on AM processes with a *moving* building surface about a fixed point of material deposition, both using plastics [8] and metals [9,10]. The aim of the research presented in this paper is to see how feasible the former approach is. Though an approach with a fixed point of material deposition shows promise, a mobile point of material deposition could make AM more applicable to a factory setting, repair work on-site etc., as it is more flexible. Joris Laarman Lab has done some work using this approach, with very promising results. They have used both stainless steel [11] and a fast-curing polymer [12] in their builds, but none of their algorithms or control methods have been made public.

AM methods such as VP or powder based DED often build with a high accuracy and resolution, and would consequentially be quite time-consuming for larger components, depending on the application. The build time of a component is generally decided by the part size, layer thickness, printing speed and build orientation: When high accuracy is necessary, the layers are often very thin. As building in the z-direction is then quite time consuming, time could be saved by orienting the structure so that the build height is kept at a minimum [2]. However, for structures that will in any case need some post-processing or machining, the resolution and layer height can be reduced in order to make the build more efficient. This could for example be the case when working with AM in metal, or more specifically wire-arc additive manufacturing (WAAM), which also falls under DED type AM methods [13,14].

This paper presents how it was possible to build structures with overhang on a horizontal surface with no need for additional support structures, and with continuous material deposition. Using welding equipment attached to a 6 DOF robot manipulator, material could be deposited using a non-vertical orientation of the welding tool. In addition, the constraints on the size of the build was greatly reduced compared to many in-box methods, as the size of the structure was only limited by the workspace of the robot. Preliminary results were presented in [15–17], and in this paper these results will be extended by experiments building structures with overhangs. Experiments with overhang were performed both with a fixed and an adjustable orientation of the tool.

In *Preliminary tests with viscous material* some preliminary experiments for a none-layer wise build using viscous glue and set-based control, are presented. *Working with metals: WAAM and CMT* explains the shift to building in metals, and the principles behind WAAM and the arc welding method cold metal transfer (CMT). *Continuous build of thin-walled structures* explores building thin-walled structured continuously using WAAM, as continuous material deposition is desirable to keep the building time low. If the structure is more complex, some challenges related to intersections and corners may arise, and this is the focus of *Avoiding double material deposition in intersections*. *Set-based control for flexibility in orientation of tool* presents how the set-based method used for the preliminary experiments from *Preliminary tests with viscous material* was also used on metal structures. Finally, *Structures with overhang focuses* on structures with overhangs, and how the workspace and flexibility of a 6 DOF robot manipulator makes it possible to deposit material with a non-vertical orientation of the tool onto a fixed substrate. Material analyses of one of the structures with intersections in addition to one of the structures with overhangs are presented in *Material analysis*, considering the differences in parts of the structures with and without intersections or overhangs.

Preliminary tests with viscous material

In order to outline the direction of this work, a review of the current status of large-scale AM was conducted, presented in [15]. A small-scale proof-of-concept experiment was designed to map how a viscous material with dynamic viscosity of 3.200.000 mpa s at 25 °C [18] could be used to build a cylindrical cup-structure in a continuous, non-layer-wise movement. The height increase was continuous, taking a step away from the strictly layer-wise approach in traditional AM methods. Several tests were carried out using a air-pressure driven caulking gun attached to a 6 DOF UR-5 robot manipulator. Using the print head of a 3D printer attached to the robot's end effector was considered, but discarded as it was preferable to deposit material more quickly (Fig. 1).

One of the resulting structures from the caulking gun experiments is shown in Fig. 2. These tests indicated that AM by robot manipulator was possible, and illustrated some of the main challenges related to continuous material deposition that had to be addressed in later work. Starting and stopping the flow of material proved especially challenging, and greatly factors into why the aim is continuous material deposition. The control method used in these experiments were later used to test how a non-vertical orientation of the tool impacts the build in a WAAM process, presented in *Set-based control for flexibility in orientation of tool*. More details regarding the control methods and approach from the preliminary experiments, as well as the state-of-the-art review, can be found in [15]. Full details on the set-based control method can be found in [19,20].

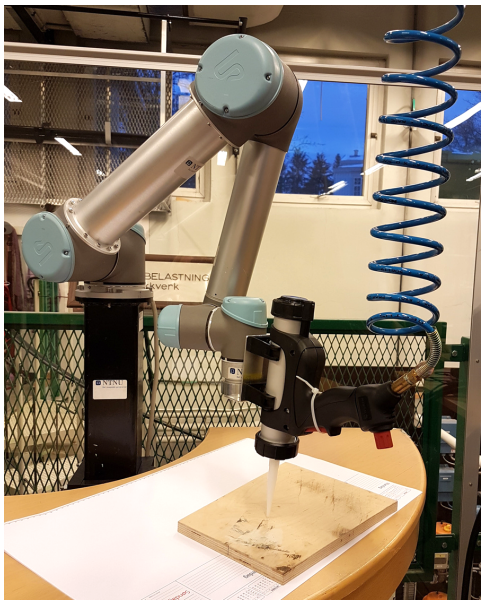

Fig. 1. Robot cell used in preliminary experiments presented in Preliminary tests with viscous material: 6 DOF UR-5 robot manipulator with air-pressure driven caulking gun.

Working with metals: WAAM and CMT

Building structures in metal using AM could be useful in many different industries. Post-processing of structures in metal is often required, even for relatively quick procedures such as metal casting. This reduces the necessary resolution of the build, which makes it more feasible to get the production time down compared to traditional AM methods. AM in metals could be applied in repair work, for example on ships or other structures that would benefit from having repairs done on-site, as well as in building custom-designed metallic parts or end-products.

Fig. 2. Cylindrical cup-structure built in preliminary experiments described in *Preliminary tests with viscous material.* Approx. 4 cm tall, built using a viscous glue.

The work presented here will focus on WAAM, a method where welding equipment is generally attached to the end effector of an industrial robot manipulator. Gas metal arc welding (GMAW), often referred to as metal inert gas welding (MIG), is preferred as a method for robotised WAAM as it is generally easier to implement. While for example gas tungsten arc welding (GTAW), also known as tungsten inert gas welding (TIG), has external feeding of the welding material, the welding material in MIG is fed through the nozzle of the welding gun, thereby acting as the electrode [21]. This means that there is only the nozzle of the welding gun to consider when designing the path for the robot's end effector, as opposed to the additional external obstacle that the wire feed in a TIG process would introduce.

The modified metal inert gas welding method cold metal transfer (CMT) has a more stable arc than traditional GMAW, which reduces metal spattering or 'welding sparks'. It also has a reduced heat input, which reduces residual stresses and distortions [22]. These properties make CMT well suited for WAAM, and the objective was consequently to focus on CMT in this research. A series of different experiments were done in collaboration with SINTEF Industry using a 6 DOF IRB 2400/10 robot manipulator from ABB robotics [23], shown in Fig. 3, equiped with Fronius TPS 400i CMT welding equipment [24]. For some of the experiments, the heat-input provided by CMT was not sufficient for the deposited material to properly adhere to the substrate. For these instances, pulsed-MIG welding was used for either the first few layers or the entire build. Pulsed-MIG is a modified GMAW welding method with a higher heat input than for CMT, but where the current alternates between a high and a low current level [25]. This makes it possible to transfer material with a lower heat input than for standard spray arc GMAW welding, as the melt bath does not have time to solidify between pulses, and the welding method is less vulnerable to spatter [21].

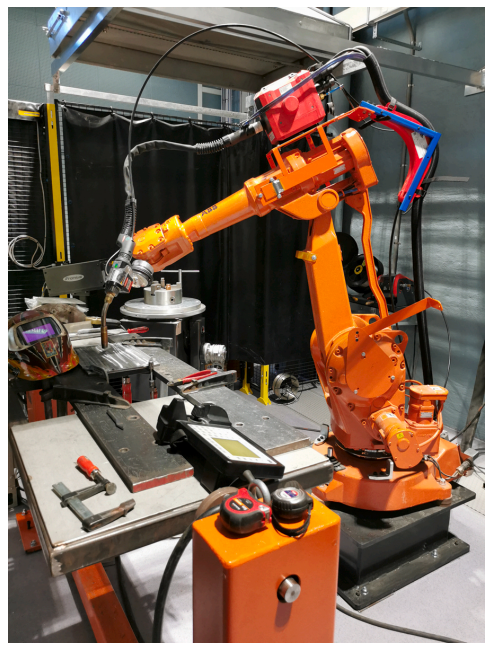

Fig. 3. Lab set-up: Robot cell used in WAAM experiments. 6 DOF ABB IRB2400 robot manipulator with CMT welding equipment from Fronius. This set-up was used in all the experiments presented here.

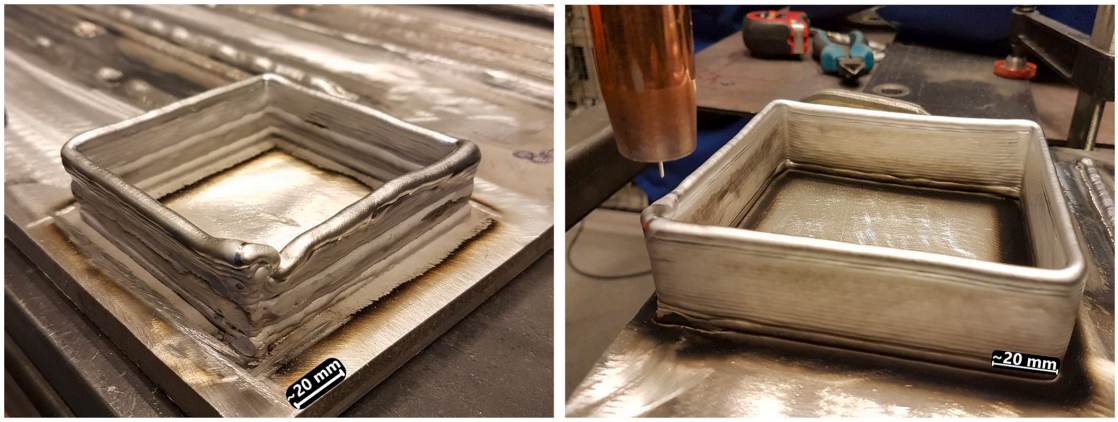

(a) First CMT box build with clear visual flaws due to accumulated errors.

(b) Second, modified CMT box build with smoother walls and few distortions.

Fig. 4. Square-box: Adjusting the structure to have smoother layer transitions, blunter corners and longer sides clearly improved the visual appearance of the structure.

Continuous build of thin-walled structures

Though WAAM in many ways differs greatly from deposition of glue through a caulking gun, the challenges related to beginning and ending the material deposition are quite similar. Just as the variations in the material flow created imprecisions in the viscous glue build, arc initiation and flame-out will generally create irregularities due to uneven material deposition for WAAM [26]. Achieving a building process that is as continuous as possible can help remove some of the challenges related to starting and stopping the material deposition revealed through the preliminary experiments [15]. A continuous building process can also make the build less time-consuming, which in an industrial setting is important in order to make production cost-effective.

In order to investigate how the heat development of prolonged deposition would impact the structure on a superficial level, the first tests focused on constructing a square, thin-walled box by continuous material deposition and CMT welding. The building material was aluminium, and the alloys AA4043 and AA4047 were used. For details related to the welding parameters, see [16].

The robot path was programmed using linear arc welding functions in the programming language Rapid, developed by ABB. Unlike the structure build in the preliminary glue experiments, this square structure did not have a continuous height increase, but was constructed in a semi-layer-wise manner. The height increase necessary to begin building the next layer was carried out evenly over the last few centimetres of each layer, which resulted in a smooth build with no visible irregularities. The difference between increasing the height of the welding gun in a *single point* vs. over a few centimetres can be seen in Fig. 4. Seemingly, increasing the height in a single point lead to a heap-up of material, while a gradual height increase resulted in a smooth transition between layers. This method was kept for further experiments with a semi-layer-wise design, and later adjusted to a completely continuous movement in the z-direction. However, for simple structures the difference between a fully continuous height increase and an increase over a few centimetres for each layer seemed negligible.

The results of the two first tests are shown in Fig. 4. The experience from these tests made it possible to later build much taller, similar structures with continuous material deposition. Some of these are shown in Fig. 5 and Fig. 19. Heat accumulation did not seem to impact the shape of the structures in any significant way, so these builds could have gone on for much longer without any difficulty. The latter is built using the Ni-Cr-Mo alloy UTP 759 instead of an aluminium alloy, which seemed to make the heat accumulation quite insignificant even for a more complex structure, see *Avoiding double material deposition in intersections*.

Avoiding double material deposition in intersections

The box builds presented in *Continuous build of thin-walled structures* are relatively simple geometrical structures. For more complex shapes built in a semi-layer-wise manner, issues related to intersections might appear. When deposing material continuously, which is desired for efficiency, intersections within the same layer will potentially lead to double deposition of material in the point of the intersection. Starting and stopping the welding process before and after crossing a welding bead is not considered to be a good solution, as arc initiation and arc flame-out leads to uneven material deposition [26].

One solution to this challenge was examined: avoiding actual intersections by designing non-crossing paths within each layer, as

Fig. 5. Taller builds: After initial tests with square structures in aluminium, it was possible to build guide tall structures using material deposition.

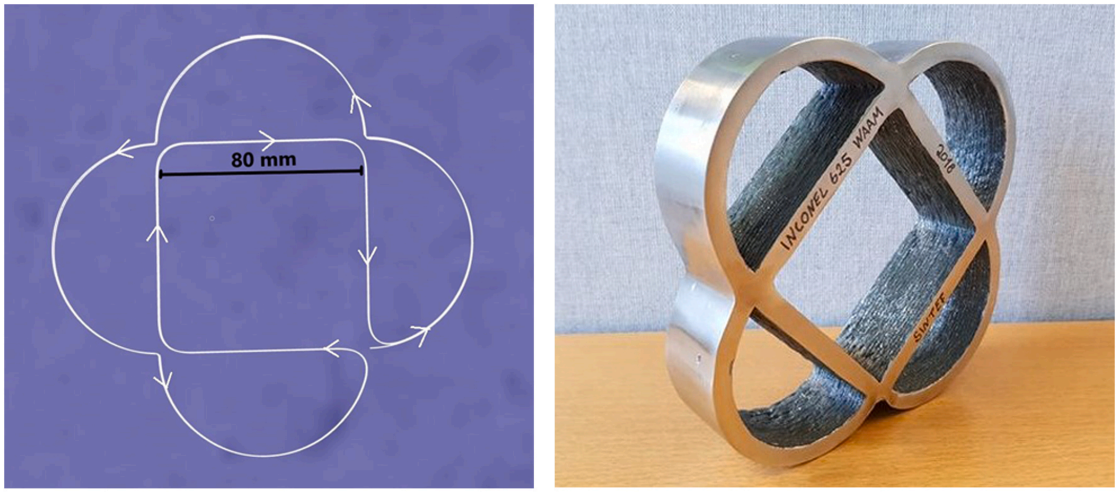

(a) First CMT box build with clear visual flaws due to accumulated errors.

(b) Second, modified CMT box build with smoother walls and few distortions.

Fig. 6. Path design: Intersections are avoided altogether by instead designing a path consisting of closely placed opposite corners. After post processing on the Inconel 625 structure shown in Fig. 7, it was evident that the structure had welded together adequately. (a) and (b) have the same scale.

shown in Fig. 6. This method, where intersections are created by opposing corners, is described in [27]. Experiments were done using this method to build what will from here-on be described as flower structures, as shown in Fig. 6 and 7. The building material was aluminium AA4043 and AA4047, as well as the nickel-based alloy Inconel 625 and the Ni-Cr-Mo alloy UTP 759. Building in different materials helped assess the effect of the physical properties of the welding material, as the aluminium alloys had a much lower melting point than the nickel alloys. The aluminium builds were done using CMT and pulsed-MIG welding. The builds in nickel-based alloys were done using only pulsed-MIG, as this material requires a higher heat input that available when using CMT.

The non-crossing paths strategy used in these tests seemed to work well when building with relatively hard materials with a higher melting point, such as Inconel 625. When building with aluminium, the inner walls of the flower structure began to slope. The heat dissipation was hampered by the surrounding walls, closing the heat in, and leaving the deposited material liquid for a longer time period. The material would therefor spread out over a larger area before solidifying, resulting in considerable differences in the height of the deposited welding bead within each layer. In addition, the intersections became points of heat accumulation, with even more severe contortions. The inaccuracies caused by the uneven cooling and deposition of material would accumulate over time, introducing a need to periodically pause the continuous process to manually grind the structure down to an even height. It was possible to improve the aluminium structures by tuning the heat input and other welding parameters, as shown in Fig. 7. However, it was much easier to build this structure using a metal with a higher melting point, because this material would solidify faster, and thereby make the structure less vulnerable to contortions caused by accumulated heat as the build progressed. The structure built in Inconel 625 was cut from the base plate and polished, and after post processing it was possible to determine that the path had in fact welded together adequately in the intersection points, as shown in Fig. 6. Further details on this experiment can be found [16].

Set-based control for flexibility in orientation of tool

One of the main advantages of depositing material using a 6 DOF robot arm is the ability to orient the tool so that material can be deposited in any direction, not just strictly vertically. Therefore, the next step after building simple, thin-walled structures using continuous material deposition was to vary the orientation of the tool. An overhang is a part of the structure that sticks out over a lower part of the structure without being supported by an preceding layer in a directly vertical direction. AM using non-vertical material deposition makes it possible to build structures with overhangs without additional support structures, and geometries that might not be available when using methods such as PBF or VP.

The method for set-based control used in the preliminary experiments in *Preliminary tests with viscous material* can also be applied to WAAM with a non-vertical deposition of material. This framework works well for robotic systems with a large number of DOFs and several tasks to solve. It combines set-based tasks defined by a valid interval, for example collision avoidance, with equality tasks defined by a desired value, such as position control for the end effector [19]. While the desired behaviour of the robot can often be described in such a task space, the robot control is actually done in the joint space, i.e. feeding the controller a specific set of desired joint values. Set-based control is a kinematic control framework which calculates reference states based on the desired behaviour and the current state of the system. For a detailed description of this framework, please refer to [19,20].

For experiments with material deposition by robot manipulator, there are two tasks that need to be handled: Position control to make sure the end effector follow the desired welding trajectory, and orientation control of the end effector. Position control can be defined with an equality task that must be met at all times. This ensures that the position of the nozzle is accurate and predictable, which is increasingly important when deposition material in a relatively narrow bead. If more material is deposited at a time, resulting in a wider building surface, the position of the tool can

(a) Aluminium AA4047.

(b) Nickel-based alloy Inconel 625.

(c) Aluminium AA4043.

(d) Ni-Cr-Mo alloy UTP 759.

Fig. 7. Varying results: The resulting thin-walled structures based on the pattern in Fig. 6, built using four different welding materials. The scale of these structures matches that of the sketch in Fig. 6a, i.e. the sides of the inner square are 80 mm long.

potentially be allowed to deviate more than the guaranteed position control accuracy of under 1 mm for the IRB2400/10 [23]. For the preliminary experiments presented in *Preliminary tests with viscous material*, the orientation control can also be considered an equality task, as the tool has to stay perpendicular to the welding surface. However, changing the control of the orientation of the tool to instead be considered a set-based task can add freedom in the orientation of the tool. This allows the orientation of the tool to deviate with a few degrees from a set orientation, while keeping control of how large such a deviation can become by adjusting the size of the valid set. Such an approach shows promise in other applications such as spray painting [20].

Using set-based control method that give us some deviation in the orientation of the tool will make the movements smoother and less demanding for the robot compared to a strictly vertical orientation, as one less constraint has to be considered while the orientation stays within the defined set. Keeping a constant speed for the movement of the tool, especially at a relatively high speed, is demanding for the robotic system due to the large torques that are needed. The set-based method designed by Moe et al. may reduce the required torques, as the freedom in orientation helps enable a smoother trajectory for the tool [20]. This also expands the robot's work-space, and can allow for movements that would not be feasible using a constant orientation of the welding gun.

The WAAM experiment using the set-based control framework was designed to build a structure with the same kind of path as for the initial experiments using glue [15], which resulted in the structure in Fig. 2. The orientation control was designed so that the orientation of the tool had to stay within the interval of a few degrees defined by the set-based task, e.g. 10°. As long as this set-based task was met, the motion was controlled only by the equality task defining the path. A bottom layer was built in an outwards spiralling path, as shown in Fig. 8, which then continued on in a helix-path with steady height increase.

It was desired to build these structures using CMT welding, as this had worked well for the simple geometrical shapes described in *Continuous build of thin-walled structures*. Using CMT had resulted in smooth surfaces and builds that seemed to could continue for a long time without excessive heat build-up and bead overflow [16]. However, the base plates available for use in the set-based experiments were thicker than those using in previous experiments. This required a higher heat input in order for the first few welding beads to adhere sufficiently to the substrate. As this helix structure also included a bottom layer, the heat input had to be high enough for the

Fig. 8. Set-based: The structure was a cylindrical shape. The bottom layer was constructed in a outwards spiral, while the path for the wall was an upwards helix with a constant radius and a constant height increase.

spiral to melt together to create a smooth surface. Therefore, the spiralling bottom layer was built using pulsed-MIG, while CMT, with a lower heat input, was used for the rest of the build.

Structures with overhang

One of the main motivations for depositing material with a 6 DOF robot manipulator is to be able to build structures with overhangs. Due to strictly vertical deposition of material, overhangs can traditionally not be build using extrusion based AM methods without adding support structures that must be removed in post-processing. Depositing material non-vertically can remove the need for support structures, which simplifies the building process, and helps save time and materials. It can also allow for a non-layer-wise approach to the AM process, as demonstrated by Laarman Lab and their artistic builds done in a fast-curing polymer [12,15].

Two different methods for creating overhangs were examined: First, testing how overhangs can be “forced" by depositing material vertically onto a lower part of the structure which only partially overlaps with the current path. Material analyses were performed to examine the quality of two the final structures, i. e. optical microscopy and hardness measurements. This will be examined further in *Material analysis*. Then, two different structures with more prominent overhangs were constructed by modifying the orientation of the tool's nozzle to follow the incline of the overhang (Fig. 9).

Fixed orientation of tool: Twisting hexagon

Using the same robot cell as for the former welding experiments (ABB IRB2400/10 6DOF robot manipulator and Fronius TPS 400i GMAW welding equipment with CMT) a thin-walled structure similar to those described in *Continuous build of thin-walled structures* was constructed. The geometric shape making out the foundation for the build was changed to a regular hexagon instead of a square. The linear movement functions in the Rapid programming language were used to build the structure, which made it necessary to define the path using Cartesian coordinates relative to a start point p_c. A regular hexagon as shown in Fig. 10 has 6 equal angles and six equal sides, and the distance from the centre point p_c to each vertex equals the radius r of the circumscribed circle. The apothem, i.e. the shortest distance l from the centre point p_c to each side, equals the radius of the inscribed circle, and $l = \frac{\sqrt{3}}{2}r$ [28]. The points describing the position of the six vertices in Fig. 10, relative to the Cartesian centre point $p_c = [x, y, z]$ of the hexagon were found using these geometrical relations:

$$p_1 = p_c + [-r, 0, 0] \tag{1}$$

$$p_2 = p_c + \left[-\frac{1}{2}r, \frac{\sqrt{3}}{2}r, 0\right] \tag{2}$$

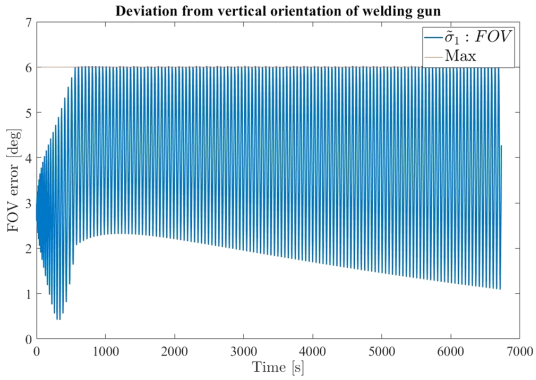

(a) Deviation from a strictly vertical orientation of the welding gun, between 1 and 6 degrees.

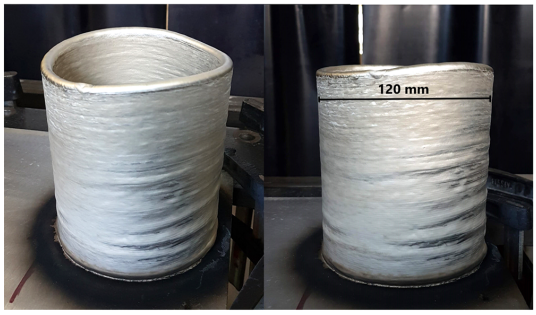

(b) Final structure built using set-based control.

Fig. 9. Build using set-based control, with deviation for vertical orientation of welding too.

$$p_3 = p_c + \left[\frac{1}{2}r, \frac{\sqrt{3}}{2}r, 0\right] \tag{3}$$

$$p_4 = p_c + [r, 0, 0] \tag{4}$$

$$p_5 = p_c + \left[\frac{1}{2}r, -\frac{\sqrt{3}}{2}r, 0\right] \tag{5}$$

$$p_6 = p_c + \left[-\frac{1}{2}r, -\frac{\sqrt{3}}{2}r, 0\right] \tag{6}$$

The base layer was approx. 14 cm wide, as the length r in Fig. 10 was set to be 7 cm. In order to generate an overhang, this hexagonal shape was rotated slightly for each layer. The orientation of the welding gun was fixed, keeping it orthogonal on the base plate. The height increase between layers were spread out over the sixth side of the hexagon, between point p_6 and p_1. For each layer, the hexagon was rotated with an angle $\theta = 1.2^{\circ}$ about the centre, leading the structure to twist as the build grew taller.

How this creates an overhang can be understood studying Fig. 10: The distance r from the centre of the hexagon to the vertex p_5 corresponds to the hypotenuse of a right-angled triangle. As vertex p_5 rotates about the centre with an angle θ, this distance remains the same. As the hypotenuse of a right-angled triangle is longer than its legs, the vertex p_5 will end up outside the side p_5p_6 of the first layer. With no support structures added, this creates a small overhang as the build continues.

The structure was built using CMT welding, except from the first two layers: As for the structure described in *Set-based control for flexibility in orientation of tool*, these had do be welded using pulsed-MIG for the heat-input to be high enough for the deposited metal to adhere sufficiently to the substrate. The welding wire was made of the Ni-Cr-Mo alloy UTP 759, and the substrate was made of carbon steel S355G10. The parameters for the welding process are listed in Table 1. This build went on for approx. 45 layers, which meant that each corner of the hexagon had rotated about 53° away from its starting point.

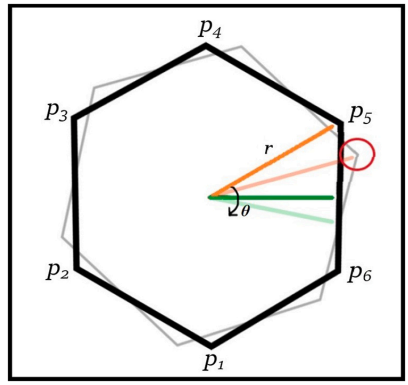

Fig. 10. Hexagon: As corner A rotates with an angle θ about the centre in an arc with radius r, it creates an overhang, as marked with a red circle.

As the aim of this experiment was to study the overhang, a rotation close to 60° was enough, as vertex p_5 in Fig. 10 at this point of the build would have rotated all the way to overlap with vertex p_6. After only 25 layers each of the vertices would have rotated 30°, and be at the point where the overhang was largest relative to the first layer. When studying Fig. 10, the orange line r for the current layer would then overlap with the original green line making out the longest leg of a right-angled triangle with hypotenuse r. The size of the overhang would be equal to the difference between r and l, which meant that the overhang protruded

$$r - l = r - \frac{\sqrt{3}}{2}r = 70 - \frac{\sqrt{3}}{2}\cdot 70 = 9.38$$

millimetres over the base layer of the structure. As the welding bead was approx. 4 mm wide, this equals more than twice the width of the welding bead (Fig. 11).

Non-vertical material deposition: Vase

Next, a structure with a significant structure was constructed by depositing material non-vertically. This design was a variation of the cylindrical structures from the experiments presented in *Preliminary tests with viscous material* and *Set-based control for flexibility in orientation of tool*. The difference is to have a varying radius, which in

Table 1
Welding parameters for twisting hexagon structure: Fixed orientation of tool mainly using CMT welding.

Hexagonal structure shown in Fig. 11						
CMT, fixed orientation of tool						
Method	Layer	Current (A)	Wire-feed speed (m/min)	Voltage (V)	Bead height (mm)	Rotation (degrees)
P-MIG	≈ **1**	182	7.1	25.5	1.5	0.0
P-MIG	≈ **2**	154	7.1	25.1	1.5	1.2
CMT	≈ **3**	130	3.8	20.9	1.5	2.4
CMT	≈ **4**	108	3.8	15.4	1.5	3.6
CMT	≈ **5–44**	95	3.8	15.9	1.5	4.8 + =1.2
CMT	≈ **45**	95	3.8	15.9	1.5	52.8

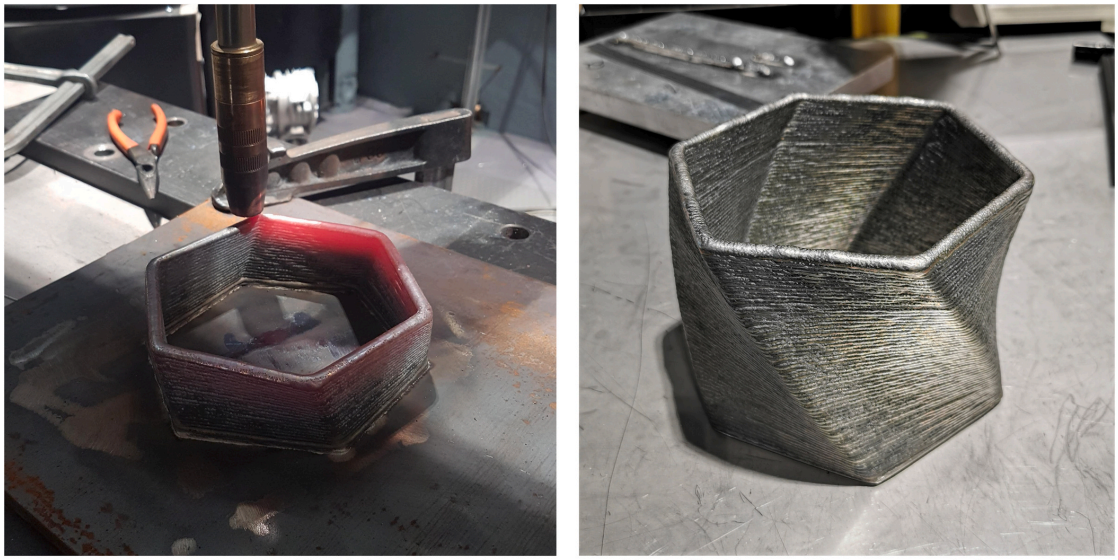

(a) The structure glowed red hot during construction. (b) The final hexagon shape, approx. 45 layers tall.

Fig. 11. Using a fixed vertical orientation of the welding gun, it was possible to construct a structure with a slight overhang. Spiralling hexagon, built in UTP 759.

turn creates an outwards or inwards overhang. A simulation of this path is shown in Fig. 12, and the design will from here-on be referred to as a vase shape.

As explained in *Set-based control for flexibility in orientation of tool*, the set-based method described in [19,20] prioritises the ease of the robot movements in order to create a smooth trajectory. However, the deviation in the orientation of the tool is not necessarily distributed symmetrically. For a traditional cylindrical shape, this imbalance in the change in the orientation resulted in the tool being almost vertical on the part of the build closest to the robot manipulator, and tilted slightly outwards on the opposite side. This in turn resulted in a saddle form at the top of the constructed cylinder, as shown in Fig. 9 [16]. The method was still tested on the vase shape in order to see how this would impact a structure with overhang. The build was done using UTP759, the same Ni-Cr-Mo alloy used for the hexagonal structure in Fig. 11.

The experiment using set-based control to build a vase structure was terminated after just a few layers. The non-symmetrical change in the orientation of the tool followed the pattern of the cylinder structure from Fig. 9, with the welding gun being almost vertical on one side of the build. This showed the significance of the orientation of the welding gun: On the side where the tool remained almost vertical, the deposited material did not adhere evenly with the previous layer, as the overlap with the previous layer was not large enough. This resulted in cladding of material, which only grew worse from one layer to the next. Welding parameters etc. for this interrupted experiment were not included in this paper, as a close analysis of this test was deemed not relevant.

However, on the opposite side of the structure, the orientation of the tool was almost aligned with the tilt of the overhang, as the welding gun tilted outwards while the radius of the structure was increasing. On this side, the constructed wall was smooth and without obvious deformation. This indicated that building such a structure while forcing the orientation of the welding gun to match the angle of the tilt of the wall would likely be more successful.

For the ensuing experiment, the path was programmed directly using the linear functions in the RAPID programming language [29], with set values for the orientation of the welding gun. The orientation of the welding gun was adjusted to being close to parallel with the direction of the tilt of the wall creating the overhang. This can be better understood by studying Fig. 12, which shows a simulation of the welding process performed in ABB's simulation software Robot Studio: As long as the radius is increasing, the welding gun will be oriented slightly outwards, and vice-versa. As the nozzle is symmetrical, no rotations about the global z-axis are needed, i.e. the axis perpendicular to the substrate, pointing out of the page when studying Fig. 13. The structure is designed to first have a section with an increasing radius, then a section with a constant radius, and lastly a section with a decreasing radius. The shift in orientation is introduced gradually over a few layers in between these sections, as listed in table 2.

The RAPID functions used to control the robot during these experiments requires the desired orientation of the end effector to be presented in quaternions $\boldsymbol{q}$, defined as [30]:

$$\boldsymbol{q} = q_\omega + \boldsymbol{i}q_x + \boldsymbol{j}q_y + \boldsymbol{k}q_z \tag{7}$$

In order to control the rotation of the tool relative to the world frame, which is parallel with the build, rotation matrices are used. Given a set of quaternions, the corresponding rotation matrix $\boldsymbol{R}_0$ can be derived. The desired rotations about the world x- and y-axes can then be performed on this rotation matrix, which will result in a new rotation matrix $\boldsymbol{R_N}$ corresponding with the final orientation of the end effector. The corresponding quaternions for the new orientation, $\boldsymbol{q_N}$, can be found from the rotation matrix $\boldsymbol{R_N}$, and used as input for the built-in RAPID functions that control the robot arm [29].

When reading the quaternions $\boldsymbol{q}$ representing the orientation of the tool when placed in a vertical position, the rotation matrix $\boldsymbol{R_0}$ for the orientation of the tool was found using the following equation [31]:

$$\boldsymbol{R}_0 = \begin{bmatrix} 1-2q_y^2-2q_z^2 & 2q_xq_y-2q_zq_\omega & 2q_xq_z+2q_yq_\omega \\ 2q_x2_y+2q_zq_\omega & 1-2q_x^2-2q_z^2 & 2q_yq_z-2q_xq_\omega \\ 2q_xq_z-2q_yq_\omega & 2q_yq_z+2q_xq_\omega & 1-2q_x^2-2q_y^2 \end{bmatrix} \tag{8}$$

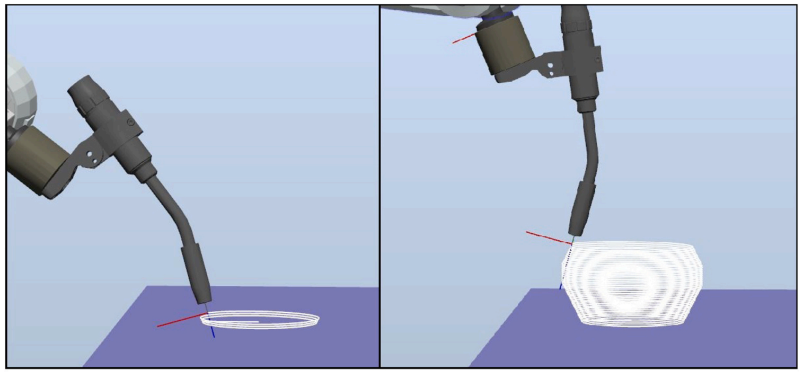

(a) The tool was oriented semi-parallel to the direction of the overhang being constructed.

(b) Vase structure, built in UTP 759.

(c) Profile of the vase.

Fig. 12. Building more prominent overhangs proved successful when orienting the tool relative to the building direction.

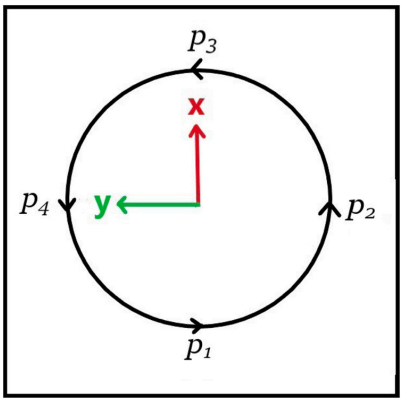

Fig. 13. Base with axes: This circle is the base for the vase structure in Fig. 12, and the axes show the global x- and y-axes that the welding gun is oriented relative to.

As can be seen from Fig. 12, the tool was tilted outwards in a given angle ϕ while the wall of the vase was tilting outwards, and vice versa. This was controlled by rotating the original rotation matrix relative to the global x- and y-axes shown in Fig. 13. The rotation matrices $\boldsymbol{R_x}$ and $\boldsymbol{R_y}$ are defined as [30]:

$$\boldsymbol{R_x} = \begin{bmatrix} 1 & 0 & 0 \\ 0 & \cos\alpha & -\sin\alpha \\ 0 & \sin\alpha & \cos\alpha \end{bmatrix} \tag{9}$$

and

$$\boldsymbol{R_y} = \begin{bmatrix} \cos\beta & 0 & \sin\beta \\ 0 & 1 & 0 \\ -\sin\beta & 0 & \cos\beta \end{bmatrix}. \tag{10}$$

The rotation angle ϕ for each layer can be read from table 2, and the rotations are given relative to the axes and points shown in Fig. 13. For the first part of the build, while the radius is increasing, the rotation angle ϕ is positive about the x- and y-axes for point p_2 and p_3, and negative for p_1 and p_4. For the last part of the build, while the radius is decreasing, the rotation angle ϕ is negative about the x- and y-axes for point p_2 and p_3, and positive for p_1 and p_4. The rotation matrix for the resulting rotation $\boldsymbol{R_N}$ at a given time is:

$$\boldsymbol{R_N} = \boldsymbol{R_0 R_{xRy}}. \tag{11}$$

Table 2
Welding parameters for vase structure: Dynamic orientation of tool and predominantly using CMT welding.

Welding parameters for the vase structure shown in Fig. 12							
CMT, varying orientation of tool							
Method	Layer	Current(A)	Wire-feed sp.(m/min)	Voltage(V)	Radius(mm)	Bead height(mm)	Angle (ϕ)(degrees)
P-MIG	≈ **1**	182	7.1	25.5	60.0	1.22	20.0
P-MIG	≈ **2**	165	7.1	25.4	60.8	1.22	20.0
CMT	≈ **3–25**	108	4.0	15.4	61.6 + = 0.8	1.22	20.0
CMT	≈ **26–29**	95	3.8	15.9	80.0	1.46	20.0 -= 5.0
CMT	≈ **30–39**	95	3.8	15.9	80.0	1.70	0.0
CMT	≈ **40–44**	95	3.8	15.9	80 -= 0.64	1.54	0.0 -= 5.0
CMT	≈ **45–100**	95	3.8	15.9	76.8 -= 0.64	1.38	-25.0

The rotation is given relative to the axes in Fig. 13. The orientation only has to be defined for each of the four points p_1-p_4 in Fig. 13, as the linear RAPID functions `MoveC/ArcC` will distribute the change in orientation evenly over the arc between two points [29]. As the rotation angle ϕ at any of the four points will only be non-zero about either the x- or the y-axis, not both of them, the rotation matrix for the non-active axis will be equal to the identity matrix $\boldsymbol{I}$. In other words: Using equations 9-10, for each of the four points in Fig. 13$\alpha = \phi$ and $\beta = 0$, or vice versa.

The quaternions $\boldsymbol{q_N}$ for this new orientation of the tool can then be found from the rotation matrix $\boldsymbol{R_N}$ using the approach presented in [32]. This approach avoids both dividing by zero and dividing by negative numbers. The rotation matrix $\boldsymbol{R_N}$ can be written as:

$$\boldsymbol{R_N} = \begin{bmatrix} r_{11} & r_{12} & r_{13} \\ r_{21} & r_{22} & r_{23} \\ r_{31} & r_{32} & r_{33} \end{bmatrix}. \tag{12}$$

Based on this, the following algorithm was used to find the quaternions [32]:

```
-----------------------------------------------
%Finding quaternions from rotation matrix

T := R[1][1] + R[2][2] + R[3][3];
IF T > 0:
    S := Sqrt(1 + T)*2;
    qw := 0.25*S;
    qx := (R[3][2] - R[2][3])/S;
    qy := (R[1][3] - R[3][1])/S;
    qz := (R[2][1] - R[1][2])/S;
ELSEIF R[1][1] >R[2][2] AND R[1][1] >R[3][3]:
    S := Sqrt(1+R[1][1] -R[2][2] -R[3][3])*2;
    qw := (R[3][2] - R[2][3])/S;
    qx := 0.25*S;
    qy := (R[1][2] + R[2][1])/S;
    qz := (R[1][3] + R[3][1])/S;                    ?.
ELSEIF R[2][2] > R[3][3]:
    S := Sqrt(1+R[2][2] -R[1][1] -R[3][3])*2;
    qw := (R[1][3] - R[3][1])/S;
    qx := (R[1][2] + R[2][1])/S;
    qy := 0.25*S;
    qz := (R[3][3] + R[3][2])/S;
ELSE:
    S := Sqrt(1+R[3][3] -R[1][1] -R[2][2])*2;
    qw := (R[2][1] - R[1][2])/S;
    qx := (R[1][3] + R[3][1])/S;
    qy := (R[2][3] + R[3][2])/S;
    qz := 0.25*S;
ENDIF
-----------------------------------------------
```

This method follows what is described in chapter 6 of [30], based on [33]. First, the trace of the rotation matrix $\boldsymbol{R_N}$ is found, i.e. the sum of the diagonal terms:

$$T = r_{11} + r_{22} + r_{33} = r_{00}. \tag{13}$$

If defining $\boldsymbol{z} = 2\boldsymbol{q}$, this gives us the set of equations [30]:

$$z_0^2 = 1 + 2r_{00} - T \tag{14}$$

$$z_1^2 = 1 + 2r_{11} - T \tag{15}$$

$$z_2^2 = 1 + 2r_{22} - T \tag{16}$$

$$z_3^2 = 1 + 2r_{33} - T, \tag{17}$$

and

$$z_0 z_1 = r_{32} - r_{23} z_2 z_3 = r_{32} + r_{23} \tag{18}$$

$$z_0 z_2 = r_{13} - r_{31} z_3 z_1 = r_{13} + r_{31} \tag{19}$$

$$z_0 z_3 = r_{21} - r_{12} z_1 z_2 = r_{21} + r_{12}. \tag{20}$$

Using the ten expressions from equations 14-20, the four unknowns z_0-z_3 can be found using many different approaches, as the variables r_{00-33} are known [33]. The quaternions $\boldsymbol{q_N}$ describing the new rotation can then be found, as

$$\boldsymbol{z} = 2\boldsymbol{q_N}. \tag{21}$$

The radius of each approx. layer of the vase, which determines how much each layer shifted relative to the previous layer, are listed in table 2. This shift, and the angle of the tilt of the wall of the vase, impacted on how much the deposited material would spread out before cooling down and solidifying, as explored in [34]. This implies that the estimated layer height became lower the steeper the building angle. This was accounted for during the build by setting the layer height to be a function of the change in angle, and the different layer heights are listed in Table 2. The correlation between layer height, tilt angle and change in radius, was linear, and set based on trial and error until finding a tilt angle for the welding gun that followed the tilt of the wall to some extent, though not accurately. A large angle would give a significant reduction in layer height and a large change in radius. The values used for the height increase, and how the angle of the tool was adjusted relative to the inclination of the wall, is based on experience from the experiments presented in *Continuous build of thin-walled structures–Fixed orientation of tool: Twisting hexagon.*

The build continued for approx. 100 layers, and was stopped because the welding material ran out. The final layer was shifted several centimetres relative to the vertical part of the structure, which shows that it was possible to build a significant overhang using non-vertical material deposition.

Table 3
Welding parameters for bowl structure: Dynamic orientation of tool and predominantly using CMT welding.

Welding parameters for bowl structure shown in Fig. 15							
CMT, varying orientation of tool							
Method	Layer	Current(A)	Wire-feed sp.(m/min)	Voltage(V)	Radius(mm)	Bead height(mm)	Angle (ϕ)(degrees)
P-MIG	≈ **1**	180	7.1	25.9	40.0	1.30	0.0
P-MIG	≈ **2**	156	7.1	25.2	40.0	1.30	0.0
CMT	≈ **3**	140	6.6	18.8	40.0	1.30	0.0
CMT	≈ **4**	108	3.9	15.8	40.0	1.30	0.0
CMT	≈ **5**	108	3.9	15.8	40.0	1.30	0.0
CMT	≈ **6–48**	96	3.5	14.0	40.0 + = 1.30·sin ϕ	1.30·cos ϕ	1.0 + = 1.0
CMT	≈ **49–96**	96	3.5	14.0	55.7 + = 0.89	0.95	43.0

Non-vertical material deposition: Bowl

After the build described in *Non-vertical material deposition: Vase*, a structure with a more significant overhang was constructed using non-vertical material deposition. Another variation of the cylinder structures presented in *Continuous build of thin-walled structures* and *Set-based control for flexibility in orientation of tool* was chosen, the alteration this time being a constantly increasing radius. This would result in a kind of bowl, in parts similar to the bottom part of the vase structure in Fig. 12, described in *Non-vertical material deposition: Vase*. The aim was to see how successful a continuous build of a structure with an increasing overhang would be, and if a overhang of more than 25° would prove challenging considering the material deposition when building in a similar material. The build was done using the nickel alloy Inconel 625, which is the same material used to build the flower structure shown in Fig. 6b. The substrate was made of carbon steel S355G10.

As in earlier builds, the increase in height of the welding gun accounting for each added layer was distributed over the last quadrant of each circular layer, thereby avoiding the issues that came with a height increase in a single point shown in Fig. 4. The initial layer height was slightly lowered compared to the vase build: from 1.7 mm to 1.3 mm in the part where the welding gun had a strictly vertical orientation. The radius and layer height was kept constant for the first 5 layers of the build, and the orientation of the tool was kept strictly vertical. This to get a good foundation for the rest of the build. As with all previous builds, the first few layers demanded a higher heat input than the rest of the build in order for the material to adhere properly to the substrate. The first two layers of the bowl structure were welded using pulsed MIG, as with the vase structure. The welding procedure was then paused momentarily to switch to CMT welding. The welding parameters for the complete build were based on parameters of the vase build in *Non-vertical material deposition: Vase*, and are described in detail in Table 3.

After the 5 first layers, the orientation of the tool was adjusted to increase by 1° per layer. The orientation of the welding gun was controlled as described in *Non-vertical material deposition: Vase*, always tilting inwards as shown in Fig. 12a. As explained in *Non-vertical material deposition: Vase*, the symmetry of the nozzle meant that the rotations only had to be performed relative to the global x- and y-axis. Because the angle would only increase relative to a vertical position, the bowl build was similar to the bottom-most part of the vase build, only with an increasing rather than decreasing overhang. While the angle increased, the radius would also increase slightly, creating a wall with a stronger tilt. As these changes were made in parallel, the angle of the welding gun would follow the building direction of the wall.

The larger the angle of the welding gun became, the more the radius would increase per layer. This made sense considering that a larger angle meant that the gravity to a larger extent could pull on the deposited, melted material so that it would spread out more before becoming solid. As the liquid material would spread out more horizontally, the layer height would simultaneously decrease. For the vase structure, these values were adjusted in a similar fashion, but there was no exact correlation between the angle of the welding gun and the tilt of the wall: the values were set more based on trial-and-error. For the bowl structure, the angle ϕ was increased by 1° per layer, and the initial layer height was set to 1.3 mm, based on the results from the vase structure. For this experiment, we wished to see how the build would progress when the increase in radius r_{inc} and the current layer height l_{hc} were set according to the geometrical correlation between these values as seen in a right triangle shown in Fig. 14. Following basic trigonometry, the layer height was set as

$$l_{hc} = l_h \cdot \sin\phi, \tag{22}$$

and the increase in radius for each layer was set as

$$r_{inc} = l_h \cdot \cos\phi. \tag{23}$$

For the first layers, while the angle ϕ was kept at zero, the increase in radius was also equal to zero, and the layer height was fixed at the set value 1.3 mm. Then, as the angle ϕ increased by 1° per layer, the radius would increase and the layer height would decrease. Using the simulation software Robot Studio from ABB, the designed path for this structure was simulated, as shown in Fig. 15a. During these simulations, the 6 DOF robot manipulator would face issues with singularities or joints being out of bounds when the angle ϕ got close to 50°, depending on the start position of the tool. To avoid this issue when performing the build, a maximum angle ϕ_{max} was set to 43°. As the aim of this build was to build a structure with a significantly larger overhang than that of the 20–25° overhang of the vase presented in *Non-vertical material deposition: Vase*, this was considered sufficient. When reaching this maximum angle ϕ_{max}, the build would continue on with this angle until stopped, resulting in the structure shown in Fig. 12c and d. For this final part of the build, the layer height would stay fixed at a value given by Eq. 22, and there would be an increase in the radius r_{inc} per additional layer given by Eq. 23, both with $\phi = \phi_{max}$.

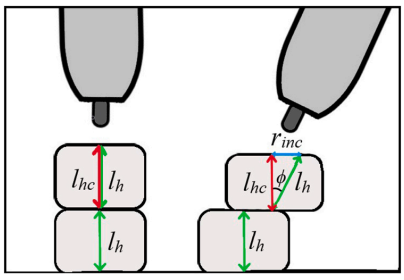

Fig. 14. Angle variation: As shown here, the layer height has a fixed value while the welding gun is strictly vertical. As the angle ϕ grows, this initial layer height becomes the hypotenuse in a right triangle. The layer height l_{hc} for the new layer, displayed in red, is described by equation 22. The increase in radius r_{inc}, displayed in blue, is described by equation 23.

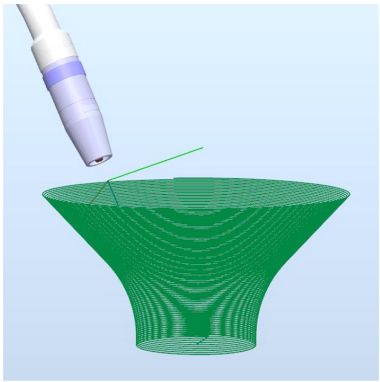

(a) The simulated path for the structure with 43° overhang.

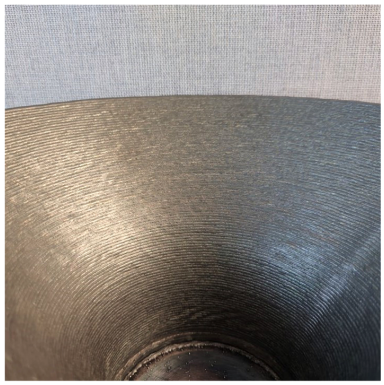

(b) The build was smooth, without clear deformations

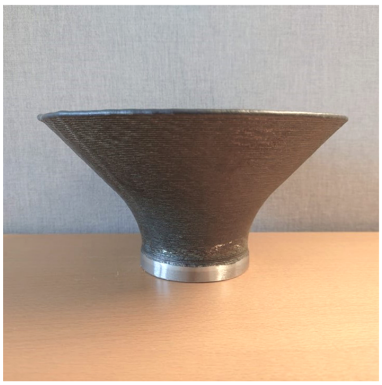

(c) The final 43° overhang of the bowl.

(d) The final bowl.

Fig. 15. The structure had a gradually increasing overhang, moving from a tilt of 0° to 43°, relative to a vertical orientation of the welding gun.

Material analysis

The conditions for heat accumulation and heat dissipation are altered when building with overhangs and intersections. As a consequence, the cooling rate and thermal gradient during solidification of the material is different along the trajectory. The different thermal history may lead to promotion of other phases and microstructures, which in turn may influence the mechanical properties and service performance. To better understand the effect of non-steady state deposition, the hexagonal structure in Fig. 11 and the flower shape in Fig. 7 were examined. Transverse sections of stable mid-wall positions, overhang corners, and intersection were examined by optical microscopy and hardness measurements to reveal any process defects or fluctuations. Both materials were manufactured with the Ni-Cr-Mo alloy UTP 759.

The hexagonal structure is shown in Fig. 16. The mid-wall position, i.e., with no overhang shows a mixed structure of columnar and equiaxed dendrites. The dendrites were nearly vertically oriented, i.e. parallel to the building direction. This structure was developed due to the strong heat sink of the already built structure by thermal conduction. The columnar dendrites grew over several layers, due to epitaxial nucleation upon remelting and solidification of a new layer. Columnar dendrites ranging over several layers are commonly seen in WAAM of nickel-based alloys like Hastelloy C276 and Inconel 625 [35–37]. A portion of equiaxed 'star-shaped' dendrites can also be seen in Fig. 16a. This morphology is uncommon in lean alloys like Hastelloy C276 and Inconel 625 processed by WAAM. However, UTP 759 has a higher alloying content, so the constitutional undercooled zone was larger during solidification compared to Hastelloy C276 and Inconel 625. This effect increased the probability of nucleation ahead of the columnar growth front and created the equiaxed dendrites.

The microstructure at the overhang position is shown in Fig. 16b. The structure was solely occupied by fine equiaxed dendrites. As the chemical composition is similar irrespective of position, the altered thermal characteristics are responsible for this microstructural change compared to the mid-wall position with no overhang. When the material is deposited with overhangs, a lower portion of the liquid weld bead is in direct contact with the former layer. Consequently, the downward thermal gradient due to conduction is decreased compared to a structure with no overhang. With a lower thermal gradient, the driving force for columnar growth is decreased and the constitutional undercooling increases. Such conditions are facilitating the nucleation of equiaxed dendrites. Overhangs can therefore influence the microstructure and the related properties of WAAM structures. Small process defects were occasionally observed at the bead interface when building with overhangs, such as the black lack-of-fusion defects depicted in Fig. 16b. Further process parameter optimisation is required to eliminate such defects.

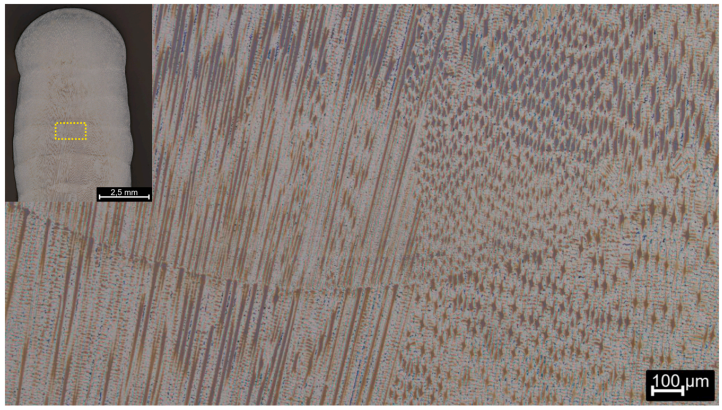

(a) Hexagon mid-wall position with no overhang. Mixture of columnar and equiaxed dendrites.

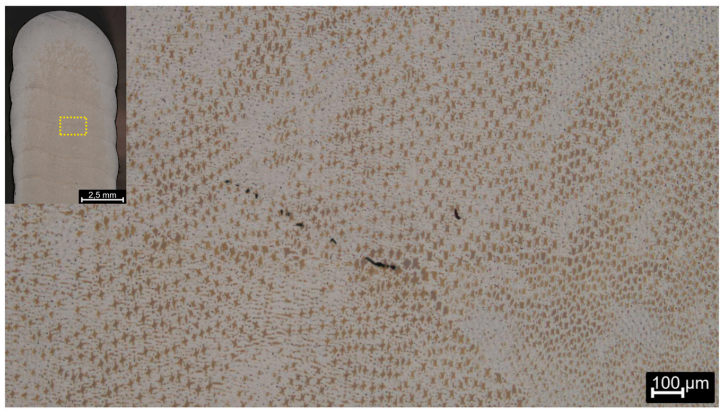

(b) Hexagon corner position with overhang. Structure with fine equiaxed dendrites.

Fig. 16. Microstructure of Ni-Co-Mo alloy UTP 759 hexagon structure in transverse section.

The microstructure of the flower shaped structure is shown in Fig. 17. This design has no overhangs, but two touching corners to create a continuous intersection. The intersection involves an extra remelting step of the structure, and two bead junctions can be observed in Fig. 17b. This effect has a minor influence on the final microstructure. The material exhibits a relatively homogeneous structure of equi-axed dendrites regardless of position. The only exception to this statement is some scattered columnar dendrites in vicinity of remelted layers at intersections, Fig. 17b. There was not observed any process defects as cracks, pores or lack of fusion in the structure.

It is evident that the microstructure during 'normal' deposition (i.e., no overhang or intersections) is different for the hexagonal structure and the flower structure. This difference is related to the increased heat input when under deposition of the flower shape. A higher heat input was necessary to ensure fusion at the intersection zone of the flower. The increased heat input lowers the temperature gradient in the molten weld pool, which in turn suppress the columnar dendritic growth. The effect of heat input and microstructure was evaluated by Vickers hardness testing, see Fig. 18. The hexagon geometry with no overhang possessed a mixture of columnar and equiaxed dendrites. The anisotropic properties of the columnar structure resulted in lower hardness values, and increased the result scatter. Further, the flower shape showed similar to somewhat higher hardness compared to the hexagon structure. Refined equiaxed dendrites accounted for the observed increase in hardness. In-depth assessments of mechanical performance, e.g. tensile strength, impact toughness, fatigue- and creep resistance was out of scope of this work, but should be assessed in further work.

Discussion

The experiments presented in this paper all take a step away from in-box, strictly layer-based AM methods. For the preliminary experiments, the trajectory for the walls resembles an upwards spiralling helix. This differs from the strictly layer-by-layer approach that you find in AM methods such as VP or PBF. After the preliminary experiments using a form of viscous glue, the focus of this research turned to metals and the DED method WAAM. Performing the builds as continuously as possible was still a priority, as the initiation or termination of the material deposition often brings with it some deformations and inaccuracies in the material deposition. In *Continuous build of thin-walled structures* it is also examined how, when deposition material continuously, a gradual transition between layers can give fewer distortions for WAAM than an height increase in a single point, as is common for many AM methods.

WAAM using CMT and pulsed-MIG gave results with few distortions when building thin-walled structures. For simple

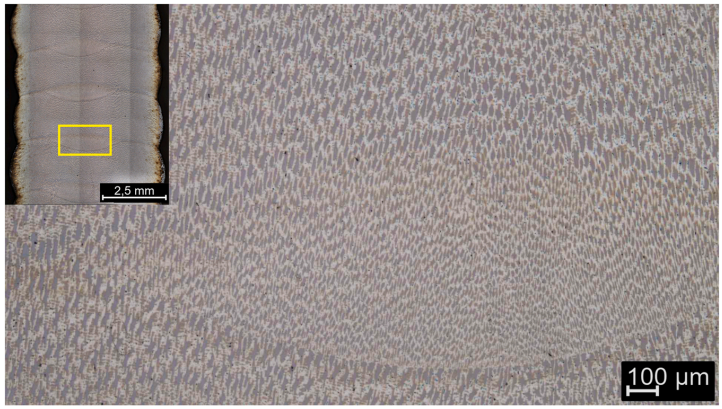

(a) Flower mid-wall position. Structure with fine equiaxed dendrites.

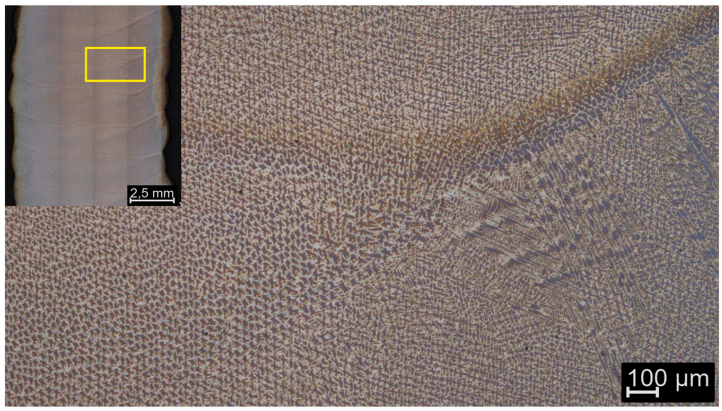

(b) Flower intersection. Mixture of columnar and equiaxed dendrites.

Fig. 17. Microstructure of Ni-Co-Mo alloy UTP 759 flower structure in transverse section.

geometrical structures such as a cylinder, both metals with a low and a high melting point resulted in structures with few deformations. These builds could have continued for a long time due to an equilibrium between heat accumulation and dissipation. For slightly more complex structures with intersections, described in *Avoiding double material deposition in intersections*, it proved easier to get a result with few deformations when using metals with a higher melting point. This is to be expected: The lower the melting point, the higher the risk of the accumulated heat impacting how long the deposited material takes to solidify, resulting in an uneven distribution of the deposited material. To cross-check the results from the experiments presented here, additional structures based on the principle described in *Continuous build of thin-walled structures* and 5 were built using the Ni-Cr-Mo alloy UTP 759. As can be seen by comparing Fig. 19 with Fig. 5 and 7, a harder material with a higher melting point helped make the surface of the structures smoother and with less superficial deformations compared to similar structures built in aluminium alloys.

The hexagonal structure presented in *Fixed orientation of tool: Twisting hexagon* shows that if the material solidifies quickly enough, it is possible to build overhangs even when depositing material from a nozzle with a vertical orientation. Future work should look into how the same structure will turn out when building in a softer material with a lower melting point, such as the aluminium-alloys used in other builds described in this paper. It would also be interesting to examine how a structure in the same material would behave with a larger rotation angle, which would lead to less overlap between two consecutive layers. The optical microscopy and hardness

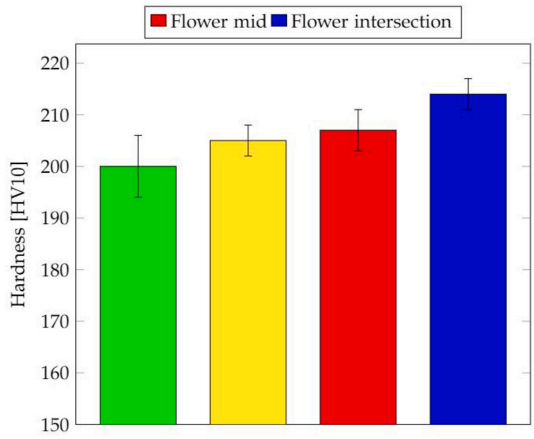

Fig. 18. Vickers hardness of Ni-Cr-Mo alloy UTP 759.

Fig. 19. Additional structures were constructed in the Ni-Cr-Mo alloy UTP 759.

measurements presented in *Material analysis* showed that such an approach will influence the micro structure of the component, but it did not seem to have significant impact on the hardness, as shown in Fig. 18.

The set-based approach used in [17] could be used for the simple thin-walled structure without overhang described in *Set-based control for flexibility in orientation of tool*. The additional freedom in orientation of the tool given by the set-based control method could potentially save energy while performing the build in the same amount of time, as shown in [20]. The method also required less torques in the turns, as the tool did not have to keep one strict orientation, which made it possible to perform sharp turns and sharp changes in the direction of the path faster and smoother. This was useful, as the earliest welding tests with the box-shape described in *Continuous build of thin-walled structures* showed that if the corners were too sharp, material would accumulate because the welding gun stayed in the same spot too long while the robot re-configured itself for the change in direction [16]. However, this structure did show some prominent deformations compared with similar structures in Fig. 5 and 19. The saddle form at the top of the finished structure was likely caused by the non-symmetric deviation in the orientation of the welding gun. This unpredictable imprecision can make the method unsuitable depending on the specifications for the built structure.

When building the vase-structure with very prominent overhangs it quickly became evident that when building a significant overhang with less vertical alignment between two consecutive layers, the orientation of the tool needed to be controlled much more closely. The freedom given by the set-based control method did not distribute the change in the orientation of the tool symmetrically, which made the method unsuited for the task. The experiment described in the first part of *Non-vertical material deposition: Vase* showed that the results could be quite unpredictable. A vertical orientation of the tool while deposition material on a wall that tilted gave a poor result, as the overlap with the previous layer was not large enough.

When constructing a vase shape with the nozzle of the welding gun following the tilt of the wall of the structure, the results were more promising. The angle of the tilt for the first part of the build showed that the build could be affected as the heat built up early in the build. In Fig. 12 it is possible to see that even though the angle of the bottom part of the vase was constant for this part of the build, the tilt of the wall seemed to decrease slightly after a few centimetres. This was caused by the accumulated heat in the structure: As the structure heated up, it took slightly longer for the deposited material to solidify, making the welding bead flatter and wider. As the angle of the top part of the vase, above the vertical part of the wall, did not have any such irregularities, it can be concluded that at this point the accumulated heat and the heat dissipation had reached equilibrium, making the welded wall smoother. The bowl structure presented in *Non-vertical material deposition: Bowl* did not have this same slope in angle. This might be because the first few layers were built straight up, with a vertical orientation of the welding gun. By the time the overhang became prominent enough for such drooping to take place, the heat dissipation had already reached equilibrium, so that the build was smooth from thereon.

The distance between the tool and surface to be welded grew too large during the vase build. If the distance between the nozzle and the surface grows too large, this can make the arc unstable and lead to deformations, as well as reduce the protective effects of the shielding gas [38]. An inaccurate estimate of the layer height was also an issue in earlier builds, most-times solved by interrupting the build to adjust the distance between the nozzle and the structure [16]. Based on the results from the vase build, the initial layer height was reduced for the bowl build, from 1.7 mm to 1.3 mm when the welding tool was vertical. In addition, the layer height for the build was set as a trigonometrical function of the angle of the welding gun relative to a vertical orientation. This seemed to be a good proximate for how the bead height and width developed as the build went on. Unlike for the vase build, the distance between the tool and the surface did not grow too large during the bowl build, and the build could have continued for longer if desired.

For future experiments, layer heights throughout the build relative to the angle of the tilt of an overhang should be adjusted more accurately. For the vase structure in *Non-vertical material deposition: Vase*, all values were estimated based on the experience from the experiments presented in Continuous build of thin-walled structures [16] and *Set-based control for flexibility in orientation of tool* [17]. More accurate estimates could be made, for example based on the results from [34] or [39]. If these values were optimised, it might be possible to build similar overhangs in other metals with a lower melting point, such as aluminium. The issue could also be solved either by adjusting the vertical position of the nozzle during the build, or by ensuring a more stable layer height [38].

Building structures with even larger overhangs can also be considered future work. As explained in *Non-vertical material deposition: Bowl*, the 6 DOF robot manipulator met challenges such as joint out of bounds or singularities when the angle of the bowl grew larger than the set maximum angle of 43°. Avoiding these issues would perhaps require an alternative control method altogether than that of the built-in functions of the RAPID programming language. At least it would have required more time adjusting the set-up of the robot cell, and the start point and orientation of the end effector. Building a basic, tilted wall would have been possible without the robot reaching singularities. Such thin-walls have been investigated by others, for example in [39]. As the main goal was to show that the construction of a prominent overhang with continuous, non-vertical material deposition was possible, a 43° angle was considered sufficient, and further adjustments are considered out of scope for the work presented here.

Concluding remarks

Building using WAAM is a relatively easily accessible way to enable non-vertical-deposition of material, as welding equipment combined with an industrial robot manipulator can be found in many labs and factories. Other projects have gotten very interesting results using other materials than metals and WAAM, such as fast-curing polymers [12]. This should be explored in future work.

Throughout the welding experiments presented in this paper, the distance between the nozzle of the welding gun and the surface to be welded was adjusted manually by the welding operator during several of these builds. A more solid solution could be to include

feedback in the process. The welding parameters, i.e. current and voltage, are impacted by this distance. If these values were monitored during the build, it could be possible to detect if this distance grew too large or too small, and the controller could then modify the path accordingly. Ideally, these adjustments could also be included in a feed-back loop and done automatically, enabling the process do correct itself during the build. This kind of feedback could potentially also be used to find an optimal orientation of the tool relative to the overhang, as the size of the contact surface is largest when the tool is orthogonal to the direction of the construction [39]. This should explored in future work.

The set-based control method designed by Moe et al. [19] was not well suited for building structures with overhangs, as the deviation in orientation was unpredictable an non-symmetrical. The method might work better if it was possible to restrict the set of valid angles for the tool further, but this would somewhat contradict the main benefits of the control method. In future work, it could be examined if this method can be modified to distribute the orientation evenly about a fixed point.

Several of the experiments showed that it is important to adjust the heat-input so that the structure does not grown too hot due to accumulated heat. This could be seen very clearly on the final vase-shape, where accumulated heat due to a large heat input early in the build made the walls of the structure slope more than estimated. Controlling that the heat input and heat dissipation is as close as possible to an equilibrium can for example be done by monitoring the accumulated heat in the structure during the build. The bowl build with an overhang of 43° shows that it is possible to construct thin-walled structures with prominent overhangs using continuous, non-vertical material deposition. Future work should examine how steep and large such an overhang could be before the structure showing significant deformations, preferably for different materials. A more thorough material analysis of structures with overhangs, including in-depth assessment of the tensile strength, impact toughness, fatigue- and creep resistance should also be examined in future work, but was out of scope for this work.

Funding

The work reported in this paper was based on activities within centre for research based innovation SFI Manufacturing in Norway, and is partially funded by the Research Council of Norway under contract number 237900.

Declaration of Competing Interest

The authors declare that they have no known competing financial interests or personal relationships that could have appeared to influence the work reported in this paper.

References

[1] Gibson, I., Rosen, D.W., Stucker, B., 2010, Additive Manufacturing Technologies, 238. Springer.
[2] Abdulhameed, O., Al-Ahmari, A., Ameen, W., Mian, S.H., 2019, Additive Manufacturing: Challenges, Trends, and Applications. Advances in Mechanical Engineering, 11/2:1687814018822880https://doi.org/10.1177/1687814018822880.
[3] Oliveira, J., LaLonde, A., Ma, J., 2020, Processing Parameters in Laser Powder Bed Fusion Metal Additive Manufacturing. Materials & Design, 193:108762https://doi.org/10.1016/j.matdes.2020.108762.
[4] Apis-cor.com, Apis-cor, accessed 2021–11-04 (2015–2021).⟨https://www.apis-cor.com⟩.
[5] Kampc.be, 3d-printing in the construction world, accessed 2021–11-04 (2018–2021).⟨https://www.kampc.be/c3po_eng⟩.
[6] Jiang, J., Ma, Y., 2020, Path Planning Strategies to Optimize Accuracy, Quality, Build Time and Material Use in Additive Manufacturing: A Review. Micromachines, 11/7: 633. https://doi.org/10.3390/mi11070633.
[7] Jiang, J., Xu, X., Stringer, J., 2018, Support Structures For Additive Manufacturing: A Review. Journal of Manufacturing and Materials Processing, 2/4: 64. https://doi.org/10.3390/jmmp2040064.
[8] Dai, C., Wang, C.C., Wu, C., Lefebvre, S., Fang, G., Liu, Y.-J., 2018, Support-free Volume Printing by Multi-axis Motion. ACM Transactions on Graphics ((TOG)), 37/4: 134. https://doi.org/10.1145/3197517.3201342.
[9] Panchagnula, J.S., Simhambhatla, S., 2018, Manufacture of Complex Thin-walled Metallic Objects Using Weld-deposition Based Additive Manufacturing. Robotics and Computer-Integrated Manufacturing, 49:194–203. https://doi.org/10.1016/j.rcim.2017.06.003.
[10] Parmar, K., Oster, L., Mann, S., Sharma, R., Reisgen, U., Schmitz, M., Nowicki, T., Wiartalla, J., Hüsing, M., Corves, B., 2021, Development of a Multidirectional Wire Arc Additive Manufacturing (waam) Process with Pure Object Manipulation: Process Introduction and First Prototypes. Journal of Manufacturing and Materials Processing, 5/4: 134. https://doi.org/10.3390/jmmp5040134.
[11] Jorislaarman.com, MX3D bridge, accessed 2019–11-11 (2015–2019).⟨https://www.jorislaarman.com/work/mx3d-bridge/⟩.
[12] Laarman, J., Jokic, S., Novikov, P., Fraguada, L.E., Markopoulou, A., 2014, Anti-gravity Additive Manufacturing. Fabricate: Negotiating Design & Making, 192–197. https://doi.org/10.2307/j.ctt1tp3c5w.27.
[13] Ramalho, A., Santos, T.G., Bevans, B., Smoqi, Z., Rao, P., Oliveira, J., 2022, Effect of Contaminations on the Acoustic Emissions During Wire and Arc Additive Manufacturing of 316l Stainless Steel. Additive Manufacturing, 51:102585https://doi.org/10.1016/j.addma.2021.102585.
[14] Ding, D., Pan, Z., Cuiuri, D., Li, H., 2015, A Practical Path Planning Methodology for Wire and Arc Additive Manufacturing of Thin-walled Structures. Robotics and Computer-Integrated Manufacturing, 34:8–19. https://doi.org/10.1016/j.rcim.2015.01.003.
[15] Evjemo, L.D., Moe, S., Gravdahl, J.T., Roulet-Dubonnet, O., Gellein, L.T., Brøtan, V., 2017, Additive Manufacturing by Robot Manipulator: An Overview of the State-of-the-art and Proof-of-concept Results. 22nd IEEE ETFA, Cyprus: 1–8. https://doi.org/10.1109/ETFA.2017.8247617.
[16] Evjemo, L.D., Langelandsvik, G., Gravdahl, J.T., 2019, Wire Arc Additive Manufacturing by Robot Manipulator: Towards Creating Complex Geometries. 5th IFAC ICONS. Elsevier, Belfast: 103–109. https://doi.org/10.1016/j.ifacol.2019.09.125.
[17] Evjemo, L.D., Moe, S., Gravdahl, J.T., 2020, Robotised Wire Arc Additive Manufacturing Using Set-based Control: Experimental Results. 21st IFAC World Congress, Berlin: 1–8. https://doi.org/10.1016/j.ifacol.2020.12.2725.
[18] Würth, SikkerhetsdatabladSTP Quickfast hvit 290 ml, rev. 3.1, ⟨https://www.wuerth.no/msds/pdf/01275205.PDF⟩ (2)2016.
[19] Moe, S., Antonelli, G., Teel, A.R., Pettersen, K.Y., Schrimpf, J., 2016, Set-Based Tasks within the Singularity-Robust Multiple Task-Priority Inverse Kinematics Framework: General Formulation, Stability Analysis, and Experimental Results. Frontiers in Robotics and AI, 3/April: 1–18. https://doi.org/10.3389/frobt.2016.00016⟨http://journal.frontiersin.org/article/10.3389/frobt.2016.00016⟩.
[20] Moe, S., Gravdahl, J.T., Pettersen, K.Y., 2018, Set-based Control for Autonomous Spray Painting. IEEE Transactions on Automation Science and Engineering, 15/4: 1785–1796. https://doi.org/10.1109/TASE.2018.2801382.
[21] Halmøy, E., 1991, Sveiseteknikk. 4th edition NTNU, Norway.
[22] Cong, B., Ouyang, R., Qi, B., Ding, J., 2016, Influence of Cold Metal Transfer Process and its Heat Input on Weld Bead Geometry and Porosity of Aluminum-copper Alloy Welds. Rare Metal Materials and Engineering, 45/3: 606–611. https://doi.org/10.1016/S1875-5372(16)30080-7.
[23] Abb.com, IRB 2400, accessed 2018–10-22 (2016–2018).⟨https://new.abb.com/products/robotics/industrial-robots/irb-2400⟩.
[24] Fronius.com, CMT - cold metal transfer: The cold welding process for premium quality, accessed 2021–07-28 (2019–2021).⟨https://www.fronius.com/en/welding-technology/world-of-welding/fronius-welding-processes/cmt⟩.
[25] Smati, Z., 1986, Automatic Pulsed Mig Welding. .
[26] Martina, F., Mehnen, J., Williams, S.W., Colegrove, P., Wang, F., 2012. Investigation of the benefits of plasma deposition for the additive layer manufacture of Ti-6Al-4V, 212 (6),1377–1386, 10.1016/j.jmatprotec.2012.02.002.
[27] Mehnen, J., Ding, J., Lockett, H., Kazanas, P., 2011, Design for Wire and Arc Additive Layer Manufacture. Global Product Development Springer: 721–727. https://doi.org/10.1007/978-3-642-15973-2_73.
[28] Cade, P., Gordon, R.A., 2005, An Apothem Apparently Appears. The College Mathematics Journal, 36/1: 52–55. https://doi.org/10.2307/30044819.
[29] ABBRobotics, Technical reference manual: RAPID Instructions, Functions and Data types (2004–2010).
[30] Egeland, O., Gravdahl, J.T., 2002, Modeling and Simulation for Automatic Control. Marine Cybernetics Trondheim, Norway.
[31] Kuipers, J.B., 1999, Quaternions and Rotation Sequences: A Primer with Applications to Orbits, Aerospace, and Virtual Reality. Princeton University Press.
[32] Euclidianspace.com, Maths - conversion matrix to quaternions, accessed 2021–04-03 (1999–2007).⟨https://www.euclideanspace.com/maths/geometry/rotations/conversions/matrixToQuaternion/⟩.

[33] Shepperd, S.W., 1978, Quaternion From Rotation Matrix. Journal of Guidance and Control, 1/3: 223–224. https://doi.org/10.2514/3.55767b.
[34] Jiang, J., Stringer, J., Xu, X., Zhong, R.Y., 2018, Investigation of Printable Threshold Overhang Angle in Extrusion-based Additive Manufacturing for Reducing Support Waste. International Journal of Computer Integrated Manufacturing, 31/10: 961–969. https://doi.org/10.1080/0951192X.2018.1466398.
[35] Qiu, Z., Wu, B., Zhu, H., Wang, Z., Hellier, A., Ma, Y., Li, H., Muransky, O., Wexler, D., 2020, Microstructure and Mechanical Properties of Wire Arc Additively Manufactured Hastelloy C276 Alloy. Materials & Design, 195:109007https://doi.org/10.1016/j.matdes.2020.109007.
[36] Qiu, Z., Wu, B., Wang, Z., Wexler, D., Carpenter, K., Zhu, H., Muránsky, O., Zhang, J., Li, H., 2021, Effects of Post Heat Treatment on the Microstructure and Mechanical Properties of Wire Arc Additively Manufactured Hastelloy C276 Alloy. Materials Characterization, 177:111158https://doi.org/10.1016/j.matchar.2021.111158.
[37] Yangfan, W., Xizhang, C., Chuanchu, S., 2019, Microstructure and Mechanical Properties of Inconel 625 Fabricated by Wire-arc Additive Manufacturing. Surface and Coatings Technology, 374:116–123. https://doi.org/10.1016/j.surfcoat.2019.05.079.
[38] Shen, H., Deng, R., Liu, B., Tang, S., Li, S., 2020, Study of the Mechanism of a Stable Deposited Height During Gmaw-based Additive Manufacturing. Applied Sciences, 10/12: 4322. https://doi.org/10.3390/app10124322.
[39] Xiong, J., Lei, Y., Chen, H., Zhang, G., 2017, Fabrication of Inclined Thin-walled Parts in Multi-layer Single-pass Gmaw-based Additive Manufacturing with Flat Position Deposition. Journal of Materials Processing Technology, 240:397–403. https://doi.org/10.1016/j.jmatprotec.2016.10.019.

ISBN 978-82-326-6853-3 (printed ver.)
ISBN 978-82-326-6624-9 (electronic ver.)
ISSN 1503-8181 (printed ver.)
ISSN 2703-8084 (online ver.)

NTNU

Norwegian University of
Science and Technology